ISSN 2686-7575 (Online)

ТОНКИЕ ХИМИЧЕСКИЕ ТЕХНОЛОГИИ

Fine Chemical Technologies

- Theoretical Bases of Chemical Technology
- Chemistry and Technology of Organic Substances
- Chemistry and Technology of Medicinal Compounds and Biologically Active Substances
- Synthesis and Processing of Polymers and Polymeric Composites
- Chemistry and Technology of Inorganic Materials
- Analytical Methods in Chemistry and Chemical Technology
- Mathematical Methods and Information Systems in Chemical Technology

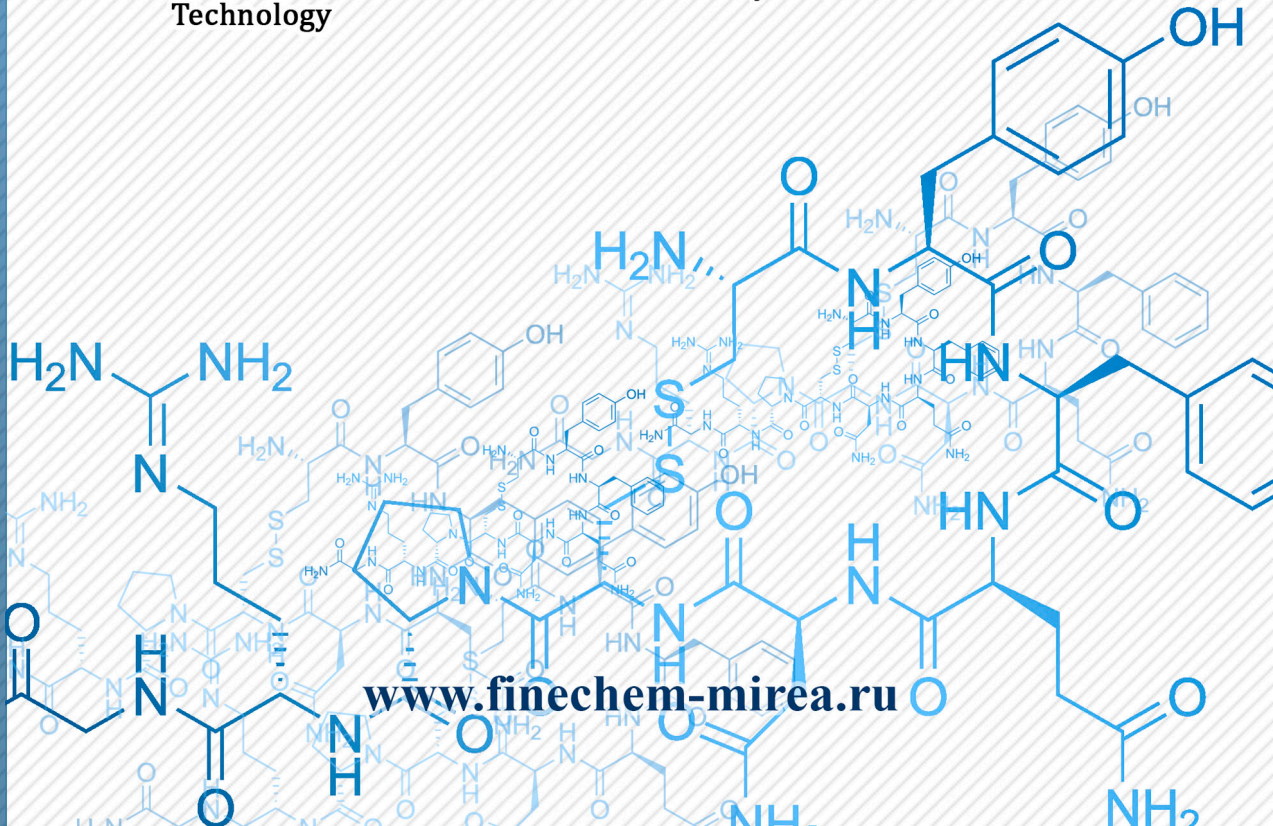

16(2)
2021

www.finechem-mirea.ru

ISSN 2686-7575 (Online)

ТОНКИЕ ХИМИЧЕСКИЕ ТЕХНОЛОГИИ

Fine Chemical Technologies

- Theoretical Bases of Chemical Technology
- Chemistry and Technology of Organic Substances
- Chemistry and Technology of Medicinal Compounds and Biologically Active Substances
- Synthesis and Processing of Polymers and Polymeric Composites
- Chemistry and Technology of Inorganic Materials
- Analytical Methods in Chemistry and Chemical Technology
- Mathematical Methods and Information Systems in Chemical Technology

Tonkie Khimicheskie Tekhnologii =
Fine Chemical Technologies
Vol. 16, No. 2, 2021

Тонкие химические технологии =
Fine Chemical Technologies
Том 16, № 2, 2021

https://doi.org/10.32362/2410-6593-2021-16-2
www.finechem-mirea.ru

https://doi.org/10.32362/2410-6593 ***www.finechem-mirea.ru***

Tonkie Khimicheskie Tekhnologii =
Fine Chemical Technologies
2021, Vol. 16, No. 2

The peer-reviewed scientific and technical journal Fine Chemical Technologies highlights the modern achievements of fundamental and applied research in the field of fine chemical technologies, including theoretical bases of chemical technology, chemistry and technology of medicinal compounds and biologically active substances, organic substances and inorganic materials, synthesis and processing of polymers and polymeric composites, analytical and mathematical methods and information systems in chemistry and chemical technology.

Founder and Publisher

Federal State Budget
Educational Institution
of Higher Education
"MIREA – Russian Technological University"
78, Vernadskogo pr., Moscow, 119454, Russian Federation.

Publication frequency: bimonthly.
The journal was founded in 2006. The name was Vestnik MITHT until 2015 (ISSN 1819-1487).

The journal is included into the List of peer-reviewed science press of the State Commission for Academic Degrees and Titles of the Russian Federation.
The journal is indexed:
DOAJ, Chemical Abstracts, Science Index, RSCI, Ulrich's International Periodicals Directory

86, Vernadskogo pr., Moscow, 119571, Russian Federation.
Phone: +7(495) 246-05-55 (#2-88)
E-mail: *seredina@mirea.ru*

Registration Certificate ПИ № ФС 77–74580, issued on December 14, 2018 by the Federal Service for Supervision of Communications, Information Technology, and Mass Media of Russia

The subscription index of *Pressa Rossii*: **36924**

Тонкие химические технологии =
Fine Chemical Technologies
2021, том 16, № 2

Научно-технический рецензируемый журнал «Тонкие химические технологии» освещает современные достижения фундаментальных и прикладных исследований в области тонких химических технологий, включая теоретические основы химической технологии, химию и технологию лекарственных препаратов и биологически активных соединений, органических веществ и неорганических материалов, синтез и переработку полимеров и композитов на их основе, аналитические и математические методы и информационные системы в химии и химической технологии.

Учредитель и издатель

федеральное государственное бюджетное
образовательное учреждение
высшего образования
«МИРЭА – Российский технологический университет»
119454, РФ, Москва, пр-кт Вернадского, д. 78.

Периодичность: один раз в два месяца.
Журнал основан в 2006 году. До 2015 года издавался под названием «Вестник МИТХТ» (ISSN 1819-1487).

Журнал входит в Перечень ведущих рецензируемых научных журналов ВАК РФ.
Индексируется:
DOAJ, Chemical Abstracts, РИНЦ (Science Index), RSCI, Ulrich's International Periodicals Directory

119571, Москва, пр. Вернадского, 86, оф. Л-119.
Тел.: +7(495) 246-05-55 (#2-88)
E-mail: *seredina@mirea.ru*

Свидетельство о регистрации СМИ: ПИ № ФС 77-74580 от 14.12.2018 г. выдано Федеральной службой по надзору в сфере связи, информационных технологий и массовых коммуникаций (Роскомнадзор)

Индекс по Объединенному каталогу «Пресса России»: **36924**

ТОНКИЕ ХИМИЧЕСКИЕ ТЕХНОЛОГИИ | Fine Chemical Technologies

16(2)
2021

CONTENTS

СОДЕРЖАНИЕ

THEORETICAL BASES OF CHEMICAL TECHNOLOGY

ТЕОРЕТИЧЕСКИЕ ОСНОВЫ ХИМИЧЕСКОЙ ТЕХНОЛОГИИ

ISSN 2686-7575 (Online)

https://doi.org/10.32362/2410-6593-2021-16-2-105-112

UDC 66-9,661;544.653.3

RESEARCH ARTICLE

Manufacturing of nanopillar (ultra-dispersed) catalytically active materials through chemical engineering

Alexey P. Antropov, Nikolay K. Zaytsev, Yegor D. Ryabkov, Nikolay A. Yashtulov[@], Polina N. Mudrakova

MIREA – Russian Technological University (M.V. Lomonosov Institute of Fine Chemical Technologies), Moscow, 119571 Russia
[@]Corresponding author, e-mail: yashtulovna@mail.ru

Abstract

Objectives. *Catalytically active materials are required in different chemical engineering processes. This makes the development of new materials with high efficiency and original ways in which to obtain them of significant interest. The present work investigates the synthesis of catalytically active material including electrode materials, as well as their improved efficiency due to the nanodecoration of their surface.*

Methods. *An aluminum folio was nanoperforated (nanoscalloped) by high-voltage anodization in an acidic medium. The effective electrode material was obtained as a metallic nickel replica rather than an oxide layer of the product. To study the surface state of aluminum obtained in this manner, a scanning electron microscope (Hitachi-SU8200) was used. The elementary composition of the aluminum was determined by back-scattered X-ray irradiation.*

Results. *The nickel replica obtained in the above-described process exceeded the catalytic activity estimated by methanol oxidation of the unprocessed nickel 70–150 times.*

Conclusions. *The present paper demonstrates the potential of creating effective catalytically active nanopillar materials using the metallic rather than metal-oxide part of a layer of anodized aluminum as a matrix template.*

Keywords: *distillation, binary mixtures, relative volatility, reflux ratio, distribution coefficient, internal energy saving in distillation*

For citation: Antropov A.P., Zaytsev N.K., Ryabkov Ye.D., Yashtulov N.A., Mudrakova P.N. Manufacturing of nanopillar (ultra-dispersed) catalytically active materials through chemical engineering. *Tonk. Khim. Tekhnol. = Fine Chem. Technol.* 2021;16(2):105–112 (Russ., Eng.). https://doi.org/10.32362/2410-6593-2021-16-2-105-112

НАУЧНАЯ СТАТЬЯ

Химико-технологический подход к созданию нановорсистых (ультрадисперсных) каталитически активных материалов

А.П. Антропов, Н.К. Зайцев, Е.Д. Рябков, Н.А. Яштулов@, П.Н. Мудракова

МИРЭА – Российский технологический университет (Институт тонких химических технологий им. М.В. Ломоносова), Москва, 119571 Россия
@Автор для переписки, e-mail: yashtulovna@mail.ru

Аннотация

Цели. *Каталитически активные материалы остаются востребованными в различных химико-технологических процессах, поэтому актуальными являются исследования, направленные на поиск новых эффективных материалов и оригинальных путей их получения. Настоящая работа посвящена созданию ленточных каталитических, в том числе электродных материалов, эффективность которых увеличена за счет нанорифления поверхности.*

Методы. *Методом высоковольтной анодной обработки на поверхности алюминиевой фольги формировалось нанорифление. Эффективный каталитически активный материал получали как никелевую реплику с металлической алюминиевой ленты. Для определения состояния поверхности алюминия использовали сканирующий электронный микроскоп Hitachi-SU8200 (Япония), для элементного анализа состава поверхности – обратную рентгеновскую фотоэлектронную микроскопию.*

Результаты. *Полученный нановорсистый никелевый материал превосходит по каталитической активности гладкий никель при окислении метанола в 70–150 раз.*

Выводы. *Продемонстрирована возможность использования в качестве темплатной матрицы для создания эффективных нановорсистых никелевых ленточных катализаторов, в том числе электродов, не алюминий-оксидной (как предлагалось ранее), а металлической части алюминиевой фольги, подвергнутой высоковольтному анодированию.*

Ключевые слова: *высоковольтное анодирование алюминия, нанорифление поверхности, ленточные катализаторы, нановоросистые электроды, ультрадисперсные электроды*

Для цитирования: Антропов А.П., Зайцев Н.К., Рябков Е.Д., Яштулов Н.А., Мудракова П.Н. Химико-технологический подход к созданию нановорсистых (ультрадисперсных) каталитически активных материалов. *Тонкие химические технологии*. 2021;16(2):105–112. https://doi.org/10.32362/2410-6593-2021-16-2-105-112

INTRODUCTION

Modern chemical technology enables the production of not only substances of a specific composition and structure, but also materials with a given dispersion and surface conditions that can serve as effective catalysts, afterburning catalysts for automobile exhaust, high-performance electrode materials for electrolyzers, and as chemical current sources. Chemical–technological approaches show great promise for creating materials with specific surface profiles because mechanical or thermophysical methods are not applicable in this case. Such materials include metal strips and plates with guaranteed roughness in the form of micro-and nanoscale needles or columns, so-called nanofilaments, or ultrafine materials, which are characterized by high catalytic activity. These materials can be used in numerous applications in small-tonnage production [1–13] but are typically not employed in large-tonnage production. The reason for this is because nanofilament materials are obtained in the form of samples with an area of several square centimeters only, making samples of a sufficiently large area unavailable.

Increasing demands regarding environmental, information, and technological security aspects have necessitated the search for new catalysts and

alternative energy sources, based on using renewable resources and enabling the more efficient use of non-renewable resources, as well as finding autonomous power sources for various technical devices and aircraft. The task of increasing the efficiency of fuel cells and water electrolysis systems is relevant for two primary reasons. First, the systems of electrolyzer fuel cells represent the most real energy buffers required for the operation of alternative energy sources, common among which is variable power. Effective operation of such energy sources is impossible without energy buffers; that is, systems that allow for shading (smoothing) or compensating for fluctuations in the power of the original energy sources.

The first stage in the manufacturing of nanofilament materials is the single/double relatively high-voltage anodic treatment of aluminum or titanium surfaces with suitable electrolytes, among which the most commonly used are oxalic, sulfuric, and phosphoric acids. In this case, an oxide layer is formed on the surface of aluminum, comprising hexagonal cells arranged in a honeycomb formation and permeated with nanopores throughout. Paszanski and Schneider [14] suggested the emergence of a dissipative microcirculation system similar to Rayleigh–Benard cells, where on the surface of aluminum the electric potential gradient acted instead of the temperature gradient, and the diffusion process instead of Archimedean force. In the case of aluminum anodizing, the oxide layer comprises aluminum hydroxide nanoparticles in various degrees of hydration that have pores with a very large aspect ratio; this pore diameter can be up to 1 nm, and its length can be up to several microns. Concurrently, the surface of metallic aluminum is also grooved, which reflects uneven propagation of the oxidation front deep into the aluminum plate [15]. The fluting of aluminum is much smaller in aspect ratio compared with that in the oxide layer; however, unlike the aluminum-oxide membrane, which does not have mechanical strength, metal tape can be used in a tape-drawing mechanism, as well as storage and transportation in a rolled state, and is much more technologically advanced for creating large-area nanofilament matrices. In all of the publications we found [1–13], the use of an aluminum-oxide layer as the initial (template) matrix was described; the typical samples that the authors of these works worked with were several square centimeters in size. The question on the possibility of the practical use as a starting matrix for the creation of functional electrodes the metal part of anodized aluminum instead of aluminum-oxide remains unexplored.

This work investigated the possibility of obtaining nanofilament nickel replicas with a higher catalytic activity compared with smooth nickel, using a replica method not based on an aluminum-oxide layer but using metallic aluminum. Finding a solution to this problem can help to determine the feasibility of developing chemical and technological installations for creating initial (template) matrices based on aluminum tape.

EXPERIMENTAL

The formation of aluminum matrices was performed on aluminum foil samples with a purity of 98.5%; 0.3 M orthophosphoric acid (analytical reagent (AR) grade) was used as a background electrolyte. Oxygen was removed from the solution by purging spectrally pure argon (American Chemical Society (ACS) grade) and during anodization, gas purging continued. The auxiliary electrode was a platinum wire with a diameter of 0.5 mm and a length of 10 cm. A potentiostat with an operating voltage range from 0 to 300 V was used as a voltage source; a maximum current of up to 10 A was allowed and the accuracy of maintaining the voltage at 0.5 V was ensured. A sample of aluminum foil with an uninsulated area of 2 cm^2 was placed in a cell (a 500 mL laboratory beaker) equipped with a RITM-01 magnetic stirrer (*Econix-Expert*, Moscow, Russia). The aluminum-oxide layer for obtaining a purified aluminum surface was removed by placing in a 0.1 M sodium carbonate solution (AR) for 30 min at 100°C.

The sample processed during the selected time and at the selected voltage was washed with bi-distilled water and dried in air for 24 h. An enlarged image of the surface of aluminum was obtained using an optical microscope, photographed, and examined on a Hitachi-SU8200 scanning electronic microscope (SEM; *Hitachi*, Japan) in a low-voltage low-temperature mode (at accelerating voltages of 15 kV and 77 K). Scanning electron microscopy was the main method for determining the number and size of holes (depressions) on the surface of the aluminum. In addition, reverse X-ray photoelectron microscopy was used for elemental analysis of the surface composition. The primary image processing of electronic micrographs was performed using the Digimizer (v.5.4.7) software program.

As catalytically active surface modifiers, palladium nanoclusters were synthesized from palladium dichloride (AR) through water microemulsions in octane (AR) stabilized with a non-ionic surfactant (Triton X-100), followed by the reduction of palladium ions with sodium tetrahydroborate (AR), similar to the process effected in our previous works [16–18]. For the preparation of nickel replicas, nickel plating solutions containing 150 g/L of nickel nitrate (AR), 80 g/L ammonium sulfate (AR), and 50 g/L of the disodium salt of ethylenediaminetetraacetic acid

(AR) was used. Nickel plating was carried out in the same electrochemical cell as anodization but a cathode voltage of −5 V was applied to the sample. Copper replicas were similarly prepared. The composition of the copper plating electrolyte was as follows: 80 g/L copper sulfate pentahydrate (AR), 80 g/L sodium thiosulfate (AR), and 80 g/L sodium acetate (AR). The time taken for the electrochemical reduction of metals to the surface of the nanoperforated membrane for each of the samples was 120 min.

After applying the replicas to the surface of the nanoperforated matrix, the aluminum template material was removed by keeping the resulting "sandwich" for 24 h in a 4 M solution of sodium hydroxide (AR), which was then repeatedly washed with bi-distilled water, and dried in air for 24 h at 21°C. Following on, the replicas were investigated by optical and electron microscopy as described above.

To study the electrochemical activity of the obtained replicas, we used the cyclic voltammetry method on the Ecotest-VA (*Econix-Expert*) voltammetric analyzer. In the case of nickel replicas, aqueous methanol solutions were used as the main substrate. For copper replicas, aqueous glucose solutions were used. The specific composition of the background electrolytes is indicated on the signatures ofthe voltammograms.

RESULTS AND DISCUSSION

The formation of the anode layer at the initial stage of anodization (15 min after the start of the process) is shown in Fig. 1. As can be seen from the figure, light contours—the boundaries of the initial metal crystallites—appeared on the sample surface. The black dots of micropore nuclei were evenly distributed over the sample surface, which is consistent with Thompson's observations [9].

With further anodization, dimples formed on the metal surface. The dependence of the average pore size on the surface of the aluminum foil on the applied voltage and the anodizing time is shown in Fig. 2.

As shown, the average size of the pores that represent the imprint of the propagation front of the Keller layer depends not only on the magnitude of the applied voltage but also on the exposition time. This suggested that the dynamic evolution of the anodized layer occurred not only at the boundary of the Keller and Thompson layers (as Thompson suggested [19]) but also at the Keller metal-layer boundary. During further anodization, depressions formed on the metal surface [20, 21].

The dependence of the current density on time at a fixed voltage (70 V) during the sample's anodization process is shown in Fig. 3.

Figures 4 and 5 show SEM images of aluminum foil samples subjected to anodization at 70 V in 0.3 M phosphoric acid after removing the aluminum-oxide

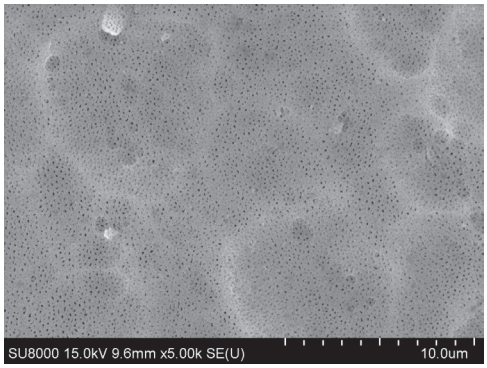

Fig. 1. Scanning electronic microscope (SEM) micrograph of an aluminum sample after anodization (U = 90 V, t = 15 min, T_{el} = 21°C, 0.3 M H_3PO_4).

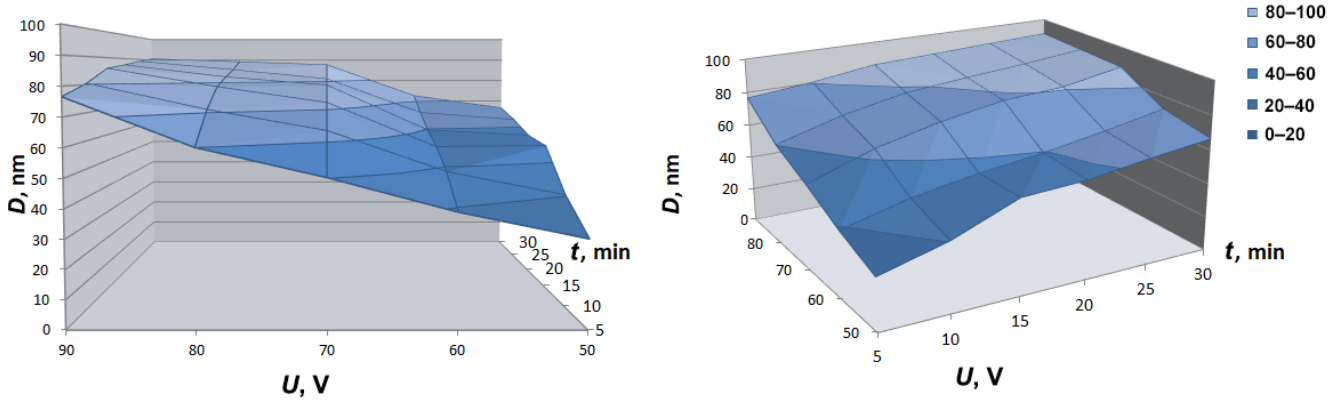

Fig. 2. A three-dimensional diagram of the dependence of the average diameter of holes formed on the aluminum surface during anodization on the voltage and time of anodizing (T_{el} = 21°C, 0.3 M H_3PO_4).

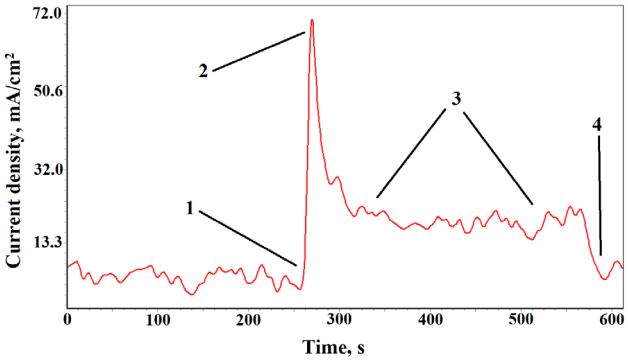

Fig. 3. Change in the current density during anodization in the mode of 70 V, 5 min, T_{el} = 21°C in 0.3 M H_3PO_4:
(1) the start of the anodization process (voltage supply);
(2) the formation of an aluminum-oxide layer;
(3) electrical breakdowns with the formation of nanoscale holes;
(4) the end of the anodization process (voltage shutdown).

layer, as well as replicas taken from it, respectively. The photo clearly shows the presence of nanoscale corrugation on the surface.

The chronoamperogram shown in Fig. 6 confirms the increase in the efficiency of the electrode material due to its nanostructuring. The applied voltage in all cases is 0.8 V (relative to the silver chloride electrode), the electrolyte is 0.1 M NaOH, and the electrode area is 1 cm^2.

As shown in Fig. 6, the resulting nickel replicas provided a current return during oxidation of the model fuel (methanol) for fuel cells at 70–150 times greater amounts compared with smooth nickel. This result can be directly used to create improved and permanent sensors for methanol. To date, the reason for such a large increase in the efficiency of the electrodes in nanofilament remains unclear; whether it is a result of

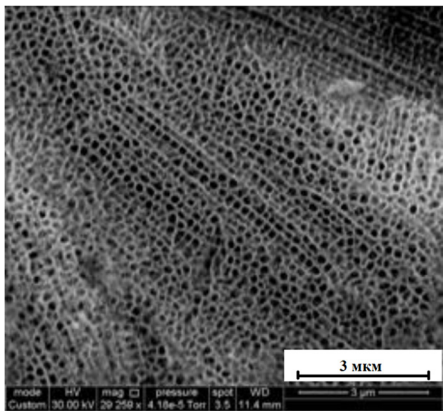

Fig. 4. An SEM image of an aluminum foil sample subjected to anodization at 70 V in 0.3 M phosphoric acid after removing the aluminum-oxide layer.

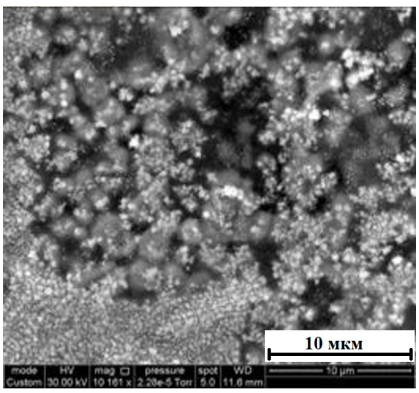

Fig. 5. An SEM image of a nickel replica sample from an aluminum foil subjected to anodization at 70 V in 0.3 M phosphoric acid after removing the aluminum-oxide layer.

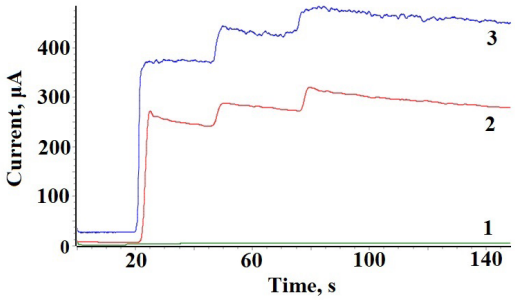

Fig. 6. Chronoamperograms when three 200-μL portions of methanol were sequentially added into an electrochemical cell with a volume of 100 mL:
(1) compact nickel electrode; (2) nickel nanostructured material; (3) nickel nanostructured material with palladium nanoparticles.

an increase in the surface of the electrode or because geometric factors and a surface structure are also important. It is expected that in the future, the proposed approach will improve the performance of fuel cells and hydrogen-source electrolyzers.

CONCLUSIONS

The high-voltage anodic treatment of aluminum foil was used to form a nanoperforated aluminum-oxide layer on a metal surface, and a nickel replica was formed on the surface of the treated aluminum. When testing the catalytic activity of the obtained replicas, using the electrochemical method on the example involving methanol oxidation, current densities were obtained at 70–150 times higher levels than on smooth nickel. Thus, it was found that the metal part of the anodized aluminum/aluminum-oxide-layer sandwich, despite having a much lower aspect ratio than the oxide part, was suitable as a template matrix for the creation of catalytically active materials and ultrafine electrodes made of nickel and other metals.

The results obtained herein can be used as a basis in chemical–technological installation aimed at creating initial (template) matrices for catalytically active materials.

Acknowledgments

The study was supported by the state assignment of the Russian Federation No. 0706-2020-0020.

Authors' contribution

A.P. Antropov – formulation of the scientific concept, aims, and objectives of the study, processing and interpretation of experimental results;

N.K. Zaitsev – general management;

Y.D. Ryabkov – planning and conducting experiments;

N.A. Yashtulov – writing the manuscript, work group management;

P.N. Mudrakova – conducting experiments.

The authors declare no conflicts of interest.

REFERENCES

1. Roslyakov I.V., Kolesnik I.V., Levina E.E., Katorova N.S., Pestrikov P.P., Kardash T.Yu., Solovyov L.A., Napolskii K.S. Annealing induced structural and phase transitions in anodic aluminum oxide prepared in oxalic acid electrolyte. *Surf. Coat. Technol.* 2020;381:125159. https://doi.org/10.1016/j.surfcoat.2019.125159

2. Goncharova A.S., Napolskii K.S., Skryabina O.V., Stolyarov V.S., Levin E.E., Egorov S.V., Eliseev A.A., Kasumov Y.A., Ryazanov V.V., Tsirlina G.A. Bismuth nanowires: electrochemical fabrication, structural features, and transport properties. *Phys. Chem. Chem. Phys.* 2020;22(26):14953–14964. https://doi.org/10.1039/D0CP01111H

3. Aslam S., Das A., Khanna M., Kuanr B. Concentration gradient Co-Fe nanowire arrays: Microstructure to magnetic characterizations. *J. Alloys Compd.* 2020;838:155566. https://doi.org/10.1016/j.jallcom.2020.155566

4. Li J., Wei H., Zhao K., Wang M., Chen D., Chen M. Effect of anodizing temperature and organic acid addition on the structure and corrosion resistance of anodic aluminum oxide films. *Thin Solid Films.* 2020;713:138359. https://doi.org/10.1016/j.tsf.2020.138359

5. Chumnanwat S., Watanabe Y., Taniguchi N., Higashi H., Kodama A., Seto T., Otani Y., Kumita M. Pore structure control of anodized alumina film and sorption properties of water vapor on $CaCl_2$-aluminum composites. *Energy.* 2020;208:118370. https://doi.org/10.1016/j.energy.2020.118370

6. Noormohammadi M., Arani Z.S., Ramazani A., Kashi M.A., Abbasimofrad S. Super-fast fabrication of self-ordered nanoporous anodic alumina membranes by ultra-hard anodization. *Electrochim. Acta.* 2020;354:136766. https://doi.org/10.1016/j.electacta.2020.136766

7. Kawai S., Ueda R. Magnetic Properties of Anodic Oxide Coatings on Aluminum Containing Electrodeposited Co and Co-Ni. *J. Electrochem. Soc.* 1975;122(1):32–36. https://doi.org/10.1149/1.2134152

8. Shiraki M., Wakui Y., Tokushima T., Tsuya N. Perpendicular magnetic media by anodic oxidation method and their recording characteristics. *IEEE Trans. Magn.* 1985;21(5):1465–1467. https://doi.org/10.1109/TMAG.1985.1064078

9. Saito M., Kirihara M., Taniguchi T., Miyagi M. Micropolarizer made of the anodized alumina film. *Appl. Phys. Lett.* 1989;55(7):607–609. https://doi.org/10.1063/1.101572

10. Miller C.J., Majda M. Microporous aluminum oxide films at electrodes. *J. Am. Chem. Soc.* 1985;107(5):1419–1420. https://doi.org/10.1021/ja00291a056

11. Tierney M.J., Martin C.R. New Electrorelease Systems Based on Microporous Membranes. *J. Electrochem. Soc.* 1990;137(12):3789–3792. https://doi.org/10.1149/1.2086302

12. Yoshino T., Baba N. Electrochromism of Oxalatotungstate(V) Complexes Chemically Deposited onto Micropores of Anodic Oxide Films on Aluminum. *Nippon Kagaku Kaishi.* 1983;1983(6):955–957. https://doi.org/10.1246/nikkashi.1983.955

13. Mizuki I., Yamamoto Y., Yoshino T., Baba N. Electrochemical Incorporation of Electroluminescent Mn Activator into Porous Anodic Al_2O_3 Films on Al. *J. Met. Surf. Finish. Soc. Japan.* 1987;38(12):561–563. https://doi.org/10.4139/sfj1950.38.561

14. Pashchanka M., Schneider J.J. Origin of self-organisation in porous anodic alumina films derived from analogy with Rayleigh–Bénard convection cells. *J. Mater. Chem.* 2011;21(46):18761–18767. https://doi.org/10.1039/C1JM13898G

15. Keller F., Hunter M.S., Robinson D.L. Structural Features of Oxide Coatings on Aluminum. *J. Electrochem. Soc.* 1953;100(9):411. https://doi.org/10.1149/1.2781142

16. Yashtulov N.A., Lebedeva M.V., Patrikeev L.N., Zaitcev N.K. New polymer-graphene nanocomposite electrodes with platinum-palladium nanoparticles for chemical power sources. *Express Polym. Lett.* 2019;13(8):739–748. https://doi.org/10.3144/expresspolymlett.2019.62

17. Yashtulov N.A., Lebedeva M.V., Ragutkin A.V., Zaitsev N.K. Electrode Materials Based on Porous Silicon with Platinum Nanoparticles for Chemical Current Sources. *Russ. J. Appl. Chem.* 2018;91(2):280–285. https://doi.org/10.1134/S1070427218020167

[Original Russian Text: Yashtulov N.A., Lebedeva M.V., Ragutkin A.V., Zaitsev N.K. Electrode Materials Based on Porous Silicon with Platinum Nanoparticles for Chemical Current Sources. *Zh. Prikl. Khim.* 2018;91(2):232−237 (in Russ.).]

18. Yashtulov N.A., Patrikeev L.N., Zenchenko V.O., Lebedeva M.V., Zaitsev N.K., Flid V.R. Palladium–platinum–porous silicon nanocatalysts for fuel cells with direct formic acid oxidation. *Nanotechnol. Russia.* 2016;11(9–10):562–568. https://doi.org/10.1134/S1995078016050207

[Original Russian Text: Yashtulov N.A., Patrikeev L.N., Zenchenko V.O., Lebedeva M.V., Zaitsev N.K., Flid V.R. Palladium–platinum–porous silicon nanocatalysts for fuel cells with direct formic acid oxidation. *Rossiiskie Nanotekhnologii.* 2016;11(9–10):45–50 in Russ.).]

19. Thompson G.E., Furneaux R.C., Wood G.C., Richardson J.A., Gode J.S. Nucleation and Growth of Porous Anodic Films on Aluminum. *Nature.* 1978;272(5652):433–435. https://doi.org/10.1038/272433a0

20. Wu J., Li Z, Li Z., Li S., Shen I., Hu X., Ling Z. Ultra-slow growth rate: Accurate control of the thickness of porous anodic aluminum oxide films. *Electrochem. Commun.* 2019;109:106602. https://doi.org/10.1016/j.elecom.2019.106602

21. Mishra P., Heberet K.R. Self-organization of anodic aluminum oxide layers by a flow mechanism. *Electrochim. Acta.* 2020;340:135879. https://doi.org/10.1016/j.electacta.2020.135879

About the authors:

Alexey P. Antropov, Cand. Sci. (Eng.), Associate Professor, Department of Energy Technologies, Systems and Installations, M.V. Lomonosov Institute of Fine Chemical Technologies, MIREA – Russian Technological University (86, Vernadskogo pr., Moscow, 119571, Russia). E-mail: alexeyantrop@yandex.ru. Scopus Author ID 36772761300, https://orcid.org/0000-0002-4702-753X

Yegor D. Ryabkov, Postgraduate Student, Department of Energy Technologies, Systems and Installations, M.V. Lomonosov Institute of Fine Chemical Technologies, MIREA – Russian Technological University (86, Vernadskogo pr., Moscow, 119571, Russia). E-mail: yegordryabkov@gmail.com. https://orcid.org/0000-0003-1201-7347

Nikolay K. Zaitsev, Dr. Sci. (Chem.), Assistant Professor, Head of the Department of Energy Technologies, Systems and Installations, M.V. Lomonosov Institute of Fine Chemical Technologies, MIREA – Russian Technological University (86, Vernadskogo pr., Moscow, 119571, Russia). E-mail: nk_zaytsev@mail.ru. Scopus Author ID 57193485921, https://orcid.org/0000-0003-4132-0097

Nikolay A. Yashtulov, Dr. Sci. (Chem.), Professor, Department of Energy Technologies, Systems and Installations, M.V. Lomonosov Institute of Fine Chemical Technologies, MIREA – Russian Technological University (86, Vernadskogo pr., Moscow, 119571, Russia). E-mail: yashtulovna@mail.ru. Scopus Author ID 6507694451, https://orcid.org/0000-0002-7709-4186

Polina N. Mudrakova, Master Student, Department of Energy Technologies, Systems and Installations, M.V. Lomonosov Institute of Fine Chemical Technologies, MIREA – Russian Technological University (86, Vernadskogo pr., Moscow, 119571, Russia). E-mail: polinapolin97@gmail.com. https://orcid.org/0000-0002-6139-8126

Об авторах:

Антропов Алексей Петрович, к.т.н., доцент кафедры энергетических технологий, систем и установок Института тонких химических технологий им. М.В. Ломоносова ФГБОУ ВО «МИРЭА – Российский технологический университет» (119571, Россия, Москва, пр-т Вернадского, д. 86). E-mail: alexeyantrop@yandex.ru. Scopus Author ID 36772761300, https://orcid.org/0000-0002-4702-753X

Рябков Егор Данилович, аспирант кафедры энергетических технологий, систем и установок Института тонких химических технологий им. М.В. Ломоносова ФГБОУ ВО «МИРЭА – Российский технологический университет» (119571, Россия, Москва, пр-т Вернадского, д. 86). E-mail: yegordryabkov@gmail.com. https://orcid.org/0000-0003-1201-7347

Зайцев Николай Конкордиевич, д.х.н., доцент, заведующий кафедрой энергетических технологий, систем и установок Института тонких химических технологий им. М.В. Ломоносова ФГБОУ ВО «МИРЭА – Российский технологический университет» (119571, Россия, Москва, пр-т Вернадского, д. 86). E-mail: nk_zaytsev@mail.ru. Scopus Author ID 57193485921, https://orcid.org/0000-0003-4132-0097

Яштулов Николай Андреевич, д.х.н., профессор кафедры энергетических технологий, систем и установок Института тонких химических технологий им. М.В. Ломоносова ФГБОУ ВО «МИРЭА – Российский технологический университет» (119571, Россия, Москва, пр-т Вернадского, д. 86). E-mail: yashtulovna@mail.ru. Scopus Author ID 6507694451, https://orcid.org/0000-0002-7709-4186

Мудракова Полина Николаевна, магистрант кафедры энергетических технологий, систем и установок Института тонких химических технологий им. М.В. Ломоносова ФГБОУ ВО «МИРЭА – Российский технологический университет» (119571, Россия, Москва, пр-т Вернадского, д. 86). E-mail: polinapolin97@gmail.com. https://orcid.org/0000-0002-6139-8126

The article was submitted: March 05, 2021; approved after reviewing: March 19, 2021; accepted for publication: April 08, 2021.

Translated from Russian into English by N. Isaeva
Edited for English language and spelling by Enago, an editing brand of Crimson Interactive Inc.

THEORETICAL BASES OF CHEMICAL TECHNOLOGY

ТЕОРЕТИЧЕСКИЕ ОСНОВЫ ХИМИЧЕСКОЙ ТЕХНОЛОГИИ

ISSN 2410-6593 (Print), ISSN 2686-7575 (Online)

https://doi.org/10.32362/2410-6593-2021-16-2-113-124

UDC 548.737

RESEARCH ARTICLE

Structural characterization of hydrogen bonding for antipyrine derivatives: Single-crystal X-ray diffraction and theoretical studies

Nataliya S. Rukk[1,@], Ravshan S. Shamsiev[1], Dmitry V. Albov[2], Svetlana N. Mudretsova[2]

[1]MIREA – Russian Technological University (M.V. Lomonosov Institute of Fine Chemical Technologies), Moscow, 119571 Russia

[2]Faculty of Chemistry, Lomonosov Moscow State University, Leninskie Gory, Moscow, 119992 Russia

[@]Corresponding author, e-mail: roukkn@inbox.ru

Abstract

Objectives. *The paper is devoted to the crystal structure characterization of 5-methyl-2-phenyl-4H-pyrazol-3-one (compound **I**) and 2-(4-chlorophenyl)-5-methyl-4H-pyrazol-3-one (compound **II**).*

Methods. *Single-crystal X-ray diffraction studies and theoretical calculations: Density functional theory and quantum theory of atoms in molecules.*

Results. *In the solid state, the crystal structure of compound **I** is characterized by the alternation of OH and NH tautomers connected via O–H---O and N–H---N hydrogen bonds. For compound **II**, the existence of chains built from the NH monomers via hydrogen bonding can be explained by the peculiarities of cooperative effects. In the framework of quantum theory of atoms in molecules, the following topological characteristics are calculated for all dimers: electron density, Laplacian of electron density, density of kinetic, potential, and total energy in the critical point of the intermolecular hydrogen bond. It is concluded that the hydrogen bond in dimers **1**–**4**, **7** (compound **I**), and **8**–**11** (compound **II**) can be assigned to the intermediate (between covalent and dispersion types) interaction owing to hydrogen bond formation with the participation of electronegative oxygen- (and/or nitrogen-) atoms, whereas H-bond in dimers **5** and **6** (compound **I**) can be attributed to the dispersion one (no hydrogen bond formation or weak H-bond formation), and it represents the weak interaction, being in agreement with length for intermolecular hydrogen bond in dimers. The electron density and total energy density values demonstrate that the strongest intermolecular H-bonds take place in dimers **1** (OH---O), **4** (OH---O), **7** (OH---N), **8** (OH---O), **9** (NH---N), and **11** (OH---N). The results obtained for compounds **I** and **II** are compared with data for antipyrine (1,2-dihydro-1,5-dimethyl-2-phenyl-3H-pyrazol-3-one; compound **III**).*

Conclusions. *An important role of intermolecular hydrogen bonding in the crystal packing, molecule association and self-organization via dimer- or more extended species formation has been demonstrated.*

Keywords: *antipyrine and its derivatives, 5-methyl-2-phenyl-4H-pyrazol-3-one, 2-(4-chlorophenyl)-5-methyl-4H-pyrazol-3-one, tautomers, hydrogen bonding, density functional theory (DFT) and quantum theory of atoms in molecules (QTAIM) calculations, crystal structure*

For citation: Rukk N.S., Shamsiev R.S., Albov D.V., Mudretsova S.N. Structural characterization of hydrogen bonding for antipyrine derivatives: Single-crystal X-ray diffraction and theoretical studies. *Tonk. Khim. Tekhnol. = Fine Chem. Technol.* 2021;16(2):113–124. https://doi.org/10.32362/2410-6593-2021-16-2-113-124

НАУЧНАЯ СТАТЬЯ

Структурное описание водородной связи в производных антипирина: рентгеноструктурные и теоретические исследования

Н.С. Рукк[1,@], Р.С. Шамсиев[1], Д.В. Альбов[2], С.Н. Мудрецова[2]

[1]МИРЭА – Российский технологический университет (Институт тонких химических технологий им. М.В. Ломоносова), Москва, 119571 Россия
[2]Московский государственный университет им. М.В. Ломоносова, химический факультет, Москва, 119962 Россия
[@]Автор для переписки, e-mail: roukkn@inbox.ru

Аннотация

Цели. *Работа посвящена рассмотрению особенностей кристаллического строения для 5-метил-2-фенил-4H-пиразол-3-она,* ***I****, и 2-(4-хлорфенил)-5-метил-4H-пиразол-3-она,* ***II****, в сравнении с результатами теоретических расчетов.*
Методы. *Рентгеноструктурный анализ и расчеты в рамках теории функционала плотности и квантовой теории атомов в молекулах.*
Результаты. *Показано, что кристаллическая структура* ***I*** *в твердом агрегатном состоянии характеризуется альтернацией OH и NH таутомеров, связанных посредством водородных связей O–H---O и N–H---N. Для соединения* ***II*** *существование цепочек из связанных водородной связью мономеров NH объясняется особенностями кооперативных эффектов и с теоретической точки зрения. В рамках квантовой теории атомов в молекулах (QTAIM) для всех димеров в критической точке межмолекулярной водородной связи были рассчитаны топологические параметры: электронная плотность, лапласиан электронной плотности, плотность кинетической, потенциальной и полной энергии. Показано, что водородная связь в димерах* ***1–4****,* ***7*** *(соединение* ***I****) и* ***8–11*** *(соединение* ***II****) относится к взаимодействию промежуточного типа (между ковалентным и дисперсионным взаимодействием) за счет образования водородных связей с участием электроотрицательных атомов кислорода (и/или атомов азота), а водородная связь в димерах* ***5*** *и* ***6*** *(соединение* ***I****) – к дисперсионному типу (отсутствие водородной связи или образование слабой H-связи) и представляет собой слабое взаимодействие, что коррелирует с длиной межмолекулярной водородной связи в димерах. На основании анализа значений электронной плотности и плотности полной энергии показано, что наиболее сильные межмолекулярные H-связи реализуются в димерах* ***1*** *(OH---O),* ***4*** *(OH---O),* ***7*** *(OH---N),* ***8*** *(OH---O),* ***9*** *(NH---N) and* ***11*** *(OH---N). Результаты, полученные для* ***I*** *и* ***II****, сопоставлены с данными для 1,2-дигидро-1,5-диметил-2-фенил-3H-пиразол-3-она,* ***III****.*
Выводы. *Показана важная роль межмолекулярной водородной связи в кристаллической упаковке, ассоциации и самоорганизации молекул.*

Ключевые слова: *антипирин и его производные, 5-метил-2-фенил-4H-пиразол-3-он, 2-(4-хлорфенил)-5-метил-4H-пиразол-3-он, таутомеры, водородная связь, теория функционала плотности, квантовая теория атомов в молекулах, кристаллическая структура*

Для цитирования: Рукк Н.С., Шамсиев Р.С., Альбов Д.В., Мудрецова С.Н. Структурное описание водородной связи в производных антипирина: рентгеноструктурные и теоретические исследования. *Тонкие химические технологии.* 2021;16(2):113–124 (Eng.). https://doi.org/10.32362/2410-6593-2021-16-2-113-124

INTRODUCTION

Antipyrine (1,2-dihydro-1,5-dimethyl-2-phenyl-3*H*-pyrazol-3-one; compound **III**) and related compounds are known to possess a number of bioactive properties, such as analgesic and antipyretic ones. They form a large number of complexes with alkaline-, transition-, and rare-earth metals [1–8]. From this point of view, searching for new ligands (including representatives of antipyrine-based ones) is very important [4, 9]. Using the method of computer prognosis based on the Prediction of Activity Spectra for Substances (PASS) system [10], it has been demonstrated that some pyrazolone derivatives, such as 5-methyl-2-phenyl-4*H*-pyrazol-3-one (compound **I**) and 2-(4-chlorophenyl)-5-methyl-4*H*-pyrazol-3-one (compound **II**), possess a relatively high probability of antimetastatic activity. It should be underlined that the compound properties are determined mainly by the specific features of chemical bonding, including hydrogen bonding and intermolecular interactions, between structural units. These distinguishing features are responsible for the self-organization of ions and molecules in crystal packing with the formation of channels opened to the intercalation of small species, for example, complexes with neridronic acid (6-amino-1-hydroxyhexylidene-1,1-bisphosphonic acid) showing promise for treating osteogenesis and the Paget's disease [11]. In the case of solvation (e.g., styryl dyes of the benzoselenazole series), the system of hydrogen bonding makes the structure more rigid compared with the non-solvation one owing to the solvate molecules participation in the hydrogen bond formation [12]. This results in different photocycloaddition reactivity of the solvated and non-solvated compounds and thus a decreased reaction rate for the solvated species. The same has been demonstrated [13] for water molecules and imidazolium salts with respect to the interaction and formation of guest(H_2O)@host (ionic liquid [IL]) complexes through strong H-bonds involving the hydrogen atoms of water molecules and nitrogen atoms of IL anions to produce a quest@host supramolecular structure. Many biologically active molecules contain multiple hydrogen-bonding sites; e.g., barbiturates, a class of compounds widely used for their physiological action as sedatives and anticonvulsants, contain both donor and acceptor atoms for multiple hydrogen-bonding formation. It should be underlined that crystal engineering and design allow obtaining different solid state structures in cocrystals of barbiturate and melamine molecules (linear tape, crinkled tape, or cyclic hexamer) [14]. The hydrogen-bonding importance and its impact on drug efficacy have been demonstrated [15]. In this connection the aim of this paper is to explain structural particularities and their comparison with results of theoretical studies for compounds **I**, **II**, and **III**.

EXPERIMENTAL

Compounds **I**, **II** (*Sigma-Aldrich*, St. Louis, Missouri, USA), and **III** (All-Russian Product Classifier 931335, chem. pure) were first recrystallized from ethanol. Single crystals were grown from saturated aqueous solutions by isothermal evaporation of the solvent at ambient temperature (ca. 20°C). Thermogravimetric and differential scanning calorimetric (STA-409 Differential Scanning Calorimeter, *Netzsch*, Germany) measurements were carried out over the temperature range 293–573 K with a heating rate of 10 K/min under a helium atmosphere. Aluminum oxide was used as a reference material.

Computational methods

The tautomers of compounds **I** and **II** (Scheme 1) were examined by density functional theory using the Priroda package [16]. Calculations were made using the Perdew–Burke–Ernzerhof (PBE) exchange-correlation functional [17] and TZ2P Gaussian-type basis sets. The solvation effects were estimated in Gaussian 09 [18] using the polarizable continuum model and solvation model based on density (PCM–SMD; water used as solvent, ε = 78.3553). Vibrational harmonic frequency analysis was conducted for the optimized geometries to ensure that a true local minimum was present with no imaginary frequencies. The starting atomic coordinates of compounds were taken from the X-ray refinement results. Convergence criteria for self-consistent field

cycles and geometry optimization were 1×10^{-6} and 1×10^{-5} a.u., respectively. The quantum-topological characteristics of electron density in the critical points of the intermolecular hydrogen bond were calculated in the framework of the quantum theory of atoms in molecules (QTAIM) using the Multiwfn 3.6 program [19].

Single-crystal X-ray crystallography

Crystallographic data were collected and refined on CAD-4 EXPRESS diffractometer[1]. Data reduction was carried out using XCAD4[2]. The following programs were used for theoretical modeling: SHELXS97 for structure solving [20], SHELXL97 for structure refining [20], and Mercury for molecular graphics [21]. The results are given in Table A1 (see Appendix A, pages 125–126).

CCDC 1891632-1891634 contain the supplementary crystallographic data for this paper. These data can be obtained free of charge from The Cambridge Crystallographic Data Centre via http://www.ccdc.cam.ac.uk.

RESULTS AND DISCUSSION

There are three possible tautomers for compounds **I** and **II** (CH: **Ia**, **IIa**; NH: **Ib**, **IIb**; OH: **Ic**, **IIc**; Scheme 1, Table 1) [22]. Here we compare theoretical and single-crystal X-ray diffraction data to examine the crystal packing particularities of compounds **I–III**. The following order of stability for compound-**I** tautomers in the gas phase was derived from Table 1: **Ia** (CH) > **Ib** (NH) > **Ic** (OH) [22]. The same order of relative stability was theoretically obtained, the results of which are shown in Table 2. Calculation results of Gibbs free energy (ΔG_{298}) values considering solvation effects demonstrate a slightly lower energy gap between **Ia** and **Ib** and a slightly higher energy gap between **Ib** and **Ic** (0.0, 24.4, and 31.2 vs. 0.0, 9.1, and 28.4 kJ·mol^{-1}, respectively, Table 2). The same tendency can be observed for compound **II** (Table 2).

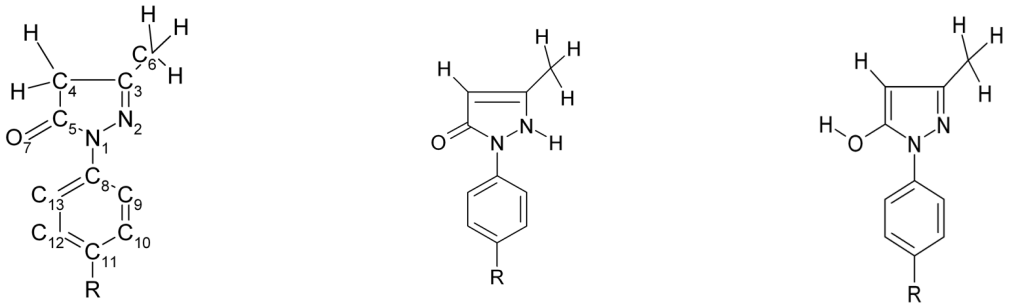

CH **Ia, IIa** | **NH** **Ib, IIb** | **OH** **Ic, IIc**

Scheme 1. Different possible tautomers for compounds **I** and **II**: R = H for the former and R = Cl for the latter.

Table 1. Calculated torsion angles (ω, °), heat of formation (ΔH_f), relative energies (ΔE), and dipole moments (μ) of the tautomers for compound **I** [22]

Method	Tautomer	ω, ° [C(O)–N_1–C_8–C_9]	ω,° [H–N_2–N_1–C_8]	ΔH_f (kJ·mol^{-1}) or ΔE (kJ·mol^{-1})	μ, Debye
AM1	**Ia (CH)**	155.6	–	0.0	2.68
	Ib (NH)	−130.9	88.9	51.51	3.99
	Ic (OH)	−142.6	–	52.80	2.06
PM3	**Ia (CH)**	124.3	–	0.0	2.46
	Ib (NH)	−98.3	86.7	18.58	3.73
	Ic (OH)	−130.7	–	34.14	2.53
HF/6-31G*	**Ia (CH)**	166.9	–	0.0	3.64
	Ib (NH)	−134.9	73.0	36.02	5.25
	Ic (OH)	−132.0	–	52.01	2.31
B3LYP/6-31G*	**Ia (CH)**	177.7	–	0.0	3.31
	Ib (NH)	−149.5	63.0	32.76	5.03
	Ic (OH)	−140.6	–	43.97	2.09

[1] Enraf_Nonius CAD_4 Software. Version 5.0. Delft (The Netherlands): Enraf_Nonius, 1989.
[2] Harms K., Wokadlo S. XCAD4. University of Hamburg, Germany.

Table 2. Calculated torsion angles (ω, °), relative energies (ΔE), Gibbs free energy (ΔG_{298}), Gibbs free energy with PCM–SMD corrections ($\Delta G_{298,solv}$), and dipole moments (μ) for the tautomers of compounds **I**, **II**, and **III**

PBE/3z	ω, °	ω, °	ΔE	ΔG_{298}	$\Delta G_{298,solv}$	μ
	$C(O)–N_1–C_8–C_9$	$H–N_2–N_1–C_8$	kJ·mol^{-1}			Debye
Ia	179.7	–	0.0	0.0	0.0	3.39
Ib	−149.5	61.8	19.3	24.4	9.1	5.15
Ic	−154.6	–	26.2	31.2	28.4	2.68
IIa	179.8	–	0.0	0.0	0.0	5.11
IIb	−148.5	63.7	20.2	25.2	8.5	6.02
IIc	−156.5	–	26.5	31.4	28.4	4.19
III	−127.7	–	–	–	–	5.36

We calculated the parameters of dimer formation from the monomers of compounds **I** and **II**, and compared the experimental and theoretical results (Table 3). The crystal structure of compound **I** is characterized by the alternation of **Ib** and **Ic** tautomers (Fig. 1a and b) connected via the O–H---O=C and N–H---N hydrogen bonds ($r_{O-H---O}$ = 2.479 Å, $r_{N–H---N}$ = 2.800 Å, Table 3, entries **1** and **2**). Extended infinite chains can be observed (Fig. 1b), as confirmed by the calculation results (Table 3, entries **1**–**7**). For the stronger O–H---O H-bonding between the **Ib** and **Ic** tautomers (r_{O---HO} = 2.62 Å, $r_{N–H---N}$ = 2.98 Å, Table 3, entries **1** and **2**) the **Ib** and **Ic** self-organization in the solid state possibly begins with the formation of the stronger O–H---O H-bonding, followed by the formation of N–H---N one. This can explain the absence of the **Ib**–**Ib** (N–H---O), **Ia**–**Ic** (O---H–O), **Ic**–**Ic** (N---H–O), and **Ia**–**Ia**, **Ia**–**Ib** (N---H–N) dimers in the solid state (Table 3, entries **3**, **4**, **7** and **5**, **6**), as confirmed by the ΔG_{298} values for the tautomer dimerization (Table 3, entries **1**–**7**, column 6).

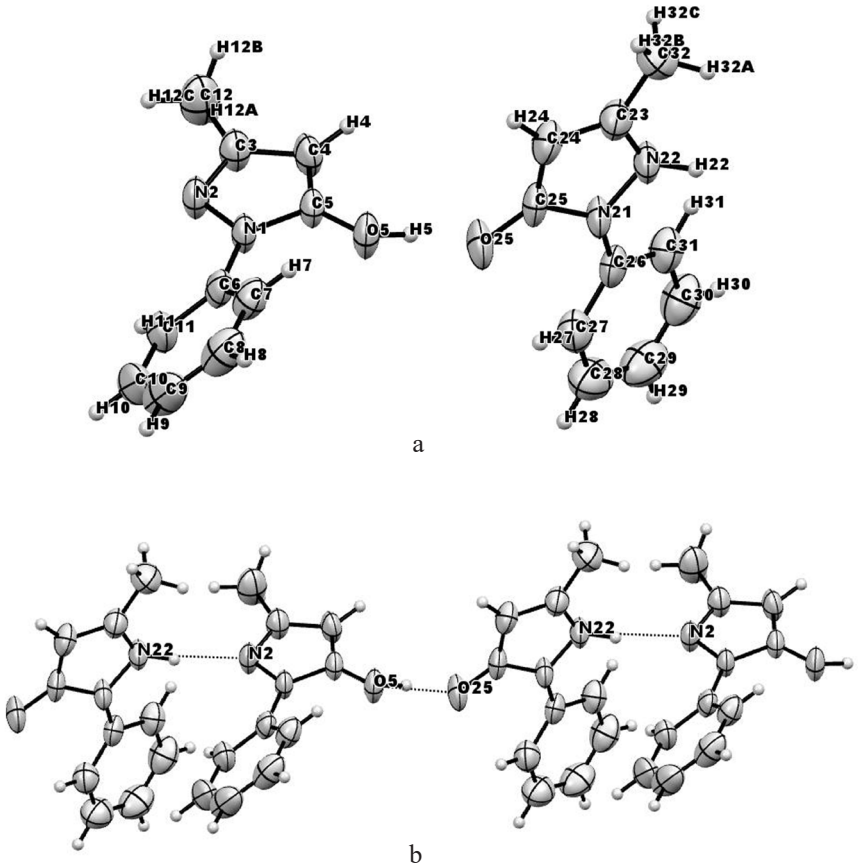

Fig. 1. Asymmetric unit of compound **I** with the crystallographic numbering scheme. Displacement ellipsoids are drawn at the 50% probability level, (a); H-bonding between **OH**- and **NH**-tautomers (b).

Compound **II** exists as the NH tautomer (Fig. 2), the molecules of which are linked by N–H---O-type H-bonds ($r_{N-H---O}$ = 2.729 Å; Fig. 2a and Table 3, entry **10**). This results in the formation of non-interacting extended chains with mutual anti-orientation (Fig. 2b). In the crystalline state, compound **II** consists of **IIb** tautomers, not **IIa** tautomers. The calculated ΔG_{298} values for **IIb** and **IIc** dimerization (**IIa** unable to form dimers with strong hydrogen bonding) demonstrate that the **IIb**–**IIc** (O-H---O) dimer is the most stable (ΔG_{298} = −13.3 kJ·mol^{-1}), followed by the **IIb**–**IIb** (N-H---O) dimer (ΔG_{298} = −3.7 kJ·mol^{-1}; Table 3, entries **8** and **10**). It is easy to imagine that the elongation of the chain built from the **IIb** monomers due to H-bonding (Fig. 2) results in energy gain growth with the number of monomers due to the predominance of the enthalpy contribution (ΔH_{298} = −39.2 kJ·mol^{-1}) over the entropy one ($-T\Delta S_{298}$ = 35.5 kJ·mol^{-1}; Table 3, entry **10**). The formation of chains built from the **Ib** tautomers is possible, but, in this case, the enthalpy contribution is approximately equal to the entropy contribution (Table 3, entry **3**), which can explain the differing mode of monomer alteration for compound **I** (**Ib**–**Ic** [O---H-O] dimer existence).

For all dimers **1**–**11**, the following topology characteristics were calculated using QTAIM theory: electron density (ρ), Laplacian of electron density ($\nabla^2\rho$), density of kinetic (*G*), potential (*V*), and total energy (*H*) in the critical point of the intermolecular hydrogen bond (Table 4). On the basis of the $\nabla^2\rho$ and *H* signs as well as the *V*/*G* (1 < |*V*|/*G* < 2) ratio, it can be concluded that hydrogen bond in dimers **1**–**4** and **7**–**11** can be assigned to the intermediate (between covalent and dispersion types) interaction, whereas the H-bond in dimers **5** and **6** can be assigned to the dispersion interaction, i.e., the weak interaction. Analysis of ρ and *H* values demonstrates that the strongest intermolecular H-bonds take place in dimers **1** (O-H---O), **4** (O-H---O), **7** (O-H---N), **8** (O-H---O), **9** (N-H---N), and **11** (O-H---N). The same dimers are characterized by the shortest X-H---Y distances and by a non-significant increase in the electron localization function (η). By comparing these results with the Gibbs free energy values for dimerization, it can be concluded that the dimer interaction energy is not sufficiently strong to overcome entropy loss during their formation. However, in spite of the H-bond-favorable topology characteristics, the formation of dimers **9** and **11** is unlikely due to the positive ΔG_{298} value.

Experimental data for compounds **I**–**III** are given in Appendix A (Tables A1–A10, pages 125–137).

Packing for compound **III** is characterized by the absence of H-bonding and is based on the presumably steric requirements (Fig. 3, Tables A1, A8–A10), the crystallographic parameters of which are consistent with the existing literature [23–25]. The experimental and theoretical results are confirmed by the thermal analysis data. The melting points for the compounds in question are as follows: 397.6–398.4 (**I**), 431.8–436.3 (**II**), and 381.5–381.9 K (**III**), the melting enthalpy being equal to 18.5, 12.3, and ca. 16.7 kJ·mol^{-1} for (**I**), (**II**), and (**III**), respectively. The order of the latter values is possibly due

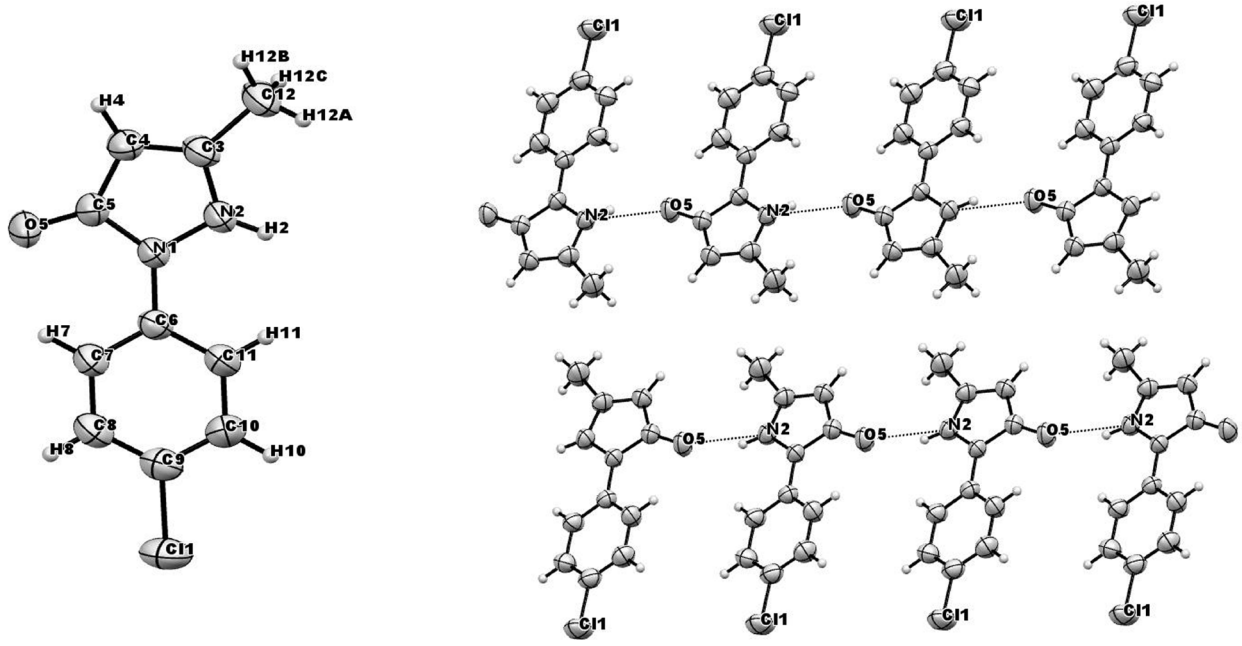

a b

Fig. 2. Asymmetric unit of compound **II** with the crystallographic numbering scheme. Displacement ellipsoids are drawn at the 50% probability level, (a); H-bonding between **NH**-tautomers (b).

Table 3. Description of dimer formation (ΔH_{298} is enthalpy and ΔS_{298} is entropy) from the corresponding monomers of compounds **I** and **II**

Entry	The species label and sketch	H-bond type and length, Å	ΔH_{298}	$-T\Delta S_{298}$	ΔG_{298}
		(calc./exp.)	kJ·mol^{-1}		
1	2	3	4	5	6
1	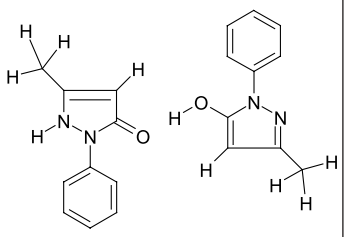 **Ib**–**Ic** dimer (O---HO)	O---H-O 2.62/2.479	−48.4	37.6	−10.8
2	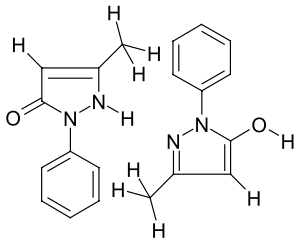 **Ib**–**Ic** dimer (NH---N)	N-H---N 2.98/2.800	−28.8	39.6	10.9
3	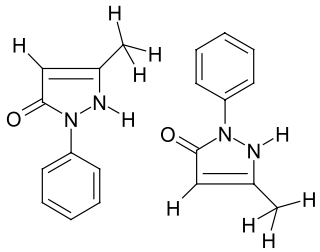 **Ib**–**Ib** dimer (NH---O)	N-H---O 2.81	−38.1	37.6	−0.6
4	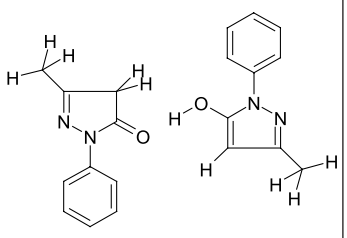 **Ia**–**Ic** dimer (O---HO)	O---H-O 2.65	−41.0	39.9	−1.1

Table 3. Continued

Entry	The species label and sketch	H-bond type and length, Å	ΔH_{298}	$-T\Delta S_{298}$	ΔG_{298}
		(calc./exp.)	kJ·mol^{-1}		
1	2	3	4	5	6
5	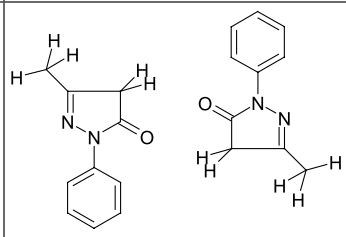 **Ia**–**Ia** dimer	–	−18.8	36.8	18.0
6	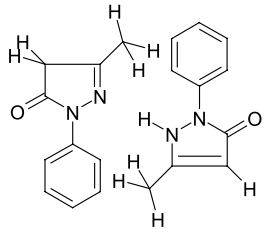 **Ia**–**Ib** dimer (N---HN)	N---H-N 3.08	−20.2	41.8	21.6
7	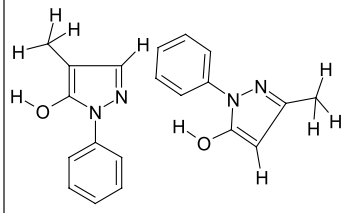 **Ic**–**Ic** dimer (N---HO)	N---H-O 2.70	−33.5	33.5	0.1
8	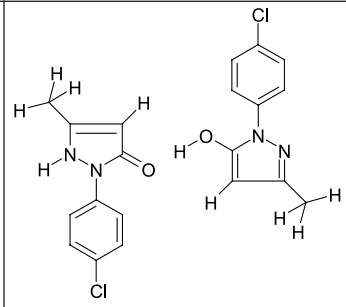 **IIb**–**IIc** dimer (O---HO)	O---H-O 2.62	−48.7	35.5	−13.3
9	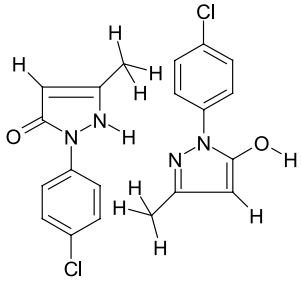 **IIb**–**IIc** dimer (NH---N)	N-H---N 2.97	−28.4	38.6	10.2

Table 3. Continued

Entry	The species label and sketch	H-bond type and length, Å (calc./exp.)	ΔH_{298}	$-T\Delta S_{298}$	ΔG_{298}
			kJ·mol^{-1}		
1	2	3	4	5	6
10	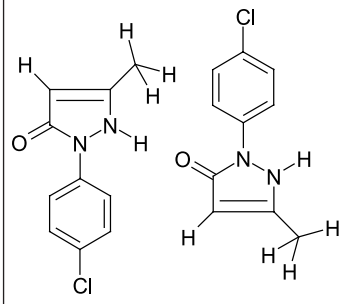 **IIb**–**IIb** dimer (NH---O)	N-H---O 2.81/2.729	−39.2	35.5	−3.7
11	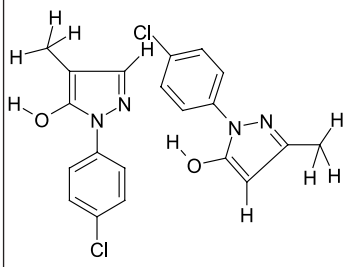 **IIc**–**IIc** dimer (N---HO)	N---H-O 2.70	−36.0	44.5	8.5

Table 4. Topology characteristics and length for the dimer intermolecular hydrogen bond

Dimer	ρ, e·Å^{-3}	$\nabla^2\rho$, e·Å^{-5}	*H*, a.u.	*V*, a.u.	*G*, a.u.	η	R(X-H---Y), Å
Compound **I**							
1	0.0294	0.1165	−0.0147	−0.0585	0.0438	0.2540	1.61
2	0.0155	0.0739	−0.0011	−0.0207	0.0196	0.1660	1.94
3	0.0201	0.1067	−0.0037	−0.0341	0.0304	0.1650	1.77
4	0.0265	0.1139	−0.0112	−0.0508	0.0397	0.2261	1.65
5	0.0070	0.0523	0.0027	−0.0076	0.0103	0.0489	2.23
5*	0.0071	0.0527	0.0027	−0.0077	0.0104	0.0493	2.23
6	0.0108	0.0619	0.0014	−0.0127	0.0141	0.0619	2.09
7	0.0270	0.0845	−0.0126	−0.0464	0.0338	0.3011	1.70
Compound **II**							
8	0.0295	0.1168	−0.0148	−0.0588	0.0440	0.2550	1.61
9	0.0296	0.1169	−0.0148	−0.0588	0.0440	0.2552	1.62
10	0.0200	0.1069	−0.0037	−0.0340	0.0304	0.1637	1.77
11	0.0275	0.0843	−0.0132	−0.0475	0.0343	0.3074	1.69

Note: **5*** is for another position of O atoms.

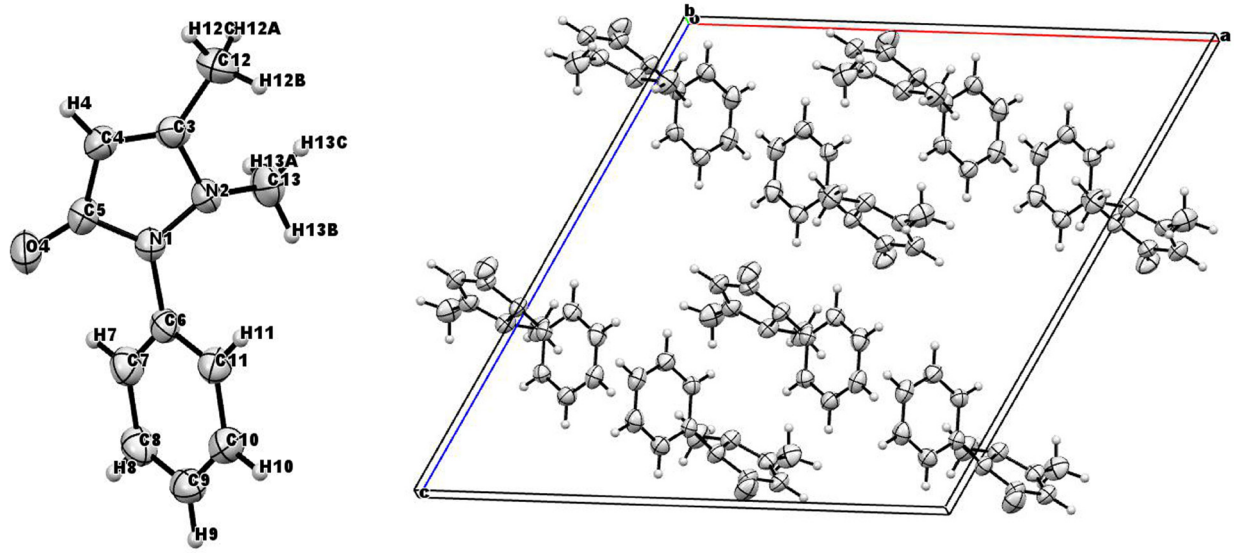

a b

Fig. 3. Asymmetric unit of compound **III** with the crystallographic numbering scheme. Displacement ellipsoids are drawn at the 50% probability level, (a); crystal structure packing (b).

to the absence of hydrogen bonding in compound **III** and the presence of comparatively longer and weaker hydrogen bonds between dimers in compound **II** compared with compound **I**. The wide melting range for compound **II** is possibly related to the intermolecular interactions with participation of chlorine atoms.

CONCLUSIONS

Our study demonstrated that intermolecular hydrogen bonding plays an important role in crystal packing, molecule association, and self-organization, and it explains some contradictions between the theoretical data for the molecules in the gas phase and experimental results for compounds in the solid state. Differentiation was determined between strong interactions due to participation of atoms with high electronegativity (O, N) and the weak (dispersion) ones, the dimer formation being the first step of extended species formation.

APPENDIX A

Supplementary data to this article can be found after this article and online at https://doi.org/10.32362/2410-6593-2021-16-2-113-124 (Supplementary files).

The authors were equally involved in the work on the article.

The authors declare no conflicts of interest.

REFERENCES

1. Vijayan M., Viswamitra M.A. A Refinement of the Structure of Calcium Hexa-antipyrine Perchlorate and a Comparative Study of Some Metal Hexaantipyrine Perchlorates. *Acta Crystallogr.* 1968;B24(8):1067–1076. https://doi.org/10.1107/S0567740868003717

2. Brassy C., Mornon J.-P., Delettre J. Dinitratobis(antipyrine) cobalt(II). *Acta Crystallogr.* 1974;B30(9):2243–2248. https://doi.org/10.1107/S0567740874006832

3. Lenarcik B., Wisniewski M., Gabryszewski M. Complexation capacity of some biologically active derivatives of 5-pyrazolone. *Pol. J. Chem.* 1980;54(10):1869–1874.

4. Maroszová J., Findoráková L., Györyvá K., Koman M., Melník M. Bis(2-chlorobenzoato-κ*O*)bis(phenazone-κ*O*)zinc(II) 0.612-hydrate. *Acta Crystallogr.* 2007;E63(5):m1406–m1407. https://doi.org/10.1107/S1600536807016765

5. Madhu N.T., Radhakrishnan P.K., Grunert M., Weinberger P., Linert F. Antipyrine and its derivatives with first row transition metals. *Rev. Inorg. Chem.* 2003;23(1):1–23. https://doi.org/10.1515/REVIC.2003.23.1.1

6. Rukk N.S., Antsyshkina A.S., Sadikov G.G., Sergienko V.S., Skryabina A.Yu., Osipov R.A., Alikberova L.Yu. Synthesis and Structure of Complex Compounds of Lanthanum, Europium and Scandium Iodides with Antipyrine. *Russ. J. Inorg. Chem.* 2009;54(4):539–542. https://doi.org/10.1134/S0036023609040081

7. Rukk N.S., Albov D.V., Shamsiev R.S., Mudretsova S.N., Davydova G.A., Sadikov G.G., Antsyshkina A.S., Kravchenko V.V., Skryabina A.Yu., Apryshko G.N., Zamalyutin V.V., Mironova E.A. Synthesis, X-ray crystal structure and cytotoxicity studies of lanthanide(III) iodide complexes with anipyrine. *Polyhedron.* 2012;44(1):124–132. https://doi.org/10.1016/j.poly.2012.06.075

8. Rukk N.S., Kuzmina L.G., Albov D.V., Shamsiev R.S., Mudretsova S.N., Davydova G.A., Retivov V.M., Volkov P.V., Kravchenko V.V., Apryshko G.N., Streletskii A.N., Skryabina A.Yu., Mironova E.A., Zamalyutin V.V. Synthesis, X-ray crystal structure and cytotoxicity studies of zinc(II) and cadmium(II) iodide complexes with anipyrine. *Polyhedron.* 2015;102:152–162. https://doi.org/10.1016/j.poly.2015.09.011

9. Li Z.-X., Fei N., Yuan W. Crystal structure of 4-((4-methoxy-benzylidene)-amino)-1,5-dimethyl-2-phenylpyrazolidin-3-ol, $C_{19}H_{19}N_3O_2$. *Z. Kristallogr. NCS.* 2007;222(2):133–134. https://doi.org/10.1524/ncrs.2007.0053

10. Rukk N.S., Skryabina A.Yu., Apryshko G.N. Search for potential antitumor complex compounds of rare earth metals. *Russ. J. Biotherapy.* 2009;8(2):14–15 (in Russ.).

11. Galantsev A.V., Drobot D.V., Dorovatovsky P.V., Khrustalev V.N. Lanthanum Complex with Neridronic Acid: Synthesis and Properties. *Tonk. Khim. Tekhnol. = Fine Chem. Technol.* 2019;14(2):70–77 (in Russ.). https://doi.org/10.32362/2410-6593-2019-14-2-70-77

12. Kuz'mina L.G, Vedernikov A.I., Howard J.A.K., Bezzubov S.I., Alfimov M.V., Gromov S.P. Peculiarities of styryl dyes of the benzoselenazole series crystal packings and their influence on solid phase [2 + 2] photocycloaddition reaction with single crystal retention. *CrystEngComm,* 2016;18:7506–7515. https://doi.org/10.1039/C6CE01426G

13. Zanatta M., Dupont J., Wentz G.N., dos Santos F.P. Intermolecular hydrogen bonds in water@IL supramolecular complexes. *Phys. Chem. Chem. Phys.* 2018;20(17):11608–11614. https://doi.org/10.1039/C8CP00066B

14. Beijer F.H. *Cooperative multiple hydrogen bonding in supramolecular chemistry*. Eindhoven: Technische Universiteit Eindhoven; 1998. 188 p. https://doi.org/10.6100/IR508563

15. Zhai C., Hou B., Peng P., Zhang P., Li L., Chen X. Hydrogen bonding interaction of ascorbic acid with nicotinamide: Experimental and theoretical study. *J. Mol. Liquids.* 2018;249:9–15. https://doi.org/10.1016/j.molliq.2017.11.034

16. Laikov D.N. Fast evaluation of density functional exchange-correlation terms using the expansion of the electron density in auxiliary basis sets. *Chem. Phys. Lett.* 1997;281(1–3):151–156. https://doi.org/10.1016/S0009-2614(97)01206-2

17. Perdew J.P., Burke K., Ernzerhof M. Generalized Gradient Approximation Made Simple. *Phys. Rev. Lett.* 1996;77(18):3865–3868. https://doi.org/10.1103/PhysRevLett.77.3865

18. Gaussian 09, Revision A.02. Frisch M.J., Trucks G.W., Schlegel H.B., Scuseria G.E., Robb M.A., Cheeseman J.R., Scalmani G., Barone V., Petersson G.A., Nakatsuji H., Li X., Caricato M., Marenich A., Bloino J., Janesko B.G., Gomperts R., Mennucci D., Hratchian H.P., Ortiz J.V., Izmaylov A.F., Sonnenberg J.L., Williams-Yang D., Ding F., Lipparini F., Egidi F., Goings J., Peng B., Petrone A., Henderson T., Ranasinghe D., Zakrewski V.G., Gao J., Rega N., Zheng D., Liang W., Hada M., Ehara M., Toyota K., Fukuda R., Hasegawa J., Ishida M., Nakajima T., Honda Y., Kitao O., Nakai H., Vreven T., Throssell K., Montgomery J.A. Jr., Peralta J.E., Ogliaro F., Bearpark M., Heyd J.J., Brothers E., Kudin K.N., Staroverov V.N., Keith T., Kobayashi R., Normand J., Raghavachari K., Rendell A., Burant J.C., Iyengar S.S., Tomasi J., Cossi M., Millam J.M., Klene M., Adamo C., Cammi R., Ochterski J.W., Martin R.L., Morokuma K., Farkas O., Foresman J.B., Fox D.J., Gaussian, Inc., Wallingford CT, 2016.

19. Lu T., Chen F. Multiwfn: A Multifunctional Wavefunction Analyzer. *J. Comput. Chem.* 2012;33(5):580–592. https://doi.org/10.1002/jcc.22885

20. Sheldrick G.M. Crystal structure refinement with SHELXL. *Acta Crystallogr.* 2015;C71:3–8. https://doi.org/10.1107/S2053229614024218

21. Macrae E.C.F., McCabe P., Pidcock E., Shields G.P. Taylor R., Towler M., van de Streek I. Mercury: visualization and analysis of crystal structures. *J. Appl. Crystallogr.* 2006;39(3):453–457. https://doi.org/10.1107/S002188980600731X

22. Dardonville C., Elguero J., Rozas I., Fernández-Castaño C., Foces-Foces C., Sobrados I. Tautomerism of 1-(2º,4º-dinitrophenyl)-3-methyl-2-pyrazolin-5-one: theoretical calculations, solid and solution NMR studies and X-ray crystallography. *New J. Chem.* 1998;22(12):1421–1430. https://doi.org/10.1039/A805415K

23. Singh T.P., Vijayan M. Structural Studies of Analgesics and Their Interactions. I. The Crystal and Molecular Structure of Antipyrine. *Acta Crystallogr.* 1973;B29:714–720. https://doi.org/10.1107/S0567740873003225

24. Chugunova G.A., Kataeva O.N., Ahlbrecht H., Kurbangalieva A.R., Movchan A.I., Lenstra A.T.H., Geise H.J., Litvinov I.A. Derivatives of 1-phenyl-3-methylpyrazol-2-in-5-thione and their oxygen analogues in the crystalline phase and their tautomeric transformations in solutions and in the gas phase. *J. Mol. Struct.* 2001;570(1–3):215–223. https://doi.org/10.1016/S0022-2860(01)00514-2

25. Wang Q., Zhang Y., Wang R., Yang Y.-L., Zhi F. 5-Methyl-2-phenyl-2H-pyrazol-3-ol. *Acta Crystallogr.* 2008;E64(10):o1924. https://doi.org/10.1107/S1600536808028559

About the authors:

Nataliya S. Rukk, Cand. Sci. (Chem.), Associate Professor, A.N. Reformatskii Department of Inorganic Chemistry, M.V. Lomonosov Institute of Fine Chemical Technologies, MIREA – Russian Technological University (86, Vernadskogo pr., Moscow, 119571, Russia). E-mail: roukkn@inbox.ru. Scopus Author ID 6506769340, Researcher ID I-3151-2016, http://orcid.org/0000-0001-7989-8009

Ravshan S. Shamsiev, Dr. Sci. (Chem.), Professor, Ya.K. Syrkin Department of Physical Chemistry, M.V. Lomonosov Institute of Fine Chemical Technologies, MIREA – Russian Technological University (86, Vernadskogo pr., Moscow, 119571, Russia). E-mail: shamsiev.r@gmail.com. Scopus Author ID 6506076152, Researcher ID L-4526-2016, http://orcid.org/0000-0002-0473-770X

Dmitry V. Albov, Cand. Sci. (Chem.), Senior Scientific Researcher, M.V. Lomonosov Moscow State University (1, Leninskie Gory, Moscow, 119992, Russia). E-mail: dmitryalbov@mail.ru. Scopus Author ID 8375436400.

Svetlana N. Mudretsova, Senior Scientific Researcher, M.V. Lomonosov Moscow State University (1, Leninskie Gory, Moscow, 119992, Russia). Scopus Author ID 6603774709.

Об авторах:

Рукк Наталия Самуиловна, к.х.н., доцент кафедры неорганической химии им. А.Н. Реформатского, Институт тонких химических технологий им. М.В. Ломоносова, ФГБОУ ВО «МИРЭА – Российский технологический университет» (119571, Россия, Москва, пр-т Вернадского, 86). E-mail: roukkn@inbox.ru. Scopus Author ID 6506769340, Researcher ID I-3151-2016, http://orcid.org/0000-0001-7989-8009

Шамсиев Равшан Сабитович, д.х.н., профессор кафедры физической химии им. Я.К. Сыркина, Институт тонких химических технологий им. М.В. Ломоносова, ФГБОУ ВО «МИРЭА – Российский технологический университет» (119571, Россия, Москва, пр-т Вернадского, 86). E-mail: shamsiev.r@gmail.com. Scopus Author ID 6506076152, Researcher ID L-4526-2016, http://orcid.org/0000-0002-0473-770X

Альбов Дмитрий Васильевич, к.х.н., научный сотрудник, МГУ им. М.В. Ломоносова, химический факультет (119992, Россия, Москва, Ленинские Горы, 1). E-mail: dmitryalbov@mail.ru. Scopus Author ID 8375436400.

Мудрецова Светлана Николаевна, старший научный сотрудник, МГУ им. М.В. Ломоносова, химический факультет (119992, Россия, Москва, Ленинские Горы, 1). Scopus Author ID 6603774709.

The article was submitted: January 24, 2020; approved after reviewing: August 17, 2020; accepted for publication: April 21, 2021.

The text was submitted by the authors in English.

Edited for English language and spelling by Enago, an editing brand of Crimson Interactive Inc.

APPENDIX A

Supplementary data to the research article: Rukk N.S., Shamsiev R.S., Albov D.V., Mudretsova S.N. Structural characterization of hydrogen bonding for antipyrine derivatives: Single-crystal X-ray diffraction and theoretical studies. *Tonk. Khim. Tekhnol. = Fine Chem. Technol.* 2021;16(2):113–124

Table A1. Crystal data and the details of data collection and refinement for compounds **I**, **II**, and **III**

Compound	I	II	III
Empirical formula	$C_{10}H_{10}N_2O$	$C_{10}H_9ClN_2O$	$C_{11}H_{12}N_2O$
Formula weight	174.20	208.64	188.23
Crystal system, Sp. gr., Z	Monoclinic, $P2_1/c$, 8	Triclinic, P–1, 2	Monoclinic, C2/c, 8
a, *b*, *c*, Å	*a* = 10.331(3) *b* = 11.155(4) *c* = 15.880(5)	*a* = 5.8551(12) *b* = 7.674(3) *c* = 11.348(3)	*a* = 16.892(9) *b* = 7.429(3) *c* = 17.776(8)
α, β, γ, °; V, Å^3	90.00, 95.06(3), 90.00; 1822.9 (10)	106.11(2), 94.669(19), 101.51(2); 475.0(2)	90.00, 116.98(5), 90.00; 1987.9(16)
F(000)	736	216	800
D_x, Mg·m^{-3}	1.269	1.459	1.258
Radiation	Cu Kα radiation, λ = 1.5418 Å, Cell parameters from 25 reflections θ = 33°–35°	Cu Kα radiation, λ = 1.5418 Å, Cell parameters from 25 reflections θ = 30°–33°	Ag Kα radiation, λ = 0.56087 Å, Cell parameters from 25 reflections θ = 15°–16°
μ, mm^{-1}	0.68	3.28	0.05
Crystal size, mm^3	0.20 × 0.20 × 0.20 Colorless prisms	0.10 × 0.10 × 0.10 Colorless prisms	0.50 × 0.50 × 0.50 Colorless prisms
Data collection: Enraf Nonius CAD4 diffractometer[3]; radiation source: fine-focus sealed tube; monochromator: graphite; non–profiled ω scans.			
3450 measured reflections, 3450 independent reflections, 2988 reflections with $I > 2\sigma(I)$; R_{int} = 0.0000; θ_{max} = 69.9°, θ_{min} = 4.3°; *h* = –12→12; *k* = 0→13; *l* = 0→19; 1 standard reflection every 120 min; intensity decay: 1%	1952 measured reflections, 1952 independent reflections, 1740 reflections with $I > 2\sigma(I)$; R_{int} = 0.0000; θ_{max} = 74.8°, θ_{min} = 4.1°; *h* = –7→7; *k* = –9→9; *l* = 0→14; 2 standard reflections every 120 min; intensity decay: 2%	9715 measured reflections, 4882 independent reflections, 2820 reflections with $I > 2\sigma(I)$; R_{int} = 0.070; θ_{max} = 28.0°, θ_{min} = 2.0°; *h* = –28→28; *k* = –12→12; *l* = –29→15; 1 standard reflection every 60 min; intensity decay: 2%	

[3] Enraf_Nonius CAD_4 Software. Version 5.0. Delft (The Netherlands): Enraf_Nonius, 1989.

Table A1. Continued

Absorption correction: multiscan [20]. Refinement on F^2. Least-squares matrix: full			
Refinement			
H-atom treatment	H atoms were treated by a mixture of independent and constrained refinement	H-atom parameters constrained	
$R[F^2 > 2\sigma(F^2)]$	0.037	0.057	0.058
w$R(F^2)$	0.102	0.158	0.175
S	1.04	1.06	1.01
Reflections/parameters/ restraints	3450/250/0	1952/128/0	4882/130/0
$\Delta\rho_{max}/\Delta\rho_{min}$, e·Å^{-3}	0.15/−0.11	0.33/−0.22	0.26/−0.30

Note: Z = the number of formula units in the unit cell;
R_{int} = merging error (measure of the precision/reproducibility);
θ_{max} = max θ angle in degrees for the reflection used for measurement of the unit cell;
θ_{min} = min θ angle in degrees for the reflection used for measurement of the unit cell;
Sp. gr. = space group;
μ = absorption coefficient;
λ = wavelength, refers to the radiation used to measure intensities;
V = unit cell volume;
a, *b*, and *c* = cell lengths; α, β, and γ = cell angles;
D_x = calculated density;
I = intensity of reflection;
R = R-factor;
w*R* = weighed R-factor;
F(000) = sum of all electrons in the unit cell;
σ = standard deviation;
S = goodness of fit;
h, *k*, and *l* = Miller indices;
$I > 2\sigma(I)$ = criterion for strong reflections.

Table A2. Fractional atomic coordinates and isotropic or equivalent isotropic displacement parameters (Å^2) for compound **I**

Atom	*x*	*y*	*z*	U_{iso}*/U_{eq}
N1	0.19338 (10)	0.37391 (8)	0.06745 (7)	0.0430 (2)
N2	0.27022 (11)	0.29948 (9)	0.02385 (7)	0.0498 (3)
C3	0.32777 (14)	0.37019 (11)	−0.02844 (9)	0.0518 (3)
C4	0.29077 (14)	0.48962 (11)	−0.01909 (9)	0.0530 (3)
H4	0.3209 (16)	0.5576 (15)	−0.0496 (10)	0.067 (5)*
C5	0.20504 (12)	0.48922 (10)	0.04174 (8)	0.0439 (3)
O5	0.13825 (10)	0.57503 (8)	0.07625 (7)	0.0570 (3)
H5	0.1924 (18)	0.6493 (19)	0.0784 (12)	0.087 (6)*
C6	0.11839 (13)	0.32597 (10)	0.12979 (8)	0.0455 (3)
C7	−0.00259 (14)	0.37340 (13)	0.14200 (9)	0.0555 (3)
H7	−0.0347	0.4389	0.1105	0.067*
C8	−0.07485 (17)	0.32197 (17)	0.20172 (12)	0.0747 (5)
H8	−0.1553	0.3543	0.2110	0.090*
C9	−0.0297 (2)	0.22383 (18)	0.24762 (12)	0.0854 (6)
H9	−0.0802	0.1886	0.2865	0.102*
C10	0.0912 (2)	0.17804 (15)	0.23559 (11)	0.0802 (6)
H10	0.1224	0.1122	0.2670	0.096*
C11	0.16638 (17)	0.22889 (12)	0.17740 (9)	0.0598 (4)
H11	0.2484	0.1984	0.1702	0.072*
C12	0.41644 (18)	0.31848 (16)	−0.08831 (12)	0.0780 (5)
H12A	0.5048	0.3378	−0.0694	0.117*
H12B	0.3954	0.3514	−0.1437	0.117*
H12C	0.4061	0.2330	−0.0904	0.117*
N21	0.30234 (11)	0.96602 (8)	0.07065 (7)	0.0473 (3)
N22	0.26333 (12)	1.04936 (9)	0.00912 (8)	0.0517 (3)
H22	0.2696 (16)	1.1302 (18)	0.0200 (11)	0.075 (5)*
C23	0.16953 (14)	0.99970 (12)	−0.04340 (9)	0.0546 (3)
C24	0.15371 (15)	0.88297 (12)	−0.02102 (10)	0.0564 (4)
H24	0.0945 (16)	0.8289 (15)	−0.0484 (10)	0.068 (5)*
C25	0.23756 (13)	0.85971 (10)	0.05141 (9)	0.0486 (3)
O25	0.26042 (11)	0.76589 (8)	0.09483 (7)	0.0646 (3)
C26	0.41009 (12)	0.98926 (10)	0.12963 (9)	0.0468 (3)
C27	0.42958 (16)	0.92134 (13)	0.20319 (10)	0.0606 (4)

Table A2. Continued

Atom	*x*	*y*	*z*	U_{iso}*/U_{eq}
H27	0.3720	0.8601	0.2137	0.073*
C28	0.53456 (18)	0.94523 (17)	0.26046 (11)	0.0752 (5)
H28	0.5485	0.8987	0.3090	0.090*
C29	0.61888 (18)	1.03716 (19)	0.24653 (13)	0.0799 (5)
H29	0.6887	1.0536	0.2859	0.096*
C30	0.59944 (16)	1.10417 (17)	0.17444 (13)	0.0750 (5)
H30	0.6563	1.1665	0.1652	0.090*
C31	0.49607 (14)	1.08054 (13)	0.11487 (11)	0.0595 (4)
H31	0.4847	1.1256	0.0655	0.071*
C32	0.10490 (19)	1.07208 (16)	−0.11336 (11)	0.0751 (5)
H32A	0.0953	1.1532	−0.0947	0.113*
H32B	0.0208	1.0389	−0.1301	0.113*
H32C	0.1568	1.0710	−0.1606	0.113*

Note: The sign * indicates the isotropic displacement parameters, Å^2.

Table A3. Atomic displacement parameters (Å^2) for compound **I**

Atom	U^{11}	U^{22}	U^{33}	U^{12}	U^{13}	U^{23}
N1	0.0534 (6)	0.0206 (4)	0.0566 (6)	−0.0024 (4)	0.0141 (5)	−0.0016 (4)
N2	0.0611 (7)	0.0248 (5)	0.0661 (7)	0.0017 (4)	0.0207 (5)	−0.0021 (4)
C3	0.0578 (7)	0.0343 (6)	0.0656 (8)	−0.0016 (5)	0.0180 (6)	0.0004 (6)
C4	0.0654 (8)	0.0278 (6)	0.0681 (8)	−0.0062 (6)	0.0182 (7)	0.0068 (6)
C5	0.0535 (7)	0.0206 (5)	0.0582 (7)	−0.0031 (5)	0.0080 (6)	−0.0013 (5)
O5	0.0680 (6)	0.0238 (4)	0.0819 (7)	−0.0005 (4)	0.0224 (5)	−0.0055 (4)
C6	0.0581 (7)	0.0275 (6)	0.0522 (7)	−0.0118 (5)	0.0124 (6)	−0.0068 (5)
C7	0.0565 (8)	0.0460 (7)	0.0652 (8)	−0.0128 (6)	0.0128 (6)	−0.0136 (6)
C8	0.0718 (10)	0.0743 (11)	0.0825 (11)	−0.0306 (9)	0.0328 (9)	−0.0272 (9)
C9	0.1175 (16)	0.0750 (12)	0.0694 (10)	−0.0501(12)	0.0415 (11)	−0.0159 (9)
C10	0.1320 (17)	0.0452 (9)	0.0659 (10)	−0.0267(10)	0.0222 (10)	0.0051 (7)
C11	0.0854 (10)	0.0328 (6)	0.0628 (8)	−0.0065 (6)	0.0152 (7)	0.0018 (6)
C12	0.0865 (12)	0.0592 (10)	0.0951 (12)	0.0037 (8)	0.0462 (10)	−0.0027 (9)
N21	0.0558 (6)	0.0203 (4)	0.0649 (6)	−0.0015 (4)	−0.0003 (5)	−0.0005 (4)
N22	0.0660 (7)	0.0233 (5)	0.0648 (7)	−0.0013 (5)	−0.0004 (6)	−0.0012 (5)
C23	0.0625 (8)	0.0395 (7)	0.0613 (8)	0.0002 (6)	0.0019 (6)	−0.0059 (6)
C24	0.0623 (8)	0.0363 (7)	0.0699 (9)	−0.0102 (6)	0.0020 (7)	−0.0121 (6)

Table A3. Continued

Atom	U^{11}	U^{22}	U^{33}	U^{12}	U^{13}	U^{23}
C25	0.0540 (7)	0.0220 (5)	0.0707 (8)	−0.0033 (5)	0.0099 (6)	−0.0068 (5)
O25	0.0771 (7)	0.0234 (4)	0.0925 (8)	−0.0051 (4)	0.0027 (6)	0.0034 (4)
C26	0.0497 (7)	0.0283 (6)	0.0626 (7)	0.0039 (5)	0.0064 (6)	−0.0092 (5)
C27	0.0675 (9)	0.0459 (8)	0.0683 (9)	0.0036 (7)	0.0058 (7)	0.0002 (7)
C28	0.0793 (11)	0.0766 (11)	0.0676 (10)	0.0117 (9)	−0.0046 (8)	−0.0029 (8)
C29	0.0662 (10)	0.0902 (13)	0.0802 (11)	0.0004 (10)	−0.0099 (9)	−0.0195(10)
C30	0.0607 (9)	0.0674 (10)	0.0966 (13)	−0.0145 (8)	0.0047 (9)	−0.0190(10)
C31	0.0587 (8)	0.0446 (7)	0.0749 (9)	−0.0085 (6)	0.0050 (7)	−0.0059 (7)
C32	0.0907 (12)	0.0627 (10)	0.0691 (10)	0.0040 (9)	−0.0079 (9)	0.0032 (8)

Table A4. Geometric parameters (Å, º) for compound **I**

Atom–Atom	Bond length, Å	Atom–Atom	Bond length, Å
N1–C5	1.3581 (15)	N21–C25	1.3826 (15)
N1–N2	1.3768 (14)	N21–N22	1.3827 (15)
N1–C6	1.4147 (16)	N21–C26	1.4140 (18)
N2–C3	1.3237 (17)	N22–C23	1.3413 (19)
C3–C4	1.3976 (18)	N22–H22	0.92 (2)
C3–C12	1.493 (2)	C23–C24	1.363 (2)
C4–C5	1.367 (2)	C23–C32	1.484 (2)
C4–H4	0.966 (17)	C24–C25	1.402 (2)
C5–O5	1.3265 (15)	C24–H24	0.938 (17)
O5–H5	1.00 (2)	C25–O25	1.2640 (16)
C6–C7	1.386 (2)	C26–C31	1.3848 (19)
C6–C11	1.3870 (19)	C26–C27	1.392 (2)
C7–C8	1.382 (2)	C27–C28	1.379 (2)
C7–H7	0.9300	C27–H27	0.9300
C8–C9	1.374 (3)	C28–C29	1.376 (3)
C8–H8	0.9300	C28–H28	0.9300
C9–C10	1.378 (3)	C29–C30	1.367 (3)
C9–H9	0.9300	C29–H29	0.9300
C10–C11	1.381 (2)	C30–C31	1.388 (2)
C10–H10	0.9300	C30–H30	0.9300
C11–H11	0.9300	C31–H31	0.9300
C12–H12A	0.9600	C32–H32A	0.9600
C12–H12B	0.9600	C32–H32B	0.9600
C12–H12C	0.9600	C32–H32C	0.9600

Table A4. Continued

Angle	Angle value, °	Angle	Angle value, °
C5–N1–N2	110.46 (10)	C25–N21–C26	129.87 (10)
C5–N1–C6	129.57 (10)	N22–N21–C26	120.54 (10)
N2–N1–C6	119.97 (9)	C23–N22–N21	108.14 (11)
C3–N2–N1	105.48 (10)	C23–N22–H22	123.9 (11)
N2–C3–C4	111.05 (12)	N21–N22–H22	121.0 (11)
N2–C3–C12	120.26 (12)	N22–C23–C24	109.21 (13)
C4–C3–C12	128.67 (13)	N22–C23–C32	119.58 (13)
C5–C4–C3	105.80 (11)	C24–C23–C32	131.20 (14)
C5–C4–H4	127.9 (10)	C23–C24–C25	108.13 (12)
C3–C4–H4	126.3 (10)	C23–C24–H24	125.5 (10)
O5–C5–N1	119.74 (11)	C25–C24–H24	126.3 (10)
O5–C5–C4	133.05 (11)	O25–C25–N21	121.75 (13)
N1–C5–C4	107.21 (10)	O25–C25–C24	132.31 (12)
C5–O5–H5	107.6 (11)	N21–C25–C24	105.94 (11)
C7–C6–C11	120.33 (13)	C31–C26–C27	119.65 (14)
C7–C6–N1	120.64 (12)	C31–C26–N21	120.13 (13)
C11–C6–N1	119.01 (12)	C27–C26–N21	120.21 (12)
C8–C7–C6	119.05 (16)	C28–C27–C26	119.71 (15)
C8–C7–H7	120.5	C28–C27–H27	120.1
C6–C7–H7	120.5	C26–C27–H27	120.1
C9–C8–C7	121.06 (17)	C29–C28–C27	120.69 (17)
C9–C8–H8	119.5	C29–C28–H28	119.7
C7–C8–H8	119.5	C27–C28–H28	119.7
C8–C9–C10	119.44 (15)	C30–C29–C28	119.59 (16)
C8–C9–H9	120.3	C30–C29–H29	120.2
C10–C9–H9	120.3	C28–C29–H29	120.2
C9–C10–C11	120.72 (18)	C29–C30–C31	120.95 (17)
C9–C10–H10	119.6	C29–C30–H30	119.5
C11–C10–H10	119.6	C31–C30–H30	119.5
C10–C11–C6	119.37 (16)	C26–C31–C30	119.39 (16)
C10–C11–H11	120.3	C26–C31–H31	120.3
C6–C11–H11	120.3	C30–C31–H31	120.3
C3–C12–H12A	109.5	C23–C32–H32A	109.5
C3–C12–H12B	109.5	C23–C32–H32B	109.5
H12A–C12–H12B	109.5	H32A–C32–H32B	109.5

Table A4. Continued

C3–C12–H12C	109.5	C23–C32–H32C	109.5
H12A–C12–H12C	109.5	H32A–C32–H32C	109.5
H12B–C12–H12C	109.5	H32B–C32–H32C	109.5
C25–N21–N22	108.38 (11)	–	–
Torsion angle	**Angle value, º**	**Torsion angle**	**Angle value, º**
C5–N1–N2–C3	−0.26 (15)	C25–N21–N22–C23	4.61 (15)
C6–N1–N2–C3	−179.50 (12)	C26–N21–N22–C23	173.22 (12)
N1–N2–C3–C4	0.60 (16)	N21–N22–C23–C24	−4.54 (16)
N1–N2–C3–C12	−178.10 (14)	N21–N22–C23–C32	176.90 (14)
N2–C3–C4–C5	−0.72 (18)	N22–C23–C24–C25	2.76 (17)
C12–C3–C4–C5	177.84 (16)	C32–C23–C24–C25	−178.91 (16)
N2–N1–C5–O5	179.90 (11)	N22–N21–C25–O25	175.97 (13)
C6–N1–C5–O5	−0.9 (2)	C26–N21–C25–O25	8.8 (2)
N2–N1–C5–C4	−0.18 (15)	N22–N21–C25–C24	−2.85 (15)
C6–N1–C5–C4	178.97 (13)	C26–N21–C25–C24	−170.05 (13)
C3–C4–C5–O5	−179.57 (15)	C23–C24–C25–O25	−178.53 (16)
C3–C4–C5–N1	0.52 (16)	C23–C24–C25–N21	0.12 (16)
C5–N1–C6–C7	35.6 (2)	C25–N21–C26–C31	150.33 (14)
N2–N1–C6–C7	−145.28 (12)	N22–N21–C26–C31	−15.54 (18)
C5–N1–C6–C11	−145.78 (14)	C25–N21–C26–C27	−30.3 (2)
N2–N1–C6–C11	33.30 (17)	N22–N21–C26–C27	163.82 (12)
C11–C6–C7–C8	−0.5 (2)	C31–C26–C27–C28	−0.3 (2)
N1–C6–C7–C8	178.05 (12)	N21–C26–C27–C28	−179.65 (13)
C6–C7–C8–C9	−1.2 (2)	C26–C27–C28–C29	1.3 (2)
C7–C8–C9–C10	1.8 (3)	C27–C28–C29–C30	−1.1 (3)
C8–C9–C10–C11	−0.7 (3)	C28–C29–C30–C31	−0.3 (3)
C9–C10–C11–C6	−1.0 (2)	C27–C26–C31–C30	−1.0 (2)
C7–C6–C11–C10	1.6 (2)	N21–C26–C31–C30	178.35 (13)
N1–C6–C11–C10	−176.98 (13)	C29–C30–C31–C26	1.3 (3)

Hydrogen-bond geometry (Å, º)

D–H---A	D–H	H---A	D---A	D–H---A
O5–H5---O25	1.00 (2)	1.49 (2)	2.4794 (14)	169.8 (18)
N22–H22---N2^{i}	0.92 (2)	1.89 (2)	2.8004 (17)	170.5 (16)

Symmetry code: (i) $x, y + 1, z$.

Table A5. Fractional atomic coordinates and isotropic or equivalent isotropic displacement parameters (Å^2) for compound **II**

Atom	*x*	*y*	*z*	U_{iso}*/U_{eq}
Cl1	0.03028 (10)	0.54630 (7)	0.35235 (4)	0.0752 (3)
N1	−0.0218 (2)	0.11695 (18)	−0.17303 (11)	0.0448 (3)
N2	−0.2362 (2)	0.00890 (18)	−0.23953 (12)	0.0491 (3)
H2	−0.3709	0.0045	−0.2140	0.059*
C3	−0.1961 (3)	−0.0883 (2)	−0.35162 (15)	0.0510 (4)
C4	0.0361 (3)	−0.0560 (2)	−0.35717 (15)	0.0510 (4)
H4	0.1068	−0.1099	−0.4241	0.061*
C5	0.1557 (2)	0.0752 (2)	−0.24282 (14)	0.0487 (4)
O5	0.36892 (19)	0.14357 (19)	−0.20424 (12)	0.0616 (4)
C12	−0.3968 (3)	−0.2094 (3)	−0.44703 (18)	0.0706 (5)
H12A	−0.5131	−0.2709	−0.4079	0.106*
H12B	−0.3411	−0.3009	−0.5067	0.106*
H12C	−0.4657	−0.1344	−0.4881	0.106*
C6	−0.0052 (2)	0.21556 (19)	−0.04676 (13)	0.0431 (3)
C7	0.1996 (3)	0.3438 (2)	0.01551 (16)	0.0532 (4)
H7	0.3290	0.3629	−0.0256	0.064*
C8	0.2129 (3)	0.4441 (3)	0.13892 (17)	0.0579 (4)
H8	0.3511	0.5290	0.1816	0.070*
C9	0.0174 (3)	0.4155 (2)	0.19710 (15)	0.0544 (4)
C10	−0.1861 (3)	0.2891 (3)	0.13769 (15)	0.0565 (4)
H10	−0.3152	0.2717	0.1793	0.068*
C11	−0.1989 (3)	0.1865 (2)	0.01432 (14)	0.0520 (4)
H11	−0.3361	0.0990	−0.0270	0.062*

Note: The sign * indicates the isotropic displacement parameters, Å^2.

Table A6. Atomic displacement parameters (Å^2) for compound **II**

Atom	U^{11}	U^{22}	U^{33}	U^{12}	U^{13}	U^{23}
Cl1	0.0948 (5)	0.0763 (4)	0.0413 (3)	0.0189 (3)	0.0047 (3)	−0.0013 (2)
N1	0.0331 (6)	0.0553 (7)	0.0374 (6)	0.0073 (5)	0.0003 (5)	0.0038 (5)
N2	0.0356 (6)	0.0574 (7)	0.0438 (7)	0.0084 (5)	−0.0002 (5)	0.0019 (6)
C3	0.0473 (8)	0.0519 (8)	0.0433 (8)	0.0116 (6)	−0.0036 (6)	0.0002 (6)
C4	0.0460 (8)	0.0585 (8)	0.0416 (8)	0.0166 (6)	0.0047 (6)	0.0015 (6)
C5	0.0395 (7)	0.0617 (8)	0.0426 (8)	0.0147 (6)	0.0049 (6)	0.0104 (7)

Table A6. Continued

Atom	U^{11}	U^{22}	U^{33}	U^{12}	U^{13}	U^{23}
O5	0.0345 (5)	0.0772 (8)	0.0577 (7)	0.0102 (5)	0.0046 (5)	−0.0020 (6)
C12	0.0497 (9)	0.0786 (11)	0.0591 (11)	0.0118 (9)	−0.0054 (8)	−0.0125 (9)
C6	0.0418 (8)	0.0480 (7)	0.0350 (7)	0.0106 (6)	−0.0007 (5)	0.0072 (6)
C7	0.0411 (7)	0.0565 (8)	0.0490 (8)	0.0044 (6)	0.0035 (6)	0.0010 (7)
C8	0.0499 (9)	0.0589 (9)	0.0505 (9)	0.0031 (7)	−0.0035 (7)	0.0028 (7)
C9	0.0633 (10)	0.0550 (8)	0.0410 (8)	0.0165 (7)	−0.0005 (7)	0.0085 (7)
C10	0.0531 (9)	0.0723 (10)	0.0408 (8)	0.0107 (7)	0.0099 (6)	0.0137 (7)
C11	0.0432 (8)	0.0629 (9)	0.0401 (8)	0.0023 (6)	0.0006 (6)	0.0084 (7)

Table A7. Geometric parameters (Å, º) for compound **II**

Atom–Atom	Bond length, Å	Atom–Atom	Bond length, Å
Cl1–C9	1.7562 (18)	C12–H12B	0.9600
N1–N2	1.3843 (17)	C12–H12C	0.9600
N1–C5	1.3914 (17)	C6–C7	1.382 (2)
N1–C6	1.4077 (18)	C6–C11	1.389 (2)
N2–C3	1.349 (2)	C7–C8	1.385 (2)
N2–H2	0.8600	C7–H7	0.9300
C3–C4	1.343 (2)	C8–C9	1.377 (2)
C3–C12	1.488 (2)	C8–H8	0.9300
C4–C5	1.426 (2)	C9–C10	1.364 (3)
C4–H4	0.9300	C10–C11	1.391 (2)
C5–O5	1.2440 (19)	C10–H10	0.9300
C12–H12A	0.9600	C11—H11	0.9300
Angle	**Angle value, º**	**Angle**	**Angle value, º**
N2–N1–C5	108.65 (12)	H12B–C12–H12C	109.5
N2–N1–C6	120.36 (12)	C7–C6–C11	120.05 (14)
C5–N1–C6	129.59 (12)	C7–C6–N1	120.55 (13)
C3–N2–N1	107.82 (12)	C11–C6–N1	119.38 (13)
C3–N2–H2	126.1	C6–C7–C8	120.31 (15)
N1–N2–H2	126.1	C6–C7–H7	119.8
C4–C3–N2	110.05 (15)	C8–C7–H7	119.8
C4–C3–C12	129.74 (16)	C9–C8–C7	118.70 (16)
N2–C3–C12	120.20 (15)	C9–C8–H8	120.6

Table A7. Continued

C3–C4–C5	108.29 (14)	C7–C8–H8	120.6
C3–C4–H4	125.9	C10–C9–C8	122.01 (16)
C5–C4–H4	125.9	C10–C9–Cl1	118.99 (14)
O5–C5–N1	123.33 (14)	C8–C9–Cl1	119.01 (14)
O5–C5–C4	131.64 (14)	C9–C10–C11	119.41 (15)
N1–C5–C4	105.03 (12)	C9–C10–H10	120.3
C3–C12–H12A	109.5	C11–C10–H10	120.3
C3–C12–H12B	109.5	C6–C11–C10	119.51 (15)
H12A–C12–H12B	109.5	C6–C11–H11	120.2
C3–C12–H12C	109.5	C10–C11–H11	120.2
H12A–C12–H12C	109.5	–	–
Torsion angle	**Angle value, º**	**Torsion angle**	**Angle value, º**
C5–N1–N2–C3	−4.19 (17)	C5–N1–C6–C7	24.4 (2)
C6–N1–N2–C3	−171.92 (12)	N2–N1–C6–C11	7.6 (2)
N1–N2–C3–C4	3.76 (19)	C5–N1–C6–C11	−157.28 (15)
N1–N2–C3–C12	−176.41 (16)	C11–C6–C7–C8	0.0 (3)
N2–C3–C4–C5	−1.88 (19)	N1–C6–C7–C8	178.29 (13)
C12–C3–C4–C5	178.31 (19)	C6–C7–C8–C9	−1.1 (3)
N2–N1–C5–O5	−176.12 (15)	C7–C8–C9–C10	1.4 (3)
C6–N1–C5–O5	−9.9 (3)	C7–C8–C9–Cl1	−178.39 (12)
N2–N1–C5–C4	2.98 (16)	C8–C9–C10–C11	−0.6 (3)
C6–N1–C5–C4	169.22 (14)	Cl1–C9–C10–C11	179.25 (12)
C3–C4–C5–O5	178.28 (18)	C7–C6–C11–C10	0.9 (2)
C3–C4–C5–N1	−0.72 (17)	N1–C6–C11–C10	−177.44 (14)
N2–N1–C6–C7	−170.78 (13)	C9–C10–C11–C6	−0.6 (3)

Hydrogen-bond geometry (Å, º)

D–H---A	D–H	H---A	D---A	D–H---A
N2–H2---O5^{i}	0.86	2.02	2.7293 (18)	139

Symmetry code: (i) *x*–1, *y*, *z*.

Table A8. Fractional atomic coordinates and isotropic or equivalent isotropic displacement parameters (Å^2) for compound **III**

Atom	*x*	*y*	*z*	U_{iso}*/U_{eq}
N1	0.48507 (6)	0.37211 (12)	0.10131 (6)	0.0388 (2)
N2	0.47599 (6)	0.54096 (11)	0.13277 (6)	0.0393 (2)

Table A8. Continued

Atom	*x*	*y*	*z*	U_{iso}*/U_{eq}
C3	0.38667 (7)	0.58089 (15)	0.09304 (7)	0.0399 (2)
C4	0.33980 (7)	0.43974 (16)	0.04683 (7)	0.0432 (3)
H4	0.2783	0.4342	0.0164	0.052*
O4	0.38798 (6)	0.14436 (13)	0.02542 (6)	0.0562 (3)
C5	0.40039 (7)	0.29940 (16)	0.05233 (7)	0.0397 (2)
C6	0.56111 (6)	0.26616 (14)	0.15091 (7)	0.0357 (2)
C7	0.59414 (8)	0.14975 (16)	0.11065 (8)	0.0445 (3)
H7	0.5680	0.1449	0.0520	0.053*
C8	0.66604 (8)	0.04131 (17)	0.15833 (9)	0.0490 (3)
H8	0.6882	−0.0366	0.1315	0.059*
C9	0.70529 (8)	0.04735 (17)	0.24529 (8)	0.0475 (3)
H9	0.7532	−0.0271	0.2769	0.057*
C10	0.67305 (8)	0.16467 (17)	0.28522 (8)	0.0451 (3)
H10	0.6998	0.1699	0.3439	0.054*
C11	0.60106 (7)	0.27459 (16)	0.23843 (7)	0.0403 (2)
H11	0.5796	0.3536	0.2655	0.048*
C12	0.35505 (11)	0.75872 (19)	0.10678 (10)	0.0607 (4)
H12A	0.3672	0.8489	0.0747	0.091*
H12B	0.3853	0.7889	0.1657	0.091*
H12C	0.2923	0.7533	0.0888	0.091*
C13	0.54237 (9)	0.67445 (18)	0.14061 (10)	0.0563 (3)
H13A	0.5435	0.6874	0.0874	0.085*
H13B	0.5997	0.6361	0.1827	0.085*
H13C	0.5277	0.7879	0.1569	0.085*

Note: The sign * indicates the isotropic displacement parameters, Å^2.

Table A9. Atomic displacement parameters (Å^2) for compound **III**

Atom	U^{11}	U^{22}	U^{33}	U^{12}	U^{13}	U^{23}
N1	0.0333 (4)	0.0354 (4)	0.0417 (4)	−0.0002 (3)	0.0118 (3)	−0.0046 (3)
N2	0.0368 (4)	0.0299 (4)	0.0447 (5)	−0.0007 (3)	0.0129 (4)	−0.0017 (3)
C3	0.0398 (5)	0.0369 (5)	0.0389 (5)	0.0063 (4)	0.0142 (4)	0.0074 (4)
C4	0.0340 (5)	0.0439 (6)	0.0433 (5)	0.0023 (4)	0.0102 (4)	0.0036 (4)
O4	0.0471 (5)	0.0474 (5)	0.0614 (5)	−0.0062 (4)	0.0135 (4)	−0.0189 (4)
C5	0.0352 (5)	0.0420 (5)	0.0360 (5)	−0.0028 (4)	0.0109 (4)	−0.0027 (4)

Table A9. Continued

Atom	U^{11}	U^{22}	U^{33}	U^{12}	U^{13}	U^{23}
C6	0.0303 (4)	0.0341 (4)	0.0421 (5)	−0.0017 (3)	0.0159 (4)	−0.0018 (4)
C7	0.0435 (6)	0.0450 (6)	0.0456 (6)	0.0011 (5)	0.0209 (5)	−0.0071 (5)
C8	0.0429 (6)	0.0436 (6)	0.0635 (7)	0.0030 (5)	0.0268 (5)	−0.0089 (5)
C9	0.0347 (5)	0.0413 (6)	0.0628 (7)	0.0033 (4)	0.0190 (5)	0.0029 (5)
C10	0.0384 (5)	0.0489 (6)	0.0437 (5)	0.0019 (5)	0.0148 (4)	0.0031 (5)
C11	0.0364 (5)	0.0442 (5)	0.0415 (5)	0.0019 (4)	0.0186 (4)	−0.0027 (4)
C12	0.0625 (8)	0.0443 (7)	0.0662 (8)	0.0174 (6)	0.0212 (7)	0.0044 (6)
C13	0.0495 (7)	0.0408 (6)	0.0707 (8)	−0.0107 (5)	0.0202 (6)	0.0001 (6)

Table A10. Geometric parameters (Å, º) for compound **III**

Atom–Atom	Bond length, Å	Atom–Atom	Bond length, Å
N1–C5	1.4021 (16)	C8–C9	1.379 (2)
N1–N2	1.4098 (13)	C8–H8	0.9300
N1–C6	1.4210 (16)	C9–C10	1.3823 (18)
N2–C3	1.3770 (17)	C9–H9	0.9300
N2–C13	1.4554 (16)	C10–C11	1.3854 (18)
C3–C4	1.3457 (17)	C10–H10	0.9300
C3–C12	1.4860 (18)	C11–H11	0.9300
C4–C5	1.4329 (17)	C12–H12A	0.9600
C4–H4	0.9300	C12–H12B	0.9600
O4–C5	1.2281 (15)	C12–H12C	0.9600
C6–C11	1.3883 (17)	C13–H13A	0.9600
C6–C7	1.3904 (15)	C13–H13B	0.9600
C6–C7	1.3904 (15)	C13–H13B	0.9600
C7–H7	0.9300	–	–
Angle	**Angle value, º**	**Angle**	**Angle value, º**
C5–N1–N2	108.98 (9)	C7–C8–H8	119.6
C5–N1–C6	123.53 (10)	C8–C9–C10	119.68 (11)
N2–N1–C6	118.50 (9)	C8–C9–H9	120.2
C3–N2–N1	106.22 (9)	C10–C9–H9	120.2
C3–N2–C13	121.31 (10)	C9–C10–C11	120.42 (12)
N1–N2–C13	115.25 (10)	C9–C10–H10	119.8
C4–C3–N2	110.46 (11)	C11–C10–H10	119.8

Table A10. Continued

C4–C3–C12	129.58 (12)	C10–C11–C6	119.61 (11)
N2–C3–C12	119.94 (11)	C10–C11–H11	120.2
C3–C4–C5	108.73 (11)	C6–C11–H11	120.2
C3–C4–H4	125.6	C3–C12–H12A	109.5
C5–C4–H4	125.6	C3–C12–H12B	109.5
O4–C5–N1	123.29 (11)	H12A–C12–H12B	109.5
O4–C5–C4	131.71 (11)	C3–C12–H12C	109.5
N1–C5–C4	104.94 (10)	H12A–C12–H12C	109.5
C11–C6–C7	120.02 (10)	H12B–C12–H12C	109.5
C11–C6–N1	120.88 (10)	N2–C13–H13A	109.5
C7–C6–N1	119.08 (10)	N2–C13–H13B	109.5
C8–C7–C6	119.56 (12)	H13A–C13–H13B	109.5
C8–C7–H7	120.2	N2–C13–H13C	109.5
C6–C7–H7	120.2	H13A–C13–H13C	109.5
C9–C8–C7	120.70 (11)	H13B–C13–H13C	109.5
C9–C8–H8	119.6	–	–
Torsion angle	**Angle value, °**	**Torsion angle**	**Angle value, °**
C5–N1–N2–C3	−8.50 (11)	C3–C4–C5–O4	174.74 (13)
C6–N1–N2–C3	−156.86 (9)	C3–C4–C5–N1	−2.69 (13)
C5–N1–N2–C13	−145.85 (11)	C5–N1–C6–C11	−112.19 (12)
C6–N1–N2–C13	65.80 (14)	N2–N1–C6–C11	31.29 (14)
N1–N2–C3–C4	6.83 (12)	C5–N1–C6–C7	66.27 (14)
C13–N2–C3–C4	141.00 (12)	N2–N1–C6–C7	−150.25 (10)
N1–N2–C3–C12	−174.78 (10)	C11–C6–C7–C8	0.83 (17)
C13–N2–C3–C12	−40.61 (17)	N1–C6–C7–C8	−177.64 (11)
N2–C3–C4–C5	−2.62 (13)	C6–C7–C8–C9	0.02 (18)
C12–C3–C4–C5	179.20 (12)	C7–C8–C9–C10	−0.78 (19)
N2–N1–C5–O4	−170.83 (11)	C8–C9–C10–C11	0.70 (18)
C6–N1–C5–O4	−24.42 (17)	C9–C10–C11–C6	0.15 (18)
N2–N1–C5–C4	6.87 (11)	C7–C6–C11–C10	−0.91 (17)
C6–N1–C5–C4	153.29 (10)	N1–C6–C11–C10	177.53 (10)

CHEMISTRY AND TECHNOLOGY OF ORGANIC SUBSTANCES

ХИМИЯ И ТЕХНОЛОГИЯ ОРГАНИЧЕСКИХ ВЕЩЕСТВ

ISSN 2686-7575 (Online)

https://doi.org/10.32362/2410-6593-2021-16-2-138-147

UDC 532.783:548.3

RESEARCH ARTICLE

Dielectric properties of the system: 4-*n*-pentyloxybenzoic acid–*N*-(4-*n*-butyloxybenzylidene)-4'-methylaniline

Svetlana A. Syrbu[1,@], Mikhail S. Fedorov[2], Elena A. Lapykina[2], Victor V. Novikov[2]

[1]*Ivanovo Fire and Rescue Academy, Ivanovo, 153040 Russia*
[2]*Ivanovo State University, Ivanovo, 153025 Russia*
[@]*Corresponding author, e-mail: syrbue@yandex.ru*

Abstract

Objectives. *Our aim was to study the dielectric properties of the 4-n-pentyloxybenzoic acid–N-(4-n-butyloxybenzylidene)-4'-methylaniline system and reveal how different concentrations of N-(4-n-butyloxybenzylidene)-4'-methylaniline additives affect the dielectric properties of 4-n-pentyloxybenzoic acid.*

Methods. *System properties were investigated using polarization thermomicroscopy and dielcometry.*

Results. *We found that dielectric anisotropy changes its sign from positive to negative at the transition temperature of the high-temperature nematic subphase to the low-temperature one. The anisotropy of the dielectric constant of N-(4-n-butoxybenzylidene)-4'-methylaniline has a positive value and increases as to the system approaches the crystalline phase. The crystal structure of the 4-n-pentyloxybenzoic acid contains dimers formed by two independent molecules due to a pair of hydrogen bonds. The crystal structure of N-(4-n-butoxybenzylidene)-4'-methylaniline contains associates formed by orientational interactions of two independent molecules. 4-n-Pentyloxybenzoic acid dimers (270 nm) and associates of N-(4-n-butoxybenzylidene)-4'-methylaniline (250 nm) proved to have approximately the identical length. Considering the close length values of the structural units of both compounds and the dielectric anisotropy sign, we assume that the N-(4-n-butoxybenzylidene)-4'-methylaniline associates are incorporated into the supramolecular structure of the 4-n-pentyloxybenzoic acid. The specific electrical conductivity of the compounds under study lies between 10^{-7} and 10^{-12} $S \cdot cm^{-1}$. The relationship between the specific electrical conductivity anisotropy and the system composition in the nematic phase at the identical reduced temperature, obtained between 100 and 1000 Hz is symbatic. However, the electrical conductivity anisotropy values of the system obtained at 1000 Hz are lower compared to those obtained at 100 Hz. At N-(4-n-butoxybenzylidene)-4'-methylaniline concentrations between 30 and 60 mol %, the electrical conductivity anisotropy values are higher than those of the individual component.*

Conclusions. *A change in the sign of the dielectric constant anisotropy of the 4-n-pentyloxybenzoic acid during nematic subphase transitions was established. We showed that the system has the highest dielectric constant anisotropy value when components have an equal number of moles. Highest electrical conductivity anisotropy values are observed when the concentration of the N-(4-n-butoxybenzylidene)-4' -methylaniline system lies between 30 and 60 mol %.*

Keywords: *liquid crystals, mixtures of nematogens, dielcometry, anisotropy of dielectric constant, anisotropy of electrical conductivity*

For citation: Syrbu S.A., Fedorov M.S., Lapykina E.A., Novikov V.V. Dielectric properties of the system: 4-*n*-pentyloxybenzoic acid–*N*-(4-*n*-butyloxybenzylidene)-4'-methylaniline. *Tonk. Khim. Tekhnol. = Fine Chem. Technol.* 2021;16(2):138–147 (Russ., Eng.). https://doi.org/10.32362/2410-6593-2021-16-2-138-147

НАУЧНАЯ СТАТЬЯ

Диэлектрические свойства системы: 4-*н*-пентилоксибензойная кислота–*N*-(4-*н*-бутилоксибензилиден)-4'-метиланилин

С.А. Сырбу[1,@], М.С. Федоров[2], Е.А. Лапыкина[2], В.В. Новиков[2]

[1]Ивановская пожарно-спасательная академия ГПС МЧС России, г. Иваново, 153040 Россия
[2]Ивановский государственный университет, Иваново, 153025 Россия
[@]Автор для переписки, e-mail: syrbue@yandex.ru

Аннотация

Цель. *Изучить диэлектрические свойства системы: 4-н-пентилоксибензойная кислота–N-(4-н-бутилоксибензилиден)-4'-метиланилин. Выявить влияние добавок N-(4-н-бутилоксибензилиден)-4'-метиланилина различной концентрации на диэлектрические свойства 4-н-пентилоксибензойной кислоты.*
Методы. *Свойства системы исследовались методами поляризационной термомикроскопии и диэлькометрии.*
Результаты. *Установлено, что при температуре перехода высокотемпературной нематической субфазы в низкотемпературную диэлектрическая анизотропия меняет свой знак с положительного на отрицательный. Анизотропия диэлектрической проницаемости N-(4-н-бутоксибензилиден)-4'-метиланилина имеет положительные значения и увеличивается по мере приближения к фазовому переходу в кристаллическую фазу. В кристаллической структуре 4-н-пентилоксибензойной кислоты присутствуют димеры, образованные двумя независимыми молекулами за счет пары Н-связей. В кристаллической структуре N-(4-н-бутоксибензилиден)-4'-метиланилина присутствуют ассоциаты, образованные за счет ориентационных взаимодействий двух независимых молекул. Отмечена близость длин димеров 4-н-пентилоксибензойной кислоты (270 нм) и ассоциатов N-(4-н-бутоксибензилиден)-4'-метиланилина (250 нм). Учитывая близость длин структурных единиц обоих соединений и знак диэлектрической анизотропии, можно предположить, что ассоциаты N-(4-н-бутоксибензилиден)-4'-метиланилина встраиваются в надмолекулярную структуру 4-н-пентилоксибензойной кислоты. Удельная электропроводность исследуемых соединений лежит в диапазоне 10^{-7}–10^{-12} См·см$^{-1}$. Зависимости анизотропии удельной электропроводности от состава системы для нематической фазы при одинаковой приведенной температуре, полученные на частотах 100 и 1000 Гц, имеют симбатный характер. Однако величины анизотропии удельной электропроводности системы, определенные на частоте 1000 Гц, ниже, чем на частоте 100 Гц. При концентрации N-(4-н-бутоксибензилиден)-4'-метиланилина от 30 до 60 мол. % значения анизотропии удельной электропроводности системы выше, чем для индивидуального компонента.*

Выводы. *Установлена смена знака анизотропии диэлектрической проницаемости 4-н-пентилоксибензойной кислоты при переходе между нематическими субфазами. Показано, что самое высокое значение анизотропии диэлектрической проницаемости система имеет при эквимолярном соотношении компонентов. Наибольшие значения анизотропии удельной электропроводности наблюдаются при содержании в системе от 30 до 60 мол. % N-(4-н-бутоксибензилиден)-4'-метиланилина.*

Ключевые слова: *жидкие кристаллы, смеси нематогенов, диэлькометрия, анизотропия диэлектрической проницаемости, анизотропия удельной электропроводности*

Для цитирования: Сырбу С.А., Федоров М.С., Лапыкина Е.А., Новиков В.В. Диэлектрические свойства системы: 4-*н*-пентилоксибензойная кислота–*N*-(4-*н*-бутилоксибензилиден)-4'-метиланилин. *Тонкие химические технологии.* 2021;16(2):138–147. https://doi.org/10.32362/2410-6593-2021-16-2-138-147

INTRODUCTION

In addition to individual supramolecular mesogens, mixtures based on classical calamite liquid crystals have attracted a great deal of interest. Doping them with non-mesogenic and liquid crystal substances offers a route to developing new liquid crystal materials. Specific nematogen interactions in nematogens can considerably affect the component orientational ordering, associative state, and other mesophase properties [1–5]. Lack of systematic studies into these interactions inhibits the development of new functional liquid crystal materials with tailored properties that can find use in various areas.

A characteristic feature of materials in a liquid-crystalline state is their anisotropic properties. These include dielectric constant, magnetic susceptibility, and refractive index, among others. Moreover, a detailed study of these characteristics could boost practical applications of certain mesomorphic functional materials. Dielectric constant data and its relationship with the temperature and composition of the system under study are necessary in the development of components for electro-optical devices [6–9].

In most cases, the nematic mesophase of 4-*n*-alkyloxybenzoic acids, which are components of liquid crystal materials used in information displays, has a positive dielectric constant anisotropy [10–13].

The anisotropy value of the dielectric constant could be affected during the molecular design stage of the mesogen due to the introduction of various functional groups. Furthermore, the anisotropy of the dielectric constant can significantly change in liquid crystal compositions and mixtures, depending on the type of intermolecular interactions and the compositions of the mixtures under study [13–19].

In this work, we studied how the composition of the 4-*n*-pentyloxybenzoic acid–*N*-(4-*n*-butyloxybenzylidene)-4'-methylaniline system affects its dielectric properties (Fig. 1).

The system mesomorphic and volumetric properties were studied earlier [20]. The resulting phase diagram of the specified system with a continuous nematic phase has a eutectic equilibrium point at 40.00 mol % 4-*n*-pentyloxybenzoic acid. In this case, for a given ratio of the mixture components, the maximum temperature range of the nematic phase is observed. It should be noted that the phase transition temperature values of nematogens and their mixtures are determined by polarization thermomicroscopy, dilatometry, and dielcometry.

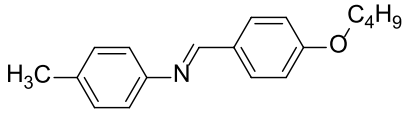

N-(4-*n*-butoxybenzylidene)-4'-methylaniline
(**4-AOBMA**)

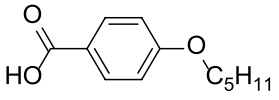

4-*n*-pentyloxybenzoic acid
(**5-AOBA**)

Fig. 1. Structural formulas of the studied compounds.

EXPERIMENTAL

The individual components of the investigated mixtures **4-AOBMA** and **5-AOBA** of analytical grade were purified by double recrystallization from ethanol followed by evacuation under 1.3 Pa from the isotropic phase to constant weight.

Evacuation helped remove volatile impurities and solvent residues after recrystallization. The purification quality was controlled by the clearing point (temperature of the nematic-isotropic phase transition) (see the table) [21–23], the absence of delamination during the nematic-isotropic phase transition, and the electrical conductivity values. The table introduces the following definitions: Cr–crystalline phase, N–nematic phase, I–isotropic liquid phase.

The phase transition temperatures of the studied compounds (°C)

Compounds	Cr		N		I
4-AOBMA	•	65.0	•	70.0	•
5-AOBA	•	124.0	•	151.0	•

Substance mixtures were prepared using the gravimetric method, homogenized at a temperature above the clearing point, and slowly cooled to complete crystallization, and then grounded in an agate mortar. The studied mixtures had the following 4-*n*-pentyloxybenzoic acid concentrations: 10.00, 20.00, 30.00, 40.00, 50.00, 60.00, 70.00, 80.00, and 90.00 mol %.

The dielectric constants of individual substances and their mixtures were measured using the method of dielcometry (immittance meter E7-15 (LCR meter), *MERATEST*, Russia). A constant magnetic field of 5000 Hz was used to determine the liquid crystal orientation. The cell for measuring the dielectric constant of the author's design, which is a flat capacitor with an area of 0.44 cm^2 and a thickness of 0.25 mm, was thermostated with an accuracy of ±0.1°C. The dielectric constant was determined at a voltage per cell of 1.2 V. The cell was calibrated against toluene, carbon tetrachloride, and benzene of chemically pure grade for spectroscopy. The error in determining the dielectric constant did not exceed 0.7%.

The electrical conductivities of individual substances and their mixtures were measured on an E7-15 immittance meter at 1 kHz and 100 Hz.

The dielectric constant anisotropy (Δε) was calculated as the difference between the values of the dielectric constant measured along the long axes of the molecules (parallel to the director) and the dielectric constant values measured across the long axes of the molecules (perpendicular to the director):

$$\Delta\varepsilon = \varepsilon_{\parallel} - \varepsilon_{\perp}$$

The electrical conductivity anisotropy was calculated as the ratio of the electrical conductivity values measured along the long axes of the molecules (parallel to the director) and the electrical conductivity values measured across the long axes of the molecules (perpendicular to the director):

$$\Delta\sigma = \sigma_{\parallel}/\sigma_{\perp}$$

RESULTS AND DISCUSSION

Since electro-optical effects expose the liquid crystal layer to an electric field, the dielectric constant and electrical conductivity are deemed extremely important parameters. The indicated values were measured for the individual components and their mixtures.

As Fig. 2 demonstrates, the compound **5-AOBA** (4-*n*-pentyloxybenzoic acid) in the nematic phase changes the sign of the dielectric constant anisotropy. The dielectric anisotropy changes its sign from positive to negative when transiting from the high-temperature nematic subphase to the low-temperature subphase. We deem that this experimental result can be explained by the "crystal structure memory" of the compound in the mesophase, which manifests when different nematic subphases are formed from different crystalline modifications of **5-AOBA**.

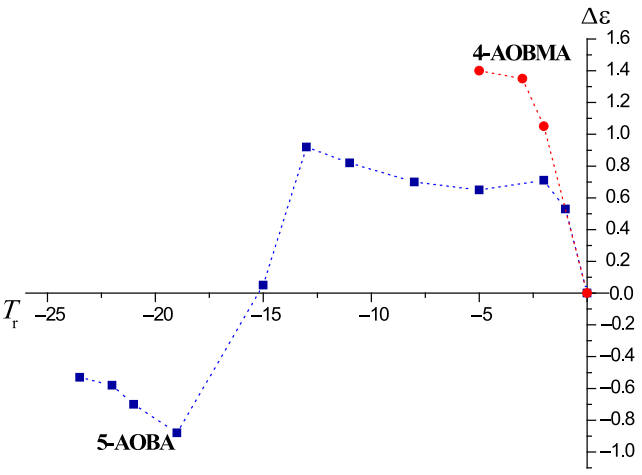

Fig. 2. Dependence of the dielectric constant anisotropy of the individual system components in the nematic phase on the reduced temperature $T_r = T - T_{N–I}$ (1 kHz frequency). $T_{N–I}$ – transition temperature from nematic (N) to isotropic liquid (I).

4-*n*-Pentyloxybenzoic acid has two crystalline modifications: triclinic and monoclinic [24]. The triclinic modification has a stacked structure that reminisces the smectogen structure. However, the interplanar distance in the stacks is much larger than that in the smectic phase. This indicates considerably weaker stacking interactions in such packing.

In the aromatic regions of the monoclinic modification, there are no stacked structural elements, but T-shaped ones, the combination of which yields a parquet packing. Such a packing causes weaker interactions among structural elements compared to those of a stacked structure. Another noteworthy observation is the disordering of the carboxyl hydrogen atom by two positions at the oxygen atoms [24, 25].

The crystal structure of 4-*n*-pentyloxybenzoic acid contains dimers formed by two independent molecules due to a pair of hydrogen bonds.

We deem that these crystalline modifications are transformed into nematic subphases that differ in both dielectric and volumetric properties [20]. The mechanism of this phase transition is still elusive. It can only be assumed that the triclinic modification turns into a low-temperature nematic subphase, while the monoclinic modification becomes a high-temperature nematic subphase. This assumption is based on the fact that the low-temperature nematic subphase has a texture that resembles that of smectogens, while the high-temperature nematic subphase has a classic schlieren texture.

The decreased anisotropy value of the dielectric constant when the system approaches the nematic-isotropic phase transition is associated with the loss of orientational ordering when the temperature increases.

The dielectric constant anisotropy of *N*-(4-*n*-butyloxybenzylidene)-4'-methylaniline has positive values and increases as the system phase approaches the crystalline phase. Associates formed due to orientational interactions of two independent molecules are also present in the crystal structure of *N*-(4-*n*-butyloxybenzylidene)-4'-methylaniline [26]. It is worth noting that the lengths of **5-AOBA** dimers and **4-AOBMA** associates are close: 270 nm for **5-AOBA** and 250 nm for **4-AOBMA** (Figs. 3 and 4). This may be due to the fact that the packing of 4-*n*-pentyloxybenzoic acid dimers [20] is denser, which is due to the acoplanarity of *N*-(4-*n*-butoxybenzylidene)-4'-methylaniline molecules.

The greatest value of the dielectric constant anisotropy in the nematic phase is observed when the components have an equal number of moles. Considering the close length values of the structural units of both compounds and the dielectric anisotropy sign, we assume that the **4-AOBMA** associates are incorporated into the supramolecular structure of **5-AOBA**. In the mixed two-phase nematic-isotropic region, the system dielectric anisotropy values do not practically change as the **4-AOBMA** concentration increases and approaches 0.1. The dielectric constant anisotropy of the system increases up to a value of 0.2 at a content of *N*-(4-*n*-butyloxybenzylidene)-4'-methylaniline of 90 mol % (Fig. 5).

In addition to dielectric anisotropy, electrical conductivity is an important property of liquid crystal materials. Thoroughly purified liquid crystals must have

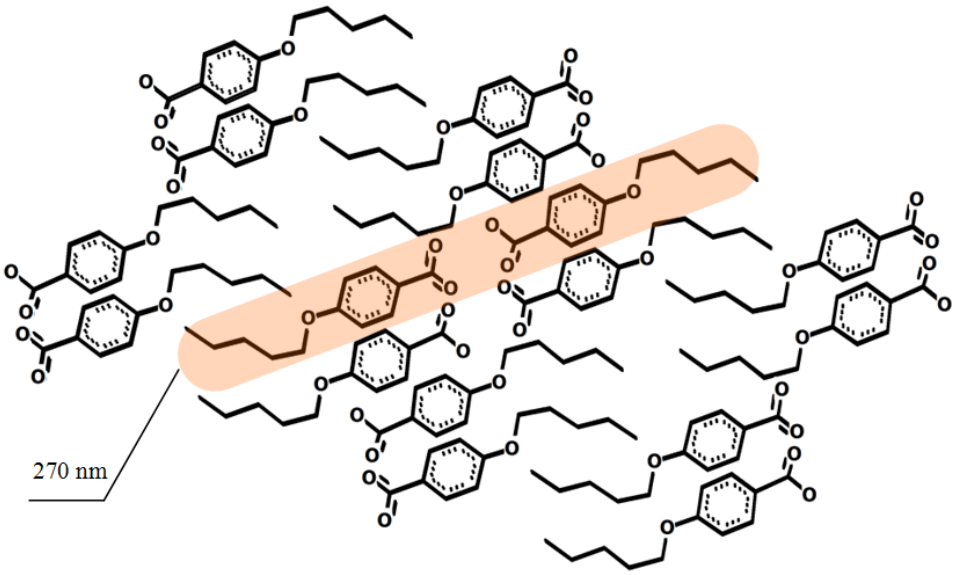

Fig. 3. The crystal packing fragment of 4-*n*-pentyloxybenzoic acid molecules [24] (the molecule long axes are in the plane of the figure).

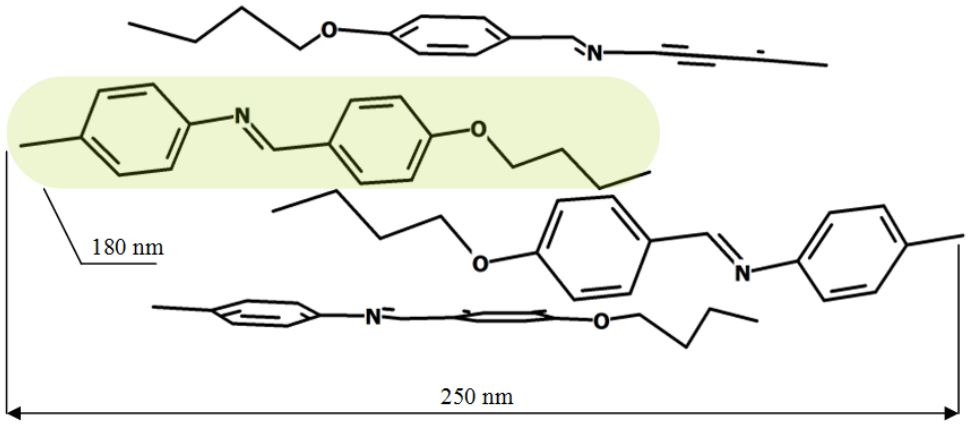

Fig. 4. The crystal packing fragment of *N*-(4-*n*-butyloxybenzylidene)-4'-methylaniline molecules [26] (the molecule long axes are in the plane of the figure).

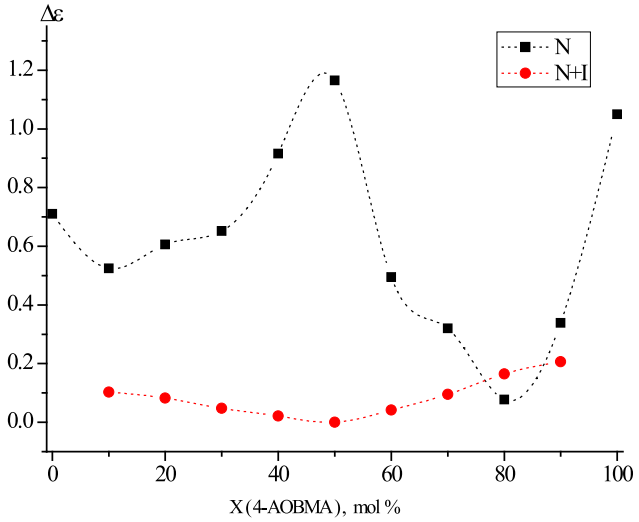

Fig. 5. Dependence of the dielectric constant anisotropy on the mixture composition for the nematic phase (N) at $T_r = -2$°C and nematic-isotropic region (N+I) $T_r = -2$°C ($T_r = T - T_{N+I-I}$), 1 kHz frequency.

extremely low intrinsic electrical conductivities. The specific electrical conductivity of liquid crystals usually ranges between 10^{-7} and 10^{-12} S·cm^{-1}. The investigated nematogens **5-AOBA** and **4-AOBMA** satisfy this requirement. For example, the specific conductivity of **5-AOBA** at 102°C is $3.9 \cdot 10^{-12}$ S·cm^{-1}, whereas the specific conductivity of **4-AOBMA** at 58°C is $1.7 \cdot 10^{-12}$ S·cm^{-1} (both conductivity values are given for the crystalline phase of the compounds).

The electrical conductivity mechanism in liquid crystals is ionic. In this case, the nature of charge carriers can be both intrinsic and impure. The electrical conductivity of mesogens is anisotropic.

Between 100 and 1000 Hz, the electrical conductivity anisotropy of *N*-(4-*n*-butyloxybenzylidene)-4'-methylaniline does not depend on the temperature in the mesophase (Fig. 6). In the 4-*n*-pentyloxybenzoic acid, the anisotropy of specific electrical conductivity sharply increases at the temperature of the phase transition between one nematic subphase to another. In the low-temperature nematic subphase, the electrical conductivity values are slightly higher than those in the high-temperature nematic subphase (Fig. 7). It should be noted that for both the **5-AOBA** acid and the **4-AOBMA** Schiff base, the anisotropy values of the electrical conductivity obtained at 100 and 1000 Hz are quite close.

Analysis results regarding the relationship between temperature and anisotropic electrical conductivity values show that the latter values exceed 1 of **4-AOBMA**. This indicates the presence of regions with a short-range smectic order in the nematic phase of **4-AOBMA**.

Let us consider how the concentration additives of

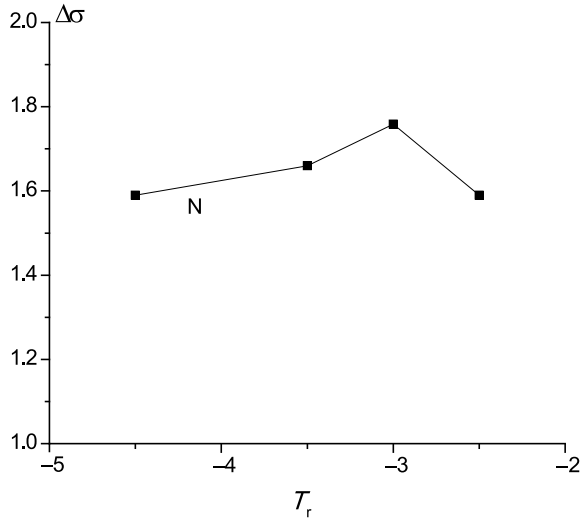

Fig. 6. Dependence of the anisotropy of specific electrical conductivity (Δσ) on the reduced temperature in the nematic phase of *N*-(4-*n*-butyloxybenzylidene)-4'-methylaniline, 1 kHz frequency.

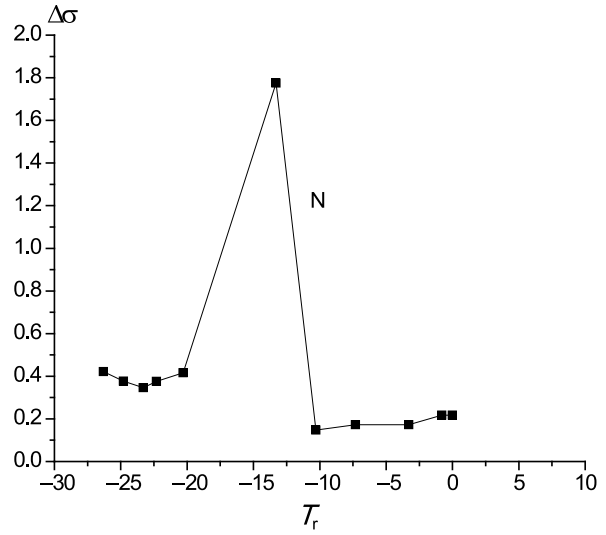

Fig. 7. Dependence of the anisotropy of specific electrical conductivity (Δσ) on the reduced temperature in the nematic phase of 4-*n*-pentyloxybenzoic acid, 1 kHz frequency.

4-AOBMA affect the electrical conductivity anisotropy of **5-AOBA** in the nematic and mixed two-phase nematic-isotropic region.

The relationship between the anisotropy of specific electrical conductivity and the system composition in the nematic phase N at T_r = −2°C, obtained at 100 and 1000 Hz, demonstrate a symbatic character. However, the anisotropy values of the system electrical conductivity at 1000 Hz are lower. The highest anisotropy values of specific electrical conductivity are observed when the system (**4-AOBMA**) concentration ranges between 30 and 60 mol %. It should be noted that, with the indicated compositions, the anisotropy values of the system electrical conductivity exceed those of **4-AOBMA** itself (Fig. 8).

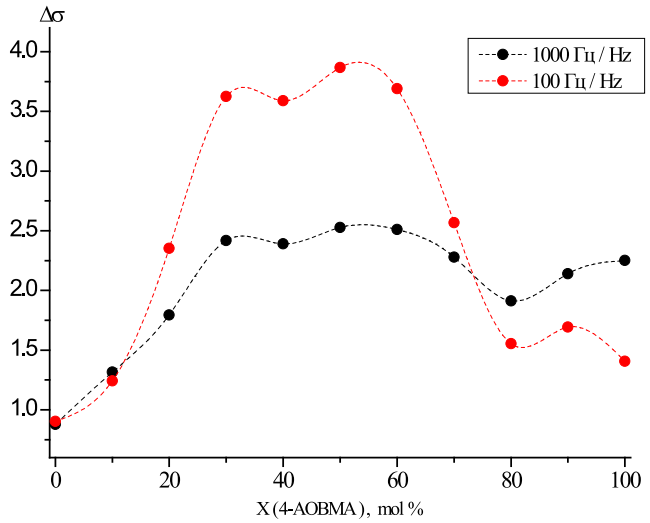

Fig. 8. Dependence of the anisotropy of specific electrical conductivity on the system composition in the nematic phase N at T_r = −2°C, 100 and 1000 Hz.

A different picture is observed for a mixed, two-phase nematic-isotropic region of the system at 100 and 1000 Hz (Fig. 9), although both dependencies have a symbatic character as in the previous case.

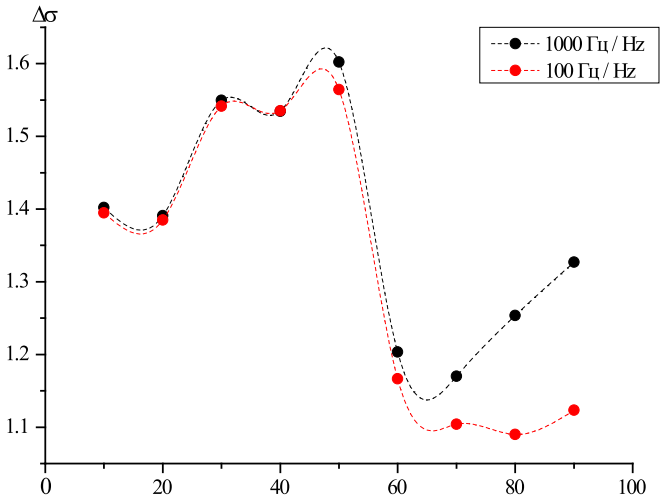

Fig. 9. Dependence of the anisotropy of specific electrical conductivity on the composition of the system in the nematic-isotropic region N+I at T_r = −2°C, 100 and 1000 Hz.

The anisotropy values of the system electrical conductivity at both frequencies are close compared to those of the previous case. Increasing the concentration of the **4-AOBMA** compound up to 50 mol % and from 70 to 90 mol % causes the anisotropic electrical conductivity of the system to increase. When the system concentration ranges between 50 and 70 mol % **4-AOBMA**, a decrease in the anisotropy of the electrical conductivity of the system is observed.

In conclusion, we note that for concentrations of *N*-(4-*n*-butyloxybenzylidene)-4'-methylaniline ranging between 30 and 80 mol % both in the nematic phase and in the mixed two-phase nematic-isotropic region, the anisotropy values of the specific electrical conductivity increase as the temperature decreases. This result indicates that the degree of orientational ordering increases.

CONCLUSIONS

Using the method of dielcometry, we studied the dielectric properties of the 4-*n*-pentyloxybenzoic acid–*N*-(4-*n*-butyloxybenzylidene)-4'-methylaniline system with a step of 10 mol % in component concentration.

Results revealed that unlike the 4-*n*-pentyloxybenzoic acid–*N*-(4-*n*-butyloxybenzylidene)-4'-methylaniline has higher dielectric constant anisotropy values.

A change in the anisotropy sign of the dielectric constant of 4-*n*-pentyloxybenzoic acid during nematic subphase transitions from negative (for a low-temperature nematic subphase) to positive (for a high-temperature nematic subphase) was established.

The system has the highest dielectric constant anisotropy when components have an equal number of moles, and the highest anisotropy values of specific electrical conductivity at concentrations of *N*-(4-*n*-butyloxybenzylidene)-4'-methylaniline ranging between 30 and 60 mol %.

Acknowledgments

This study was supported by the Russian Foundation for Basic Research (project 18-43-370027 p_a).

Authors' contribution

S.A. Syrbu – development of the concept of scientific work, consultation on planning, methodology and implementation of the study, writing the text of the article;

M.S. Fedorov – conducting research, reviewing publications on the topic of the article, processing the experimental data, preparing illustrations;

E.A. Lapykina – conducting research, analysis of literature data;

V.V. Novikov – conducting research, collecting and processing the material.

The authors declare no conflicts of interest.

REFERENCES

1. Paleos C.M., Tsiourvas D. Supramolecular hydrogen-bonded liquid crystals. *Liquid Crystals.* 2001;28(8):1127–1161. https://doi.org/10.1080/02678290110039516

2. Kato T., Uchida J., Ichikawa T., Soberats B. Functional liquid-crystalline polymers and supramolecular liquid crystals. *Polym. J.* 2018;50(1):149–166. https://doi.org/10.1038/pj.2017.55

3. Therrien B. Thermotropic Liquid-Crystalline Materials Based on Supramolecular Coordination Complexes. *Inorganics.* 2020;8(1):2. https://doi.org/10.3390/inorganics8010002

4. Syrbu S.A., Fedorov M.S., Giricheva N.I., Novikov V.V., Filippov I.A., Kiselev M.R. Supramolecular complexes based on 4-*n*-alkoxycinnamic acids and pyridine derivatives: Mesomorphic properties and prospects of applying to tribosystems. *J. Mol. Liq.* 2020;305:112796. https://doi.org/10.1016/j.molliq.2020.112796

5. Giricheva N.I., Syrbu S.A., Bubnova K.E., Fedorov M.S., Kiselev M.R., Girichev G.V. H-complexes in the "4-*n*-alkoxybenzoic acid: 4-pyridyl 4'-*n*-alkoxybenzoate" system. IR spectroscopy and quantum chemical calculations. *J. Mol. Liq.* 2019;277:833–842. https://doi.org/10.1016/j.molliq.2019.01.029

6. Gray G.W., Harrison K.J., Nash J.A., Constant J., Hulme D.S., Kirton J., Raynes E.P. Stable, Low Melting Nematogens of Positive Dielectric Anisotropy for Display Devices. In: Johnson J.F., Porter R.S. (Eds.). *Liquid Crystals and Ordered Fluids*. Springer, Boston, MA; 1974. P. 617–643. https://doi.org/10.1007/978-1-4684-2727-1_55

7. Hird M., Goodby J.W., Toyne K.J. Nematic materials with negative dielectric anisotropy for display applications. *Liquid Crystal Materials, Devices, and Flat Panel Displays*. 2000;3955:15–23. https://doi.org/10.1117/12.379979

8. Belyaev V.V., Chausov D.N., Kurilov A.D., Rybakov D.O., Solomatin A.S., Murauski A.A., Muravsky A.A., Chigrinov V.G., Fan F. Dielectric properties of liquid crystals for display and sensor applications. *J. Soc. Inf. Disp*. 2015;23(9):403–409. https://doi.org/10.1002/jsid.352

9. Ishii Y., Uchida T. Wada M. Effects of dielectric anisotropy on DSM-type display devices. *IEEE Transactions on Electron Devices.* 1978;25(3):323–329. https://doi.org/10.1109/T-ED.1978.19077

10. Verma R., Tripathi A., Dhar R. Enhancement in the thermal stability of themesophases of 4-*n*-(decyloxy) benzoic acid due to Li ion beam irradiaton. *J. Mol. Liq.* 2013;177:409–415. https://doi.org/10.1016/j.molliq.2012.10.034

11. Efremova E.I., Kydryashova Z.A., Nosikova L.A., Kovshik A.P., Dobrun L.A., Melnikov A.B. Phase Diagram and Dielectric Studies in Hydrogen-Bonded Liquid Crystal System. *Mol. Cryst. Liq. Cryst.* 2016;626(1):12–20. https://doi.org/10.1080/15421406.2015.1106220

12. Patari S., Nath A. Tunable dielectric and conductivity properties of two 4-*n* alkoxy benzoic acid. *Opto-Electronics Review.* 2018;26(1):35–43. https://doi.org/10.1016/j.opelre.2017.12.002

13. Valiskó M., Liszi J., Szalai I. Relative permittivity of a few H-bonded liquid crystals. *J. Mol. Liq.* 2004;109(1):39–43. https://doi.org/10.1016/j.molliq.2003.06.001

14. Missaoui T., Amor I.B., Soltani T., Ouada H.B., Jeanneau E., Chevalier Y. Dielectric and electro-optic properties of cybotactic nematic phase in hydrogen-bonded liquid crystals. *J. Mol. Liq.* 2020;304:112726. https://doi.org/10.1016/j.molliq.2020.112726

15. Prabu N.P.S., Mohan M.L.N.M. Thermal and Dielectric Investigations on Supramolecular Hydrogen Bonded Liquid Crystals. *Mol. Cryst. Liq. Cryst.* 2012;569(1):72–91. https://doi.org/10.1080/15421406.2012.703035

16. Nosikova L.A., Kudryashova Z.A., Iskhakova L.D., Syrbu S.A. Mesomorphic and dielectric properties of the *p*-*n*-hexyloxybenzoic acid-*p*-*n*-heptyloxybenzoic acid liquid crystal system. *Russ. J. Phys. Chem.* 2008;82(12):2065–2068. https://doi.org/10.1134/S0036024408120169

[Original Russian Text: Nosikova L.A., Kudryashova Z.A., Iskhakova L.D., Syrbu S.A. Mesomorphic and dielectric properties of the *p*-*n*-hexyloxybenzoic acid-*p*-*n*-heptyloxybenzoic acid liquid crystal system. *Zhurnal Fizicheskoi Khimii.* 2008;82(12):2292–2295 (in Russ.).]

17. Vijayakumar V.N., Madhu Mohan M.L.N. Optical, thermal and dielectric studies in linear hydrogen bonded liquid crystal homologous series. *J. Mol. Struct.* 2011;1000(1–3):69–76. https://doi.org/10.1016/j.molstruc.2011.05.054

18. Viciosa M.T., Nunes A.M., Fernandes A., Almeida P.L., Godinho M.H., Dionísio M.D. Dielectric studies of the nematic mixture E7 on a hydroxypropylcellulose substrate. Liquid Crystals. 2002;29(3):429–441. https://doi.org/10.1080/02678290110113478

19. Zheng A., Xia X., Gao S., Yang J., Lu H., Deng G., Yin Z. Dielectric properties of two high birefringence liquid crystal mixtures in the Sub-THz band. *Liquid Crystals.* 2020;47(1):83–88. https://doi.org/10.1080/02678292.2019.1630490

20. Syrbu S.A., Syrbu A.A., Bagazhkov I.V. Mesomorphic and volume properties of *p*-*n*-butyloxybenzylidene-*p*'-methylanyline – *p*-*n*-pentyloxybenzoic acid system. *Zhidk. krist. ikh prakt. ispolz. = Liq. Cryst. and their Appl.* 2010;3(33):46–56 (in Russ.).

21. Demus D., Demus H., Zaschke H. *Flussiqe Kristalle in Tabellen*. I. Leipzig: VEB, Deut. Verlag; 1974. 356 p.

22. Demus D., Zaschke H. *Flussiqe Kristalle in Tabellen*. II. Leipzig: VEB, Deut. Verlag; 1984. 468 p.

23. Fonseca J.M.S., Santos Luís M.N.B.F., Monte M.J.S. Thermodynamic Study of 4-*n*-Alkyloxybenzoic Acids, *J. Chem. Eng. Data.* 2010;55(6):2238–2245. https://doi.org/10.1021/je900776y

24. Kuz'mina L.G., Kucherepa N.S., Pectov S.M., Kochetov A.N., Rukk N.S., Syrbu S.A. Molecular and Crystal Structure of 4-Alkoxybenzoic Acids: Design of the Mesogenic Phase. *Crystallogr. Rep.* 2009;54(5):862–879. https://doi.org/10.1134/S1063774509050204

[Original Russian Text: Kuz'mina L.G., Kucherepa N.S., Pectov S.M., Kochetov A.N., Rukk N.S., Syrbu S.A. Molecular and Crystal Structure of 4-Alkoxybenzoic Acids: Design of the Mesogenic Phase. *Kristallografiya*. 2009;54(5):908–925 (in Russ.).]

25. Bryan R.F. 508. An X-ray study of the *p*-*n*-alkoxybenzoic acids. Part I. *J. Chem. Soc.* 1960;(0):2517–2519. https://doi.org/10.1039/JR9600002517

26. Kuz'mina L.G., Kucherena N.S., Rodnikova M.N. X-ray diffraction study of *p*-(alkoxybenzylidene)-*p*'-toluidines $C_5H_{11}O–C_6H_4–CH=N–C_6H_4–CH_3$ and $C_8H_{17}O–C_6H_4–CH=N–C_6H_4–CH_3$. *Crystallogr. Rep.* 2008;53(6):1016–1022. https://doi.org/10.1134/S1063774508060175

[Original Russian Text: Kuz'mina L.G., Kucherepa N.S., Rodnikova M.N. X-ray diffraction study of *p*-(alkoxybenzylidene)-*p*'-toluidines $C_5H_{11}O–C_6H_4–CH=N–C_6H_4–CH_3$ and $C_8H_{17}O–C_6H_4–CH=N–C_6H_4–CH_3$. *Kristallografiya,* 2008;53(6):1072–1078 (in Russ.).]

About the authors:

Svetlana A. Syrbu, Dr. Sci. (Chem.), Professor, Deputy Head for the Development of Extra-budgetary Activities, Ivanovo Fire and Rescue Academy of State Firefighting Service of Ministry of Russian Federation for Civil Defense, Emergencies and Elimination of Consequences of Natural Disasters (33, Stroitelei pr., Ivanovo, 153040, Russia). E-mail: syrbue@yandex.ru. Scopus Author ID 57212932207, ResearcherID R-6470-2017, https://orcid.org/0000-0002-0694-7508

Mikhail S. Fedorov, Cand. Sci. (Chem.), Associate Professor, Department of Fundamental and Applied Chemistry, Ivanovo State University (39, Ermaka ul., Ivanovo, 153025, Russia). E-mail: fedorovms@ivanovo.ac.ru. Scopus Author ID 54990030800, ResearcherID E-6231-2017, https://orcid.org/0000-0003-4945-2967

Elena A. Lapykina, Cand. Sci. (Chem.), Associate Professor, Department of Fundamental and Applied Chemistry, Ivanovo State University (39, Ermaka ul., Ivanovo, 153025, Russia). E-mail: ealapikina@yandex.ru. Scopus Author ID 26537603100, ResearcherID U-1734-2019, https://orcid.org/0000-0002-6686-4077

Victor V. Novikov, Cand. Sci. (Eng.), Associate Professor, Department of Fundamental Physics and Nanotechnology, Ivanovo State University (39, Ermaka ul., Ivanovo,153025, Russia). E-mail: novikov-ww@mail.ru. Scopus Author ID 55675223420, ResearcherID S-5851-2017, https://orcid.org/0000-0002-9036-3205

Об авторах:

Сырбу Светлана Александровна, д.т.н., профессор, заместитель начальника (по развитию внебюджетной деятельности) ФГБОУ ВО «Ивановская пожарно-спасательная академия ГПС МЧС России» (153040, Россия, Иваново, пр-т Строителей, 33). E-mail: syrbue@yandex.ru. Scopus Author ID 57212932207, ResearcherID R-6470-2017, https://orcid.org/0000-0002-0694-7508

Федоров Михаил Сергеевич, к.х.н., доцент кафедры фундаментальной и прикладной химии ФГБОУ ВО «Ивановский государственный университет» (153025, Россия, Иваново, ул. Ермака, 39). E-mail: fedorovms@ivanovo.ac.ru. Scopus Author ID 54990030800, ResearcherID E-6231-2017, https://orcid.org/0000-0003-4945-2967

Лапыкина Елена Андреевна, к.х.н., доцент кафедры фундаментальной и прикладной химии ФГБОУ ВО «Ивановский государственный университет» (153025, Россия, Иваново, ул. Ермака, 39). E-mail: ealapikina@yandex.ru. Scopus Author ID 26537603100, ResearcherID U-1734-2019, https://orcid.org/0000-0002-6686-4077

Новиков Виктор Владимирович, к.т.н., доцент кафедры фундаментальной физики и нанотехнологий ФГБОУ ВО «Ивановский государственный университет» (153025, Россия, Иваново, ул. Ермака, 39). E-mail: novikov-ww@mail.ru. Scopus Author ID 55675223420, ResearcherID S-5851-2017, https://orcid.org/0000-0002-9036-3205

The article was submitted: March 04, 2021; approved after reviewing: March 29, 2021; accepted for publication: April 28, 2021.

Translated from Russian into English by H. Moshkov
Edited for English language and spelling by Enago, an editing brand of Crimson Interactive Inc.

CHEMISTRY AND TECHNOLOGY OF MEDICINAL COMPOUNDS AND BIOLOGICALLY ACTIVE SUBSTANCES

ХИМИЯ И ТЕХНОЛОГИЯ ЛЕКАРСТВЕННЫХ ПРЕПАРАТОВ И БИОЛОГИЧЕСКИ АКТИВНЫХ СОЕДИНЕНИЙ

ISSN 2686-7575 (Online)

https://doi.org/10.32362/2410-6593-2021-16-2-148-155

UDC 577.113.4

RESEARCH ARTICLE

Study of the multiple incorporation of modified nucleotides into the growing DNA strand

Olga S. Volkova[@], Alexander V. Chudinov, Sergey A. Lapa

Engelhardt Institute of Molecular Biology, Russian Academy of Sciences, Moscow, 119991 Russia

[@]Corresponding author, e-mail: olechka.volckowa@yandex.ru

Abstract

Objectives. *This study investigated the substrate properties of the modified derivatives of triphosphates of purine and pyrimidine deoxynucleosides (5-propynyl-2'-deoxyuridine-5'-triphosphate, 5-propynyl-2'-deoxycytidine-5'-triphosphate, 5-methyl-2'-deoxycytidine-5'-triphosphate, and N^6-methyl-2'-deoxyadenosine-5'-triphosphate) during their simultaneous incorporation in enzymatic reactions (polymerase chain and primer extension reactions).*

Methods. *The real-time polymerase chain and primer extension reactions were used to study the substrate efficiency of modified deoxynucleotide triphosphates. Various pairwise combinations of modified derivatives were used; specially designed synthetic DNA fragments and libraries for the Systematic Evolution of Ligands by Exponential Enrichment technology were used as templates. Reactions were conducted using DNA polymerases: Taq, Vent (exo-), DeepVent (exo-), and KOD XL.*

Results. *In each case, a pair of compounds (modified dUTP + dCTP, dUTP + dATP, and dCTP + dATP) was selected to study the simultaneous incorporation into the growing DNA strand. The most effective combinations of nucleotides for simultaneous insertion were dU and dC, having 5-propynyl substitution. The Vent (exo-) DNA polymerase was found as the most effective for the modified substrates.*

Conclusions. *The selected compounds can be used for the enzymatic preparation of modified DNA, including aptamers with extended physicochemical properties.*
Keywords: *modified aptamers, modified nucleotides, primer extension reaction, real-time polymerase chain reaction*

For citation: Volkova O.S., Chudinov A.V., Lapa S.A. Study of the multiple incorporation of modified nucleotides into the growing DNA strand. *Tonk. Khim. Tekhnol. = Fine Chem. Technol.* 2021;16(2):148–155 (Russ., Eng.). https://doi.org/10.32362/2410-6593-2021-16-2-148-155

НАУЧНАЯ СТАТЬЯ

Изучение множественного встраивания модифицированных нуклеотидов в растущую цепь ДНК

О.С. Волкова[@], А.В. Чудинов, С.А. Лапа

Институт молекулярной биологии им. В.А. Энгельгардта Российской академии наук, Москва, 119991 Россия
[@]Автор для переписки, e-mail: olechka.volckowa@yandex.ru

Аннотация

Цели. *Целью данной работы является изучение субстратных свойств модифицированных производных трифосфатов дезоксинуклеозидов пуриновой и пиримидиновой природы (5-пропинил-2'-дезоксиуридин-5'-трифосфат, 5-пропинил-2'-дезоксицитидин-5'-трифосфат, 5-метил-2'-дезоксицитидин-5'-трифосфат, N⁶-метил-2'-дезоксиаденозин-5'-трифосфат) при их одновременном встраивании в процессе ферментативных реакций (полимеразной цепной реакции и реакции удлинения праймера).*
Методы. *В работе для изучения субстратной эффективности модифицированных трифосфатов дезоксинуклеозидов использовали методы полимеразной цепной реакции в режиме реального времени и реакции удлинения праймера. Использовали различные попарные сочетания модифицированных производных, в качестве матриц применяли специальным образом сконструированные синтетические фрагменты ДНК и библиотеки для SELEX. Реакции проводили с применением ДНК-полимераз: Taq, Vent (exo-), DeepVent (exo-) и KOD XL.*
Результаты. *В каждом случае из исследуемых соединений выбирали пару соединений (модифицированные dUTP + dCTP, dUTP + dATP, dCTP + dATP) для изучения одновременного встраивания в растущую цепь ДНК. Найдены наиболее эффективные сочетания нуклеотидов для одновременного встраивания, а именно: dU и dC, имеющие 5-пропинильный заместитель. Также найдена наиболее эффективная (из протестированных) ДНК-полимераза: Vent (exo-).*
Выводы. *Выбранные соединения можно использовать для ферментативного получения модифицированных ДНК, в частности аптамеров с расширенными физико-химическими свойствами.*

Ключевые слова: *модифицированные нуклеотиды, модифицированные аптамеры, полимеразная цепная реакция в режиме реального времени, реакция удлинения праймера*

Для цитирования: Волкова О.С., Чудинов А.В., Лапа С.А. Изучение множественного встраивания модифицированных нуклеотидов в растущую цепь ДНК. *Тонкие химические технологии.* 2021;16(2):148–155. https://doi.org/10.32362/2410-6593-2021-16-2-148-155

INTRODUCTION

Modified nucleic acids are currently used in many fields: molecular biology [1], therapy [2], diagnostics [3], and analytical chemistry [4]. Because of their chemical diversity, modified nucleic acids can be used to introduce fluorescent labels into samples and select aptamers [5, 6]. One way to obtain modified nucleic acids is the enzymatic synthesis of DNA or RNA polymerases using modified 2-deoxynucleoside triphosphates (dNTPs) as substrates [7, 8]. Modifications using functional groups (e.g., analogs of amino acid side chains) allow increasing the affinity of aptamers to protein targets [9].

Aptamers are short, single-stranded DNA or RNA molecules that can interact with target molecules. The production of aptamers is performed using the Systematic Evolution of Ligands by Exponential Enrichment (SELEX) technology. Modifying the aptamers' structure improves their physicochemical properties and binding to target molecules [10]. For introducing modifications, the enzymatic method is most often used (in most cases, the primer extension reaction is used) using modified dNTP derivatives. Producing aptamers containing different functional groups can increase their affinity for their targets because of the greater variety of types of aptamer–target interactions.

Early studies report that the simultaneous incorporation of nucleotides with different modifications can improve the properties of the resulting modified aptamers [11]. The main concern when using the enzymatic method is the modified derivatives' substrate compatibility with DNA polymerases.

In this paper, we evaluated the effectiveness of two enzymatic methods—polymerase chain reaction (PCR) and primer extension reaction (PEX)—and compared the effectiveness of different polymerases with no 3'–5' correcting exonuclease activity for the pairwise simultaneous incorporation of modified nucleotides in one growing DNA chain.

EXPERIMENTAL

Modified analogs of dNTPs: All compounds are manufactured by *TriLink BioTechnologies, Inc.* (San Diego, CA, USA): N-2016, N-2017, N-2025, and N-2026.

DNA templates: Synthetic DNA templates with a length of 49 nt were used for PEX, the sequences of which are given below:

M1U 5'-CT**AAAA**CTCT**AAA**CTCT**AA**CTCT**A**CT-*GGCTACCAGTATGGAGCTGACAG*-3'

M1A 5'-CT**TTTT**CTCT**TTT**CTCT**TT**CTCT**T**CT-*GGCTACCAGTATGGAGCTGACAG*-3'

M2UA 5'-CT**TATA**CTCT**ATA**CTCT**TA**CTCT**A**CT-*GGCTACCAGTATGGAGCTGACAG*-3'

M2AU 5'-CT**ATAT**CTCT**TAT**CTCT**AT**CTCT**T**CT-*GGCTACCAGTATGGAGCTGACAG*-3'

The synthetic templates used to study the incorporation of modified dCs have been studied earlier [12].

The nucleotides complementary to the ones under study are marked in bold. The primary areas are highlighted in italics. The sequence of the primer used is the following:

5'-CTGTCAGCTCCATACTGGTAGCC-3'

A combinatorial DNA library and corresponding primers were used for PCR [13].

DNA polymerases used: The following polymerases were used: Taq (*Thermo Scientific*, Waltham, MA, USA), Vent (*exo*-), Deep Vent (*exo*-) (*New England Biolabs*, Ipswich, MA, USA), and KOD XL (NovaTaq™, *Merck KGaA*, Darmstadt, Germany). Polymerases were used in reaction buffers and in concentrations recommended by the manufacturers.

Solid-phase synthesis of template oligonucleotides

The solid-phase synthesis of template oligonucleotides was conducted using an automatic synthesizer ABI 394 DNA/RNA (*Applied Biosystems*, Foster City, CA, USA) according to standard regulations on using commercial solvents and reagents.

Chromatographic purification of template oligonucleotides

For the chromatographic purification of oligonucleotides, a BDS Hypersil C18 (*Thermo Scientific*) column with a size of 250 × 4.6 mm and a particle size of 5 μm was used in the eluent system: buffer A contained 0.1-M TEAA, and buffer B is 50% acetonitrile in buffer A. Both buffers were prepared using Milli-Q and CH_3CN for high-performance liquid chromatography (ChromAR® HPLC, MACRON), filtered using a ZAPCAP-CR Nylon filter (0.22-μm pore size, 47-mm diameter; *Sigma-Aldrich*, St. Louis, MO, USA). The products were separated at a temperature of 25°C. The eluent feed rate is 1 mL/min. The detection was conducted at two wavelengths: λ_1 = 270 nm and λ_2 = 295 nm. BD Syringes 1 mL, without needle (*Becton Dickinson*, Franklin Lakes, NJ, USA). Replacement filters for Acrodisc® LC, 13-mm syringes with a 0.2-μm polyvinylidene fluoride (PVDF) membrane, HPLC certified (*PALL Corporation*, NY, USA).

Primer extension reaction

The reaction mixture contained natural dATP and dGTP (when studying the incorporation of modified deoxyadenosine to natural dGTP and dCTP) at a concentration of 0.2 mM each, as well as various combinations of the dNTPs indicated in Fig. 1; 1.5-U Taq-or 0.5-U Vent (*exo*-) DNA polymerase (the reaction buffer corresponded to the

applied polymerase); a primer for PEX; and one of the synthetic templates. The reaction was performed using a MiniCycler DNA amplifier (*MJ Research Inc.*, Hercules, CA, USA) according to the following program: 5 min at 95°C, 30 s at 65°C, and 40 min at 78°C.

Real-time PCR

We used a mixture similar to that used for the primer extension reaction and two flanking primers instead of one in the case of PEX. The dye EvaGreen (*Biotium*, Moscow, Russia) was added to the reaction mixture to visualize the process. Amplification was performed using an IQ5 device (*Bio-Rad Laboratories*, Inc., Hercules, CA, USA) according to the following program: after preheating at 95°C for 3 min, 40 cycles were performed at 95°C for 20 s, 66°C for 30 s, and 72°C for 40 s. After that, the final incubation was done at 72°C for 5 min.

Determination of chemical yield

The resulting PCR products were separated in a 4% agarose gel. Staining was performed using ethidium bromide. The amounts of the products were estimated from the optical density of the corresponding bands in the gel tracks using the ImageJ program (National Institutes of Health, USA).

RESULTS AND DISCUSSION

Previously, we studied the patterns of the simultaneous incorporation of pyrimidine nucleotides into DNA with complete replacement of the corresponding natural dNTPs [12]. Derivatives with less bulk functional groups have been shown to be better substrates for DNA polymerases. Probably, in the case of the use of electroneutral modifying groups, steric factors play the main role in the formation of a catalytically active “closed” conformation of DNA polymerase in the formation of a complex with a substrate [14, 15, 16].

In this study, we investigated the substrate properties of modified dNTPs (mod-dUTP, mod-dCTP, and mod-dATP) with extended sets of DNA polymerases. Modifications were introduced into the heterocyclic bases of compounds to provide structural differences and possibly create pairs with similar modifications. Nucleotides of purine and pyrimidine nature with similar modifications cannot be considered as complete analogs. Still, their comparison is of interest in identifying the patterns of influence of modifying groups.

The structures of the compounds used are shown in Fig. 1.

PCR and PEX were performed with complete substitution of dTTP, dCTP, and dATP using various pairwise combinations of the modified derivatives. DU + dC, dU + dA, and dC + dA pairs with different or identical modifications were created.

We used a combinatorial DNA library as a template for PCR, which we used earlier in preparing aptamers using SELEX [17], because the substrate

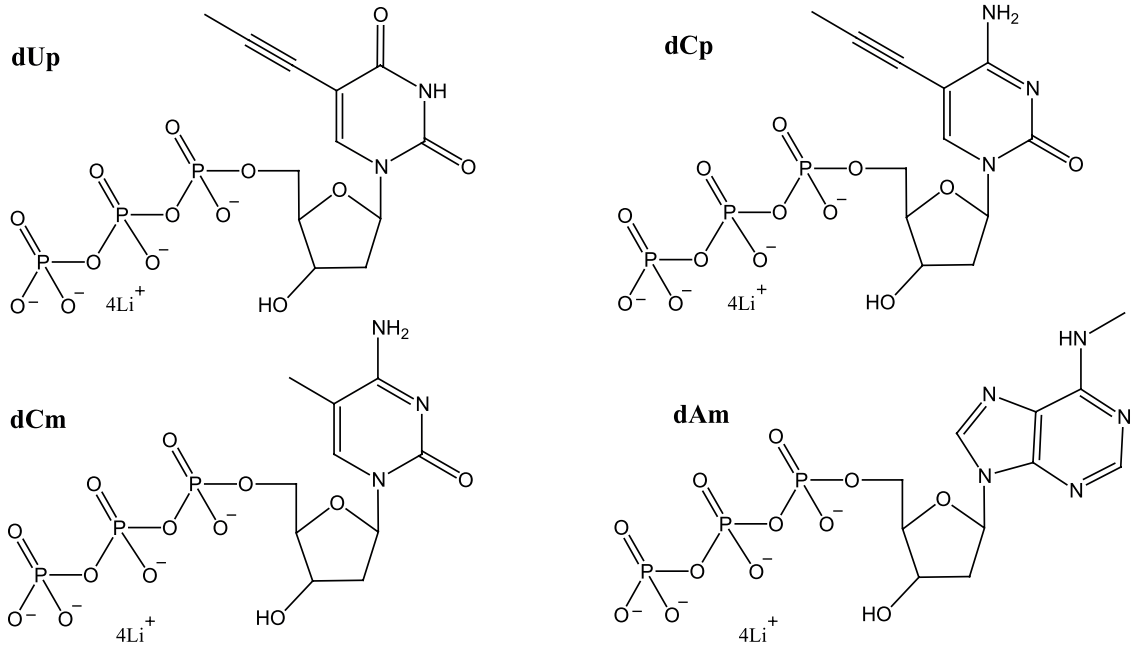

Fig. 1. Modified triphosphates of deoxyuridine, deoxycytidine, and deoxyadenosine.
dUp and dCp are derivatives containing 5-propynyl; dCm and dAm are derivatives containing a methyl group in the 5 and N^6 positions, respectively.

behavior of the modified substrates of polymerases with such template is of particular interest for producing aptamers with new properties (Fig. 2). The most complex substrate for all polymerases was dA with a methyl substituent (dAm). For this substrate, obtaining a product using only the Deep Vent polymerase was possible, but many incomplete products were obtained. When dC (dCm) and dA (dAm) with methyl substituents were simultaneously embedded, the formation of a full-size product was observed.

Using the Taq polymerase with none of the selected modified dNTPs, obtaining full-size products was impossible, except for the variant with a combination of propinyl dU (dUp) and methyl dA (dAm). Both full- and half-size products were formed. The KOD XL polymerase with none of the modified substrates used formed a full-length product, except for dUp, but even in this case, the formation of two products of different lengths was observed.

The Vent (*exo*-) polymerase in this experiment proved to be the most effective enzyme for all the selected combinations, except for dAm. Products could not be obtained using this substrate, but in combination with dCp and dUp, full-size products were reproducibly formed with high efficiency calculated from real-time PCR results.

The PCR analysis showed that the most complex substrates for all the polymerases used are modified derivatives with a methyl substituent. Interestingly, combining triphosphates with propinyl and methyl substituents resulted in a better substrate efficiency than those of derivatives with only a methyl substituent. It should also be noted that polymerases better perceive substrates that have a pyrimidine nature.

We synthesized artificial template oligonucleotides to study the individual and simultaneous integration of dU and dC into one growing DNA chain by the PEX method [12]. Additional ones (the sequences are indicated in the Experimental section) were constructed to the existing synthetic templates to study the patterns of embedding of modified deoxyadenins (nucleotides of purine nature), aimed at understanding the multiple sequential incorporation of modified dA both individually and in pairs with different modified nucleotides of the dU type.

The template M1A is designed to sequentially study the individual incorporation of modified dA 1, 2, 3, and 4 times during primer extension along the template chain. Conducting PEX allows evaluating the effectiveness of the multiple sequential incorporation of mod-dA. It can be seen that the spacer regions of the template do not contain complementary deoxyadenin nucleotides (dT). In addition, compared with the results of pairwise incorporation with dU (on the M2UA and M2AU templates), the spacer plots also do not contain dA.

The M2UA and M2AU templates are designed to study the multiple pairwise incorporation of dA and dU in different sequences, which is reflected in the names of the template oligonucleotides.

In PEX with synthetic templates (Fig. 3), the Taq and Vent (*exo*-) and Deep Vent polymerases could embed both deoxyuridine with a propyl substituent and deoxyadenosine with a methyl substituent.

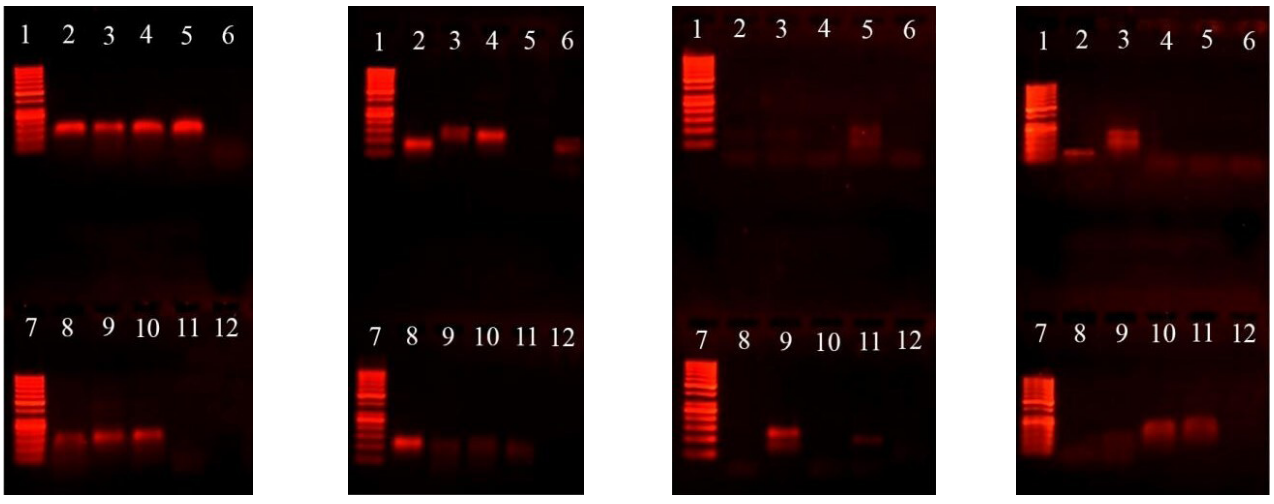

Fig. 2. Polymerase chain reaction electrophoretic analysis using different DNA polymerases and a DNA library.
In each figure: (1) and (7) are GeneRuler 50bp DNA ladder, (2) dT + dC, (3) dUp, (4) dCp, (5) dCm, (6) dAm, (8) dUp + dCp, (9) dUp + dAm, (10) dCp + dAm, (11) dCm + dAm, and (12) negative control.

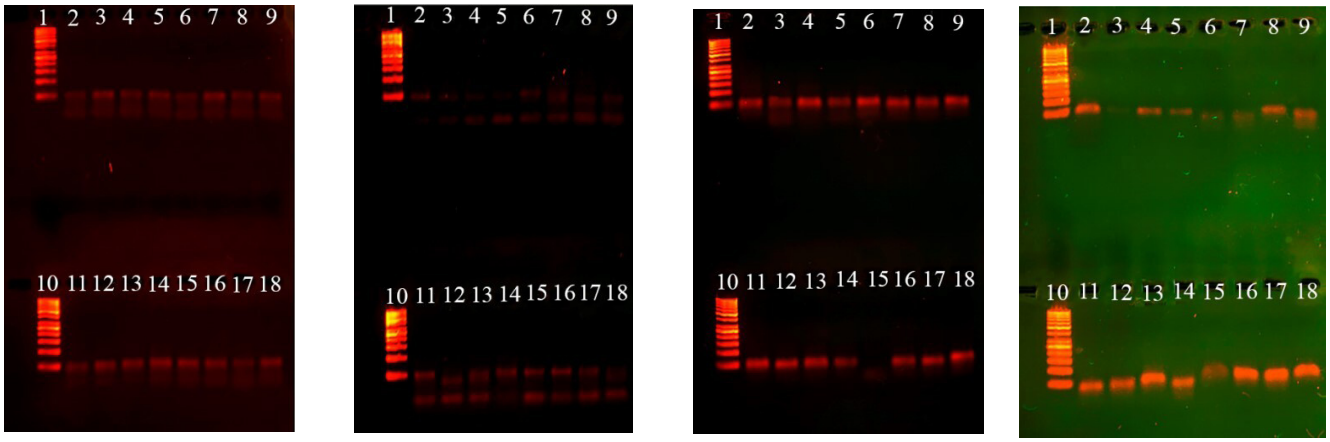

Fig. 3. PEX electrophoretic analysis with various DNA polymerases and specially designed templates. In each figure: (2–5) matrix M1U; (6–9) matrix M1A; (11–14) matrix M2UA; (15–18) matrix M2AU; (1) and (10) length marker for GeneRuler products 50 bp; (2, 6, 11, and 15) dT + dA; 3, 7, 12, and 16) dUp; (4, 8, 13, and 17) dAm; (5, 9, 14, and 18) dUp + dAm.

When using the KOD XL polymerase, products that were somewhat different in mobility were formed, presumably not fully corresponding to the theoretical length of the full-size product. This may be due to the mobility of the modified products in the gel.

It is shown that under the conditions used and for the pairs of modified substrates under study, PEX leads to the more efficient formation of target products than that of PCR. This is due to the slower incorporation kinetics of the modified substrates than those of natural oligonucleotides. Therefore, the advantage of PEX is the length of the voluion time (significantly higher than that in PCR). The results correlate well with previously obtained data [12] and the world practice of using PEX for producing modified aptamers [18].

CONCLUSIONS

The substrate efficiency of the modified compounds used in this study depends on the chemical nature of the modification (massive or compact substituents) and the nucleotide used (purine or pyrimidine bases) and varies for different DNA polymerases. In addition, the enzymatic reaction used significantly affects the formation of full-size modified products. Thus, because of its long elongation time (elongation), the primer extension reaction has an advantage over PCR.

Of the tested compounds, modified dU and dC (i.e., pyrimidine nucleotides) combined with the Vent (*exo*-) DNA polymerase showed the greatest efficiency.

As a result, we obtained DNA modified simultaneously by pairs of nucleotide derivatives of both purine and pyrimidine types. These studies are important for producing DNA with multiple modifications, including a new generation of aptamers.

Acknowledgments

The study was supported by the Russian Foundation for Basic Research, grant No. 19-04-01217.

Authors' contribution

O. S. Volkova – conducting research, preparation of the manuscript;

A.V. Chudinov – academic advising;

S.A. Lapa – design of experiments, editing the manuscript.

The authors declare no conflicts of interest.

REFERENCES

1. Lee K., Rafi M., Wang X., Aran K., Feng X., Lo Sterzo C., *et al*. *In vivo* delivery of transcription factors with multifunctional oligonucleotides. *Nat. Mater.* 2015;14(7):701–706. https://doi.org/10.1038/nmat4269

2. Smith C.I.E., Zain R. Therapeutic oligonucleotides: state of the art. *Annu. Rev. Pharmacol. Toxicol.* 2019;59:605–630. https://doi.org/10.1146/annurev-pharmtox-010818-021050

3. Wandtke T., Wozniak J., Kopinski P. Aptamers in diagnostics and treatments of viral infections. *Viruses.* 2015;7(2):751–780. https://doi.org/10.3390/v7020751

4. Peinetti A.S., Cerertti H., Mizrahi M., Gonzales G.A., Ramires S.A., Requejo F., *et al*. Confined gold nanoparticles enhance the detection of small molecules in label free impedance aptasensors. *Nanoscale.* 2015;7:7763–7769. https://doi.org/10.1039/C5NR01429H

5. Faltin B., Zengerle R., von Stetten F. Current methods for fluorescence-based universal sequence-dependent detection of nucleic acids in homogenous assays and clinical applications. *Clin.Chem.* 2013;59 (11):1567–1582. https://doi.org/10.1373/clinchem.2013.205211

6. Maier K.E., Levy M. From selection hits to clinical leads progress in aptamer discovery. *Mol. Ther. Methods & Clin. Develop.* 2016;5:16014. https://doi.org/10.1038/mtm.2016.14

7. Hocek M. Synthesis of base-modified 2′-deoxyribonucleoside triphosphates and their use in enzymatic synthesis of modified DNA for applications in bioanalysis and chemical biology. *J. Org. Chem.* 2014;79(21):9914–992. https://doi.org/10.1021/jo5020799

8. Kutyavin I.V. Use of base-modified duplex-stabilizing deoxynucleoside 5'-triphosphates to enhance the hybridization properties of primers and probes in polymerase chain reaction. *Biochemistry.* 2008;47(51):13666–13673. https://doi.org/10.1021/bi8017784

9. Rohloff J.C., Gelinas A.D., Jarvis T.C., Ochsner U.A., Schneider D.J., Gold L., Janjic N. Nucleic Acid Ligands with Protein-like Side Chains: Modified Aptamers and Their Use as Diaognostic and Therapeutic Agents. *Mol. Ther. Nucleic Acids.* 2014;3(10):e201. https://doi.org/10.1038/mtna.2014.49

10. Tolle F., Mayer G. Dressed for success – applying chemistry to modulate aptamer functionality. *Chem. Sci.* 2013;4(1):60–67. https://doi.org/10.1039/c2sc21510a

11. Gawande B.N., Rohloff J.C., Carter J.D., von Carlowitz I., Zhang C., Schneider D.J., Janjic N. Selection of DNA aptamers with two modified bases. *Proc. Natl. Acad. Sci.* 2017;114(11):2898–2903. https://doi.org/10.1073/pnas.1615475114

12. Chudinov A.V., Shershov V.E., Pavlov A.S., Volkova O.S., Kuznetsova V.E., Zasedatelev A.S., Lapa S.A. Simultaneous incorporation of modified dU and dC derivativesin the growing DNA chain using PEX and PCR. *Bioorg. Khimiya = Bioorg. Chemistry.* 2020;46(5):546–549 (in Russ.). https://doi.org/10.31857/S0132342320050061

13. Lapa S.A., Romashova K.S., Spitsyn M.A., Shershov V.E., Kuznetsova V.E., Guseinov T.O., Zasedateleva O.A., Radko S.P., Timofeev E.N., Lisitsa A.V., Chudinov A.V. Preparation of modified combinatorial DNA libraries via emulsion PCR with subsequent strand separation. *Mol. Biol.* 2018;52(6):854–864. https://doi.org/10.1134/S0026893318060110

[Original Russian Text: Lapa S.A., Romashova K.S., Spitsyn M.A., Shershov V.E., Kuznetsova V.E., Guseinov T.O., Zasedateleva O.A., Radko S.P., Timofeev E.N., Lisitsa A.V., Chudinov A.V. Preparation of modified combinatorial DNA libraries via emulsion PCR with subsequent strand separation. Molekulyarnaya Biologiya. 2018;52(6):984–996 (in Russ.). https://doi.org/10.1134/S0026898418060113]

14. Berman A.J., Kamtekar S., Goodman J.L., Lázaro de Vega M., Blanco L., Salas M., Steitz T.A. Structures of phi29 DNA polymerase complexed with subsreate: the mechanism of translocation in B-family polymerases. *EMBO J.* 2007;26(14):3494–3505. https://doi.org/10.1038/sj.emboj.7601780

15. Betz K, Malyshev DA, Lavergne T, Welte W, Diederichs K, Dwyer TJ, Ordoukhanian P, Romesberg FE, Marx A. KlenTaq polymerase replicates unnatural base pairs by inducing a Watson-Crick geometry. *Nat Chem Biol*. 2012;8(7):612–614. https://doi.org/10.1038/nchembio.966

16. Hollenstein M. Nucleoside triphosphates – building blocks for the modification of nucleic acids. *Molecules*. 2012;17(11):13569–13591. https://doi.org/10.3390/molecules171113569

17. Lapa S.A., Shershov V.E., Krasnov G.S., Volkova O.S., Kuznetsova V.E., Radko S.P., Zasedatelev A.S., Chudinov A.V. Method of terminal dissociation for the selection of DNA-aptamers. *Bioorg. Khimiya = Bioorg. Chemistry.* 2020;46(4):411–417 (in Russ.). https://doi.org/10.31857/S0132342320040156

18. Gold L., Ayers D., Bertino J., Bock C., Bock A., Brody E.N., Carter J., Dalby A.B., Eaton B.E., Fitzwater T., Flather D., Forbes A., Foreman T., Fowler C., Gawande B., Goss M., Gunn M., Gupta S., Halladay D., Heil J., Heilig J., Hicke B., Husar G., Janjic N., Jarvis T., Jennings S., Katilius E., Keeney T.R., Kim N., Koch T.H., Kraemer S., Kroiss L., Le N., Levine D., Lindsey W., Lollo B., Mayfield W., Mehan M., Mehler R., Nelson S.K., Nelson M., Nieuwlandt D., Nikrad M., Ochsner U., Ostroff R.M., Otis M., Parker T., Pietrasiewicz S., Resnicow D.I., Rohloff J., Sanders G., Sattin S., Schneider D., Singer B., Stanton M., Sterkel A., Stewart A., Stratford S., Vaught J.D., Vrkljan M., Walker J.J., Watrobka M., Waugh S., Weiss A., Wilcox S.K., Wolfson A., Wolk S.K., Zhang C., Zichi D. Aptamer-based multiplexed proteomic technology for biomarker discovery. *PLoS One.* 2010;5(12):e15004. https://doi.org/10.1371/journal.pone.0015004

About the authors:

Olga S. Volkova, Laboratory Assistant, Engelhardt Institute of Molecular Biology, Russian Academy of Sciences (32, Vavilova ul., Moscow, 119991, Russia). E-mail: olechka.volckowa@yandex.ru. https://orcid.org/0000-0003-1328-771X

Alexander V. Chudinov, Cand. Sci. (Chem.), Head of the Laboratory, Engelhardt Institute of Molecular Biology, Russian Academy of Sciences (32, Vavilova ul., Moscow, 119991, Russia). E-mail: chud@eimb.ru. Scopus Author ID 7003833018, https://orcid.org/0000-0001-5468-4119

Sergey A. Lapa, Cand. Sci. (Biol.), Researcher, Engelhardt Institute of Molecular Biology, Russian Academy of Sciences (32, Vavilova ul., Moscow, 119991, Russia). E-mail: lapa@biochip.ru. Scopus Author ID 6603461000, https://orcid.org/0000-0003-1328-771X

Об авторах:

Волкова Ольга Сергеевна, лаборант, ФГБУН Институт молекулярной биологии РАН им. В.А. Энгельгардта (119991, Россия, Москва, ул. Вавилова, д. 32). E-mail: olechka.volckowa@yandex.ru. https://orcid.org/0000-0003-1328-771X

Чудинов Александр Васильевич, к.х.н., заведующий лабораторией, ФГБУН Институт молекулярной биологии РАН им. В.А. Энгельгардта (119991, Россия, Москва, ул. Вавилова, д. 32). E-mail: chud@eimb.ru. Scopus Author ID 7003833018, https://orcid.org/0000-0001-5468-4119

Лапа Сергей Анатольевич, к.б.н., научный сотрудник. ФГБУН Институт молекулярной биологии РАН им. В.А. Энгельгардта (119991, Россия, Москва, ул. Вавилова, д. 32). E-mail: lapa@biochip.ru. Scopus Author ID 6603461000, https://orcid.org/0000-0002-9011-134X

The article was submitted: February 20, 2021; approved after reviewing: March 12, 2021; accepted for publication: April 02, 2021.

Translated from Russian into English by N. Isaeva
Edited for English language and spelling by Enago, an editing brand of Crimson Interactive Inc.

CHEMISTRY AND TECHNOLOGY OF MEDICINAL COMPOUNDS AND BIOLOGICALLY ACTIVE SUBSTANCES

ХИМИЯ И ТЕХНОЛОГИЯ ЛЕКАРСТВЕННЫХ ПРЕПАРАТОВ И БИОЛОГИЧЕСКИ АКТИВНЫХ СОЕДИНЕНИЙ

ISSN 2686-7575 (Online)

https://doi.org/10.32362/2410-6593-2021-16-2-156-166

UDC 547.464.7

RESEARCH ARTICLE

Synthesis of ethers containing 1,3-dioxolane and *gem*-dichlorocyclopropane fragments

Shakhobiddin Sh. Dzhumaev[1], Yulianna G. Borisova[1,@], Gul'nara Z. Raskil'dina[1], Ulyana Sh. Kuzmina[2], Rustem R. Daminev[3], Simon S. Zlotskii[1]

[1]Ufa State Petroleum Technological University, Ufa, 450062 Russia
[2]Institute of Biochemistry and Genetics, Ufa Federal Research Center, Russian Academy of Sciences, Ufa, 450054 Russia
[3]Ufa State Petroleum Technological University, Branch in Sterlitamak, Sterlitamak, 453118 Russia
[@]Corresponding author, e-mail: yulianna_borisova@mail.ru

Abstract

Objectives. *This study aimed to obtain ethers containing gem-dichlorocyclopropane and 1,3-dioxolane fragments and evaluate their cytotoxic properties against HEK293, SH-SY5Y, MCF-7, and A549 cell lines.*

Methods. *The qualitative and quantitative compositions of the reaction masses were determined using mass spectrometry (using a Chromatek-Kristall 5000M device with the 2012 National Institute of Standards and Technology, USA database) and nuclear magnetic resonance spectroscopy (using a Bruker AM-500 device with operating frequencies of 500 and 125 MHz).*

Results. *Ethers containing gem-dichlorocyclopropane and 1,3-dioxolane fragments were synthesized in the presence of a catamine AB catalyst. The structures of the obtained substances were confirmed using gas-liquid chromatography, mass spectrometry, and nuclear magnetic resonance spectroscopy. The cytotoxicity of the esters was studied against HEK293, SH-SY5Y, MCF-7, and A549 cell lines.*

Conclusions. *Ethers containing gem-dichlorocyclopropane and 1,3-dioxolane fragments were obtained in quantitative yields; however, only 4-{[(2,2-dichloro-3-{[(2,2-dichlorocyclopropyl) methoxy]methyl}cyclopropyl)methoxy]methyl}-2,2-dimethyl-1,3-dioxolane exhibited cytotoxic activity against HEK293, SH-SY5Y, MCF-7, and A549 cell lines.*

Keywords: *2,2-dimethyl-4-hydroxymethyl-1,3-dioxolane, carbenation, cell lines, cytotoxicity*

For citation: Dzhumaev Sh.Sh., Borisova Yu.G., Raskil'dina G.Z., Kuzmina U.Sh., Daminev R.R., Zlotskii S.S. Synthesis of ethers containing 1,3-dioxolane and *gem*-dichlorocyclopropane fragments. *Tonk. Khim. Tekhnol. = Fine Chem. Technol.* 2021;16(2):156–166 (Russ., Eng.). https://doi.org/10.32362/2410-6593-2021-16-2-156-166

НАУЧНАЯ СТАТЬЯ

Синтез простых эфиров, содержащих 1,3-диоксолановый и *гем*-дихлорциклопропановый фрагменты

Ш.Ш. Джумаев[1], Ю.Г. Борисова[1,@], Г.З. Раскильдина[1], У.Ш. Кузьмина[2], Р.Р. Даминев[3], С.С. Злотский[1]

[1]Уфимский государственный нефтяной технический университет, Уфа, 450064 Россия
[2]Институт биохимии и генетики УФИЦ РАН, Уфа, 450054 Россия
[3]Уфимский государственный нефтяной технический университет, филиал в г. Стерлитамак, Стерлитамак, 453118 Россия
[@]Автор для переписки, e-mail: yulianna_borisova@mail.ru

Аннотация

Цели. *Получить простые эфиры, содержащие гем-дихлорциклопропановый и 1,3-диоксолановый фрагменты и оценить их цитотоксические свойства в отношении клеточных линий HEK293, SH-SY5Y, MCF-7 и A549.*
Методы. *Для определения качественного и количественного состава реакционных масс были использованы следующие методы анализа: газожидкостная хроматография (на аппаратно-программном комплексе «Кристалл 2000»), масс-спектрометрия (на приборе «Хроматэк-Кристалл 5000М» с базой NIST 2012), и спектроскопия ядерного магнитного резонанса (ЯМР-спектроскопия) (на приборе «Bruker AM-500» с рабочими частотами 500 и 125 МГц).*
Результаты. *Синтезированы простые эфиры, содержащие гем-дихлорциклопропановый и 1,3-диоксолановый фрагменты в присутствии катализатора катамина АВ. Строение полученных веществ было подтверждено с помощью газожидкостной хроматографии, масс-спектрометрии и ЯМР-спектроскопии. Для эфиров изучена цитотоксическая активность в отношении клеточных линий HEK293, SH-SY5Y, MCF-7 и A549.*
Выводы. *С количественными выходами получены простые эфиры, содержащие гем-дихлорциклопропановый и 1,3-диоксолановый фрагменты. Установлено, что цитотоксическую активность в отношении клеточных линий HEK293, SH-SY5Y, MCF-7 и A549 среди ряда полученных соединений проявляет только 4-{[(2,2-дихлоро-3-{[(2,2-дихлорциклопропил)метокси]метил}циклопропил)метокси]метил}-2,2-диметил-1,3-диоксолан.*

Ключевые слова: *2,2-диметил-4-оксиметил-1,3-диоксолан, карбенирование, клеточные линии, цитотоксичность*

Для цитирования: Джумаев Ш.Ш., Борисова Ю.Г., Раскильдина Г.З., Кузьмина У.Ш., Даминев Р.Р., Злотский С.С. Синтез простых эфиров, содержащих 1,3-диоксолановый и *гем*-дихлорциклопропановый фрагменты. *Тонкие химические технологии.* 2021;16(2):156–166. https://doi.org/10.32362/2410-6593-2021-16-2-156-166

INTRODUCTION

Compounds containing cycloacetal and *gem*-dichlorocyclopropane fragments are important intermediate and final products in the pharmaceutical, perfume, and polymer industries and, depending on the structure of the substituents, exhibit a wide spectrum of biological activity [1–10]. For example, 2-{(4R)-4[(benzyloxy)-methyl]-1,3-dioxolan-2-yl}phenol, diisopropyl-(4R-5R)-2-(2-hydroxyphenyl)-1,3-dioxolane-4,5-dicarboxylate, diisopropyl-2-(2-hydroxyphenyl)-1,3-dioxolane-4,5-dicarboxylate, dimethyl 2-(2-hydroxyphenyl)-1,3-dioxolane-4,5-dicarboxylate, and 2-[(4S,5S)-4,5-bis(benzyloxymethyl)-1,3-dioxolane-2-yl] phenol have been shown to exhibit pronounced antibacterial properties against *Staphylococcus aureus* and *Staphylococcus epidermidis* as well as antifungal activity against *Candida albicans* [5].

Özkanli and co-authors, demonstrated that new derivatives of 2-acetylnaphthalene with the dioxolane structure have an anticonvulsant effect [11]. In addition, it has been shown that 1,3-dioxolane heterocyclic compounds are not only effective anticancer agents but are able to overcome the phenomenon of multidrug resistance, which is one of the main problems in successful cancer therapy [12]. We have previously reported compounds containing 1,3-dioxolane and *gem*-dichlorocyclopropane fragments with potential antitumor activity [3], and these heterocyclic compounds have also been shown to have herbicidal [1], antioxidant [3], antiviral [13, 14], anticoagulant, antiaggregatory [7], and anesthetic [15] activities. This breadth of activities and the fact that many groups are only partially studied means that the synthesis of novel 1,3-dioxolane and *gem*-dichlorocyclopropane fragment-containing compounds is a promising route to finding biologically active substances.

This study aimed to develop new methods for preparing novel bi- and polycyclic compounds, where 1,3-dioxolane and *gem*-dichlorocyclopropane fragments are bound by the stable but mobile CH_2–O–CH_2 group in acidic and alkaline media, as well as assessing their cytotoxic properties *in vitro*.

MATERIALS AND METHODS

The analysis of the reaction masses and the recording of the mass spectra of the compounds were carried out on a Chromatec-Kristall 5000M (*CHROMATEC*, Russia) hardware–software complex using the National Institute of Standards and Technology 2012 database (NIST, USA). The analysis conditions were as follows: 30 m long capillary quartz column, 20 min duration, 260°C ion source, 300°C transition line, 30–300 Da scanning range, 37–43 mTorr pressure, helium carrier gas, and a heating rate of 20°C/min. The mass spectra of the compounds were obtained using electron impact ionization. ^{1}H and ^{13}C nuclear magnetic resonance (NMR) spectra were recorded using a Bruker AM-500 spectrometer (*Bruker Corporation*, USA) with operating frequencies of 500 and 125 MHz, respectively, and a $CDCl_3$ solvent. The chemical shifts were reported on a δ (ppm) scale relative to an internal tetramethylsilane standard. Spin-spin coupling constants (*J*) were recorded in Hz.

Synthesis of 2,2-dimethyl-4-hydroxymethyl-1,3-dioxolane 1. A mixture of 0.49 mol of glycerol, 49 mol of acetone, and 0.22 g of *p*-toluenesulfonic acid was vigorously stirred at room temperature for 18 h followed by the addition of 3 g (anhydrous) K_2CO_3 and stirring for 1 h. The mixture was then filtered, concentrated, and the residue distilled at reduced pressure.

Physicochemical constants corresponded with previously reported data [16–22].

Synthesis of compounds 4–6, 11, and 15. Catamin-AB catalyst (0.22 g) and 100 g of 50% NaOH solution were added with vigorous stirring at 50°C (or 30°C for allyl chloride) to a solution of 0.06 mol 2,2-dimethyl-4-hydroxymethyl-1,3-dioxolane in 60 mL of benzene. After 2 h, 0.30 mol of the corresponding halogenated derivatives were added dropwise. Upon completion of the reaction, the mixture was washed with water, extracted with ethoxyethane (3 × 30 mL), and dried over anhydrous $MgSO_4$. Following the removal of the solvent, the residue was distilled under reduced pressure (a detailed procedure is described in [23]).

According to this method, the following were obtained:

4-[(Allyloxy)methyl]-2,2-dimethyl-1,3-dioxolane 4. The NMR spectrum of the compound is given in [24]. Yield (**4**) 90%, boiling temperature bp = 52–54°C (10 mm Hg). Mass spectrum, *m*/*z* (I_{rel}, %): 172 (≤2) [M]+, 157/70, 101/100, 73/25, 55/30.

4-({[(2Z)-4-chlorobut-2-en-1-yl]oxy}-methyl)-2,2-dimethyl-1,3-dioxolane 5. Yield (**5**) 80%, bp = 81–83°C (5 mm Hg). ^{1}H NMR spectrum ($CDCl_3$), δ, ppm (*J*, Hz): 1.33 t (3H, CH_3, *J* = 7.0), 1.40 t (3H, CH_3, *J* = 7.3), 3.44 t (1H, C^6H_a, *J* = 9.9, 5.2), 3.51 d (1H, C^6H_b, *J* = 10.0, 3.0), 3.70 t (1H, C^5H_a, *J* = 8.2, 6.4), 4.03 d (1H, C^5H_b, *J* = 8.2, 6.5), 4.09 d (2H, C^7H_2, *J* = 11.8, 7.5), 4.14 d (2H, $C^{10}H_2$, *J* = 11.1, 5.8), 4.22–4.27 m (1H, C^4H), 5.69–5.81 m (2H, C^8H, C^9H). ^{13}C NMR spectrum ($CDCl_3$), δ_C, ppm: 25.31 (CH_3), 26.68 (CH_3), 38.98 (C^{10}), 63.88 (C^5), 66.62 (C^6), 71.33 (C^7), 74.65 (C^4), 109.44 (C^2), 128.37 (C^8), 130.53 (C^9). Mass spectrum, *m*/*z* (I_{rel}, %): 220/222 (≤1) $[M]^+$, 205/207 (40/15), 115/117 (10/5), 101/100, 89/91 (55/30), 73 (25), 43 (90).

4,4-[(2Z)-but-2-en-1,4-diyl(oxymethylene)]-bis-(2,2-dimethyl-1,3-dioxolane) 6. Yield (**6**) 60%, bp = 101–103°C (3 mm Hg). ^{1}H NMR spectrum

($CDCl_3$), δ, ppm (*J*, Hz): 1.35 s (6H, 2 CH_3), 1.42 s (6H, 2 CH_3), 3.44 t (2H, $C^{6+6"}H_a$, *J* = 9.1, 6.9), 3.51 d (2H, $C^{6+6"}H_b$, *J* = 10.7, 7.0), 3.72 t (2H, $C^{5+5"}$Ha, *J* = 8.0, 6.2), 4.00 d (2H, $C^{5+5"}$Hb, *J* = 8.2, 6.1), 4.08 dt (4H, $C^{7+10}H_a$, *J* = 11.8, 7.5), 4.15 dd (4H, $C^{7+10}H_b$, *J* = 11.1, 5.8), 4.24–4.29 m (1H, $C^{4+4"}$H), 5.69–5.81 m (2H, C^8H, C^9H). ^{13}C NMR spectrum ($CDCl_3$), δ_C, ppm: 25.28 (CH_3), 26.44 (CH_3), 64.23 ($C^{5+5"}$), 66.62 ($C^{6+6"}$), 71.35 (C^{7+10}), 73.69 ($C^{4+4"}$), 109.44 ($C^{2+2"}$), 127.32 (C^8), 130.55 (C^9). Mass spectrum, *m*/*z* (I_{rel}, %): 316 (≤1) $[M]^+$, 300 (70), 215 (50), 101 (100), 73 (20), 43 (70).

4-({[(2Z)-4-(alloxy)-but-2-en-1-yl]oxy}methyl)-2,2-dimethyl-1,3-dioxolane 11. Yield (**11**) 40%, bp = 99–101°C (4 mm Hg). ^{1}H NMR spectrum ($CDCl_3$), δ, ppm (*J*, Hz): 1.41 t (3H, CH_3, *J* = 7.7), 1.45 t (3H, CH_3, *J* = 7.5), 3.45 t (1H, C^6H_a, *J* = 8.9, 5.9), 3.54 д (1H, C^6H_b, *J* = 10.0), 3.74 t (1H, C^5H_a, *J* = 8.0, 6.0), 4.11 d (1H, C^5H_b, *J* = 8.2), 3.72 t (1H, $C^{11}H_a$, *J* = 10.3, 5.8), 4.06 d (3H, $C^{11}H_b$, *J* = 5.9), 4.09 d (2H, C^7H_2, *J* = 7.7), 4.17 t (2H, $C^{10}H_2$, *J* = 10.4, 5.9), 4.25–4.29 m (1H, C^4H), 5.18 d (1H, $C^{13}H_a$, *J* = 1.3, 10.4), 5.26 d (1H, $C^{13}H_b$, *J* = 15.0), 5.83–5.93 m (1H, C^{12}H), 5.70–5.81 m (2H, C^8H, C^9H). ^{13}C NMR spectrum ($CDCl_3$), δ_C, ppm: 25.31 (CH_3), 26.68 (CH_3), 63.84 (C^{10}), 65.30 (C^5), 67.02 (C^6), 67.77 (C^7), 69.32 (C^{11}), 71.55 (C^4), 107.50 (C^2), 122.92 (C^{13}), 127.93 (C^9), 131.02 (C^8). 132.53 (C^{12}). Mass spectrum, *m*/*z* (I_{rel}, %): 242 (≤3) $[M]^+$, 300 (70), 275 (60), 215 (35), 145 (60), 101 (100), 73 (34), 43 (50).

4-[(benzyloxy)methyl]-2,2-dimethyl-1,3-dioxolane 15. ЯМР спектр соединения описан в работе [25]. Yield (**15**) 90%, bp = 138°C (5 mm Hg). Mass spectrum *m*/*z* (I_{rel}, %): 222 (≤1) $[M]^+$, 207 (27), 164 (34), 101 (41), 91 (100), 43 (23).

4-[(2-chloromethyl-benzyloxy)methyl]-2,2-dimethyl-1,3-dioxolane 16. Yield (**16**) 90%, bp = 138°C (5 mm Hg). ^{1}H NMR spectrum ($CDCl_3$), δ, ppm (*J*, Hz): 1.33 t (3H, CH_3, *J* = 7.5), 1.41 t (3H, CH_3, 6.8), 3.49 t (1H, C^6H_a, *J* = 11.5), 3.54 d (1H, C^6H_b, *J* = 11.2), 3.67 t (1H, C^5H_a, *J* = 9.6), 3.78 d (1H, C^5H_b, *J* = 10.0), 4.45–4.82 m (1H, C_4H), 4.89 (s, 1H, C^8H_a), 4.91 (s, 1H, C^8H_a), 7.07–7.16 m (4H, 4 CH). ^{13}C NMR spectrum, δ_C, ppm: 25.47 (CH_3), 26.54 (CH_3), 47.13 (C^8H_2), 66.43 (C^5H_2), 67.83 (C^6H_2), 68.37 (C^7H_2), 68.28 (C^4H), 105.29 (C^2), 127.07–139.61 (Ph). Масс-спектр *m*/*z* (I_{rel}, %): 270/272 (≤1) $[M]^+$, 255/257 (25/5), 101 (40), 73 (56), 91 (70), 77 (100), 41 (30).

Synthesis of compounds 7–9 and 12. Compounds **7**–**9** and **12** were obtained similarly to the procedure [25–27] using chloroform, 50% alkali solution, and catamine AB phase transfer catalyst.

4-{[(2,2-dichlorocyclopropyl)methoxy]-methyl}-2,2-dimethyl-1,3-dioxolane 7. Yield (**7**) 70%, bp = 74–76°C (8 mm Hg). ^{1}H NMR spectrum ($CDCl_3$), δ, ppm (*J*, Hz): 0.95–0.1.04 m (1H, C^8H), 1.37 t (3H, CH_3, *J* = 7.0), 1.43 t (3H, CH_3, 6.8), 1.62 t (1H, C^9H_a, *J* = 5.3), 1.68 d (1H, C^9H_b, *J* = 5.4), 3.45 t (1H, C^7H_a, *J* = 11.0, 7.0), 3.57 d (1H, C^7H_b, *J* = 11.2), 3.61 t (1H, C^6H_a, *J* = 9.0, 7.0), 3.69 d (1H, C^6H_b, *J* = 8.9), 3.84 d (1H, C^5H_a, *J* = 6.0), 4.02 t (1H, C^5H_b, *J* = 6.7), 4.33–4.38 m (1H, C^4H). ^{13}C NMR spectrum, δ_C, ppm: 24.52 (CH_2), 25.46 (CH_3), 27.34 (CH_3), 28.49 (CH), 61.03 (C), 67.83 (CH_2), 68.58 (CH_2), 69.42 (CH_2), 69.78 (CH), 108.96 (C). Mass spectrum, *m*/*z* (I_{rel}, %): 225/227/229 (≤3) $[M]^+$, 219/221 (40/15), 145 (45), 115/117 (30/8), 101 (100), 89/91 (60/35), 43 (80).

4-({[2,2-dichloro-3-(chloromethyl)-cyclopropyl]methoxy}methyl)-2,2-dimethyl-1,3-dioxolane 8. Yield (**8**) 50%, bp = 88–90°C (8 mm Hg). ^{1}H NMR spectrum ($CDCl_3$), δ, ppm (*J*, Hz): 1.36 t (3H, CH_3, *J* = 7.0), 1.41 t (3H, CH_3, *J* = 6.8), 1.54–1.58 m (1H, C^8H), 1.78–1.85 m (1H, C^9H), 3.46 t (1H, C^7H_a, *J* = 9.0), 3.51 d (1H, C^7H_b, *J* = 9.3), 3.63 t (1H, $C^{10}H_a$, *J* = 9.2), 3.71 d (1H, $C^{10}H_b$, *J* = 8.8), 3.88 d (1H, C^6H_a, *J* = 6.5), 3.93 t (1H, C^6H_b, *J* = 6.6), 4.04 d (1H, C^5H_a, *J* = 6.8), 4.07 t (1H, C^5H_b, *J* = 6.5), 4.28–4.35 m (1H, C^4H). ^{13}C NMR spectrum, δ_C, ppm: 24.48 (CH_3), 25.49 (CH_3), 34.87 (C^9H), 36.39 (C^8H), 43.42 ($C^{10}H_2$), 63.06 (C), 67.86 (C^6H_2), 68.73 (C^7H_2), 69.42 (C^5H_2), 71.74 (C^4H), 108.69 (C^2). Mass spectrum, *m*/*z* (I_{rel}, %): 304/306/308 (≤2) $[M]^+$, 269/271/273 (35/15/4), 219/221 (60/45), 145/65, 101/100, 89/91 (30/15), 41 (70).

4.4-[(3,3dichlorocyclopropane-1,2-diyl) bis(methyleneoxymethylene)]bis(2,2-dimethyl-1,3-dioxolane) 9. Yield (**9**) 60%, bp = 102–104°C (5 mm Hg). ^{1}H NMR spectrum ($CDCl_3$), δ, ppm (*J*, Hz): 1.29 t (3H, CH_3, *J* = 6.9), 1.34 t (3H, CH_3, *J* = 6.7), 2.24 dt (2H, 2 C^{8+9}H, *J* = 5.9, 8.9), 3.39 t (2H, 2 $C^{7+10}H_a$, *J* = 10.9), 3.42 d (2H, 2 $C^{7+10}H_b$, *J* = 10.2), 3.56 t (2H, 2 $C^{6+6"}H_a$, *J* = 9.6), 3.63 d (2H, 2 $C^{6+6"}H_b$, *J* = 8.2), 3.82 d (2H, 2 $C^{5+5"}H_a$, *J* = 6.4), 4.00 t (2H, 2 $C^{5+5"}H_b$, *J* = 6.6), 4.45–4.60 m (2H, 2 $C^{4+4"}$H). ^{13}C NMR spectrum, δ_C, ppm: 25.45 (CH_3), 26.30 (CH_3), 34.76 (2 C^{8+9}H), 64.55 (C), 67.93 (2 $C^{5+5"}H_2$), 68.81 (2 $C^{7+10}H_2$), 72.66 (2 $C^{6+6"}H_2$), 72.75 (2 $C^{4+4"}$H), 106.44 (C). Mass spectrum, *m*/*z* (I_{rel}, %): 400/402/404 (≤10) $[M]^+$, 384/386/388 (30/14/6), 298/300/302 (40/22/12), 145/40, 115/117 (32/11), 101/100, 89/91 (80/30), 43 (80), 41 (50).

4-{[(2,2-dichloro-3-{[(2,2-dichlorocyclopropyl)-methoxy]methyl}-cyclopropyl)methoxy]methyl}-2,2-dimethyl-1,3-dioxolane 12. Yield (**12**) 50%, bp = 134–136°C (2 mm Hg). ^{1}H NMR spectrum ($CDCl_3$), δ, ppm (*J*, Hz): 0.90–1.01 m (1H, C^{12}H), 1.26 t (3H, CH_3, *J* = 6.4), 1.31 t (3H, CH_3, *J* = 6.3), 1.57 t (1H, $C^{13}H_a$, *J* = 6.9), 1.62 d (1H, $C^{13}H_b$, *J* = 5.9), 2.05 qu (1H, C^8H, *J* = 9.7), 2.23 qu (1H, C^9H, *J* = 9.9), 3.56–3.61 m (4H, 2 $C^{7+10}H_2$), 3.66 t (1H, $C^{11}H_a$, *J* = 10.0), 3.73 d

(1H, $C^{11}H_b$, J = 9.9), 3.85 d (1H, C_6H_a, J = 7.9), 4.00 t (1H, C^6H_b, J = 6.9), 4.22 d (1H, C^5H_a, J = 6.9), 4.25 t (1H, C^5H_b, J = 7.8), 4.42–4.63 m (1H, C^4H). ^{13}C NMR spectrum, δ_C, ppm: 24.44 ($C^{13}H_2$), 25.45 (CH_3), 26.30 (CH_3), 28.56 ($C^{12}H$), 35.39 (2 $C^{8+9}H$), 61.20 (C), 63.91 (C), 67.58 (C^5H_2), 67.92 ($C^{10}H_2$), 69.34 ($C^{11}H_2$), 70.62 (C^6H_2), 71.28 (C^7H_2), 72.55 (C^4H), 110.29 (C). Mass spectrum, m/z (I_{rel}, %): 408/410/412/414 (≤5) $[M]^+$, 393/395/397/399 (35/40/16/9/3), 372/374/376/378 (17/25/8/3), 298/300/302 (60/35/18), 154/156/158 (55/36/14), 115/117 (32/11), 101/100, 89/91 (70/25), 41 (70).

Assessment of the cytotoxicity of the substances *in vitro*

The cytotoxicity of the substances was studied using SH-SY5Y (human neuroblastoma), A549 (human lung adenocarcinoma), and MCF-7 (adenocarcinoma of the human mammary gland ducts) tumor cell lines and the HEK293 (immortalized human embryonic kidney cells) normal cell line, which were obtained from the Russian collection of cell cultures (Institute of Cytology, Russian Academy of Sciences, St. Petersburg). HEK293 cells (25×10^3 cells per well), SH-SY5Y (50×10^3 cells per well), MCF-7 (12×10^3 cells per well), and A549 (10×10^3 cells per well) were seeded in 96-well plates in 100 μL of DMEM medium containing 10% FBS (*Gibco*, USA), 2 mM L-glutamine (*PanEco*, Russia), and 50 μg/mL gentamicin (*Biolot*, Russia). After 24 h, the candidate substances were added to the cells at concentrations of 1, 10, and 100 μM in 0.1% DMSO, followed by incubation for 48 h at 37°C in 5% CO_2. The cytotoxic properties of the substances were then assessed using PrestoBlue® vital dye according to the manufacturer's protocol (*Invitrogen*, USA), and fluorescence was detected using a 2300 EnSpire® Multimode Plate Reader (*Perkin Elmer*, USA). The IC_{50} value (substance concentration at which 50% inhibition of cell viability is observed) was calculated using the GraphPad Prizm 4.0 program (*GraphPad Software Inc.*, USA).

The selectivity index (SI) of each substance was determined to reveal the possible selectivity of its cytotoxic effects against tumor cells, i.e., its potential antitumor properties. The HEK293 cell line served as control cells of normal origin, and the SI of the substance was calculated as the ratio of the IC_{50} value in HEK293 cells to the IC_{50} in tumor cells.

Statistical analysis of the obtained data was carried out using the standard Statistica 6.1 software package (*StatSoft Inc.*, USA). The results were presented as the arithmetic mean of 3 independent experiments (M), including the standard error of the mean (±m). Analysis of variance using the Dunnett's test was used to determine the significance of differences in the IC_{50} values of the substances between cells of normal and tumor origin.

RESULTS AND DISCUSSION

The *O*-alkylation of 2,2-dimethyl-4-hydroxymethyl-1,3-dioxolane **1** with allyl chloride **2** and *cis*-1,4-dichlorobutene-2 **3** resulted in the corresponding ethers **4**–**6** being obtained in yields of 60–90%. The subsequent dichlorocarbenation of compounds **4**–**6** according to a previously reported procedure [25–27] synthesized products **7**–**9** in yields of 50–70%, which contained heterocyclic and carbocyclic fragments (Scheme 1).

Chloromethyl derivative **5** was used for the *O*-alkylation of allyl alcohol **10**, which produced compound **11** with two double bonds in a yield of 40%. Its exhaustive dichlorocarbenation led to diester **12** (50% yield), which contained one 1,3-dioxolane and two *gem*-dichlorocyclopropane fragments (Scheme 1).

Competitive kinetics was used to determine the relative reactivity of chlorides **2** and **3** in the reaction with 2,2-dimethyl-4-hydroxymethyl-1,3-dioxolane **1**. Judging by the rate of product accumulation of **4** and **5**, allyl chloride **2** was 2 times more active than *cis*-1,4-dichlorobutene-2 **3**. By considering the number of reaction centers, the CH_2Cl group in olefin **2** is 4 times more active than the analogous group in compound **3**, which is likely due to the chlorine atoms in position 1 and 4 making it difficult for the bulky alcoholate to approach the CH_2–Cl group. This assumption was confirmed by the competitive *O*-alkylation of 2,2-dimethyl-4-hydroxymethyl-1,3-dioxolane **1** with benzyl chloride **13** and 1,2-dichloromethylbenzene **14** (Scheme 2) resulting in the accumulation of esters **15** and **16**, which means that monochloride **13** is also 1.5 times more active than dichloride **14**.

The structures of **4**–**9**, **11**, **12**, **15**, and **16** were elucidated by ^1H and ^{13}C NMR spectroscopy and chromatomass spectrometry.

The initial biological screening of new substances, regardless of their intended use, is the assessment of their basic cytotoxicity *in vitro*, which is defined as the negative effect of chemical compounds on the vital functions of the cell, e.g., damage to cell membranes, disruption of the metabolic activity of cells, changes in the processes of cell division, and protein synthesis. Continuous cell lines of various origins are used in this analysis.[1] The *in vitro* cytotoxicity assessment of polycyclic compounds **7**–**9** and **12** was performed using normal (HEK293) and tumor (SH-SY5Y, MCF-7, A549) cell lines to reveal both possible cytotoxicity and also the selectivity of their action, e.g., organ specificity or antitumor activity. The PrestoBlue® test used for

[1] Vakhitova Yu.V., Tselousova O.S. *Kletochnye mekhanizmy toksichnosti ksenobiotikov* (*Cellular mechanisms of xenobiotic toxicity*). Textbook. 2nd ed., revised and add. Ufa: BSPU, 2015. 104 p.

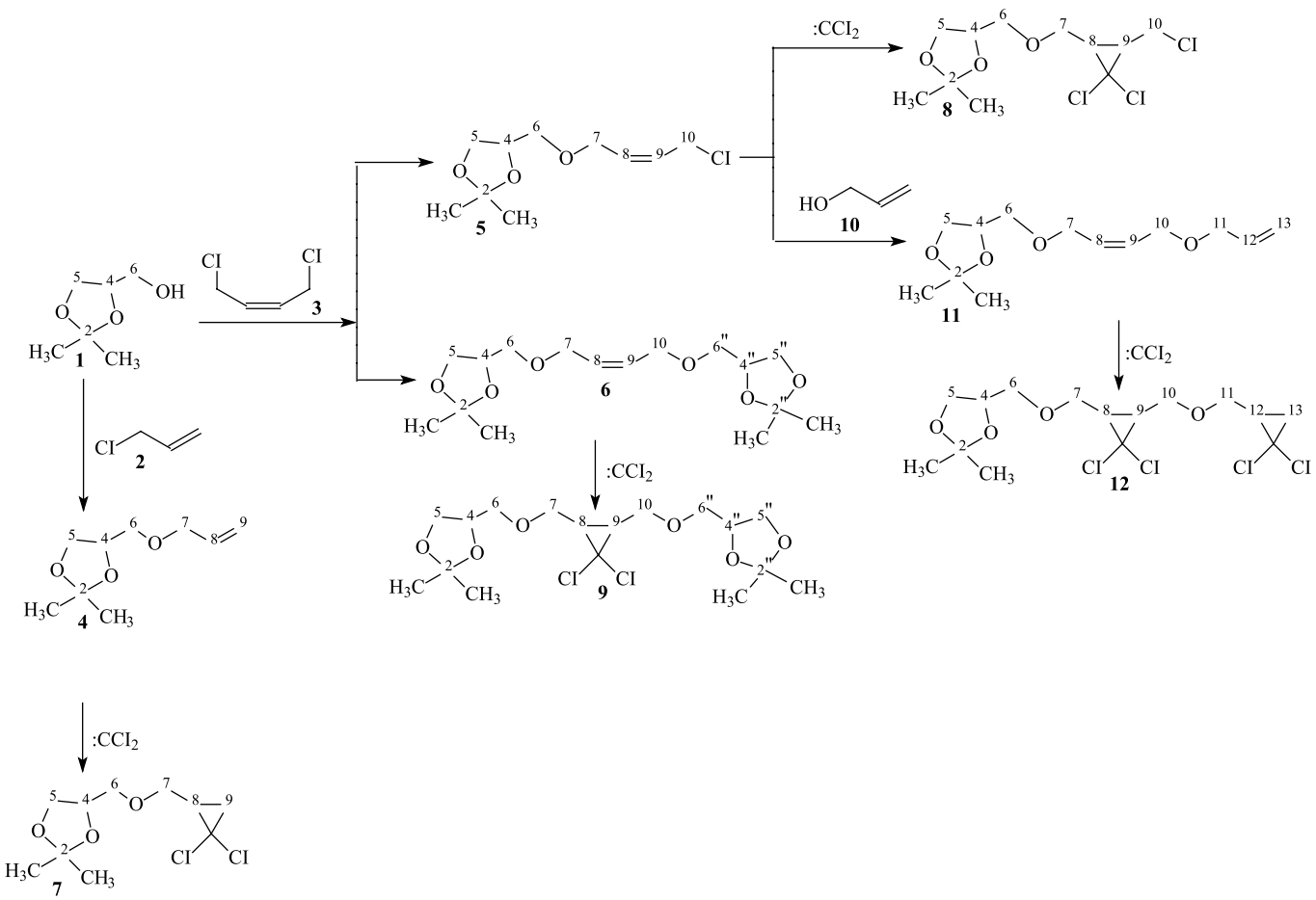

Scheme 1. Synthesis of 2,2-dimethyl-4-hydroxymethyl-1,3-dioxolane ethers **1**.

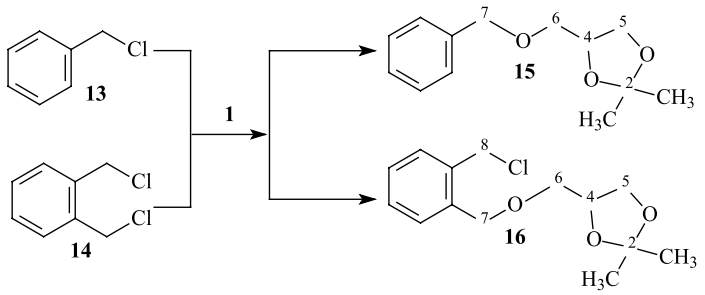

Scheme 2. Alkylation of 2,2-dimethyl-4-hydroxymethyl-1,3-dioxolane 1 by chlorides **13** and **14**.

these screens allows for the detection of changes in the metabolic activity of cells against the background of the substances under study, which acts as a proxy for cell viability.

From the obtained data (see Table) only compound **12** (IC_{50} < 100 μM) exhibited moderate cytotoxic activity against the HEK293, SH-SY5Y, MCF-7, and A549 cell lines. Substances **8** and **9** did not affect the viability of cell lines in the concentration range of 1–100 μM. The activity of the tricyclic compound **12** against the HEK293, SH-SY5Y, and A549 cell lines is in agreement with the previously studied corresponding bicyclic compound 8,8-dichloro-4-isopropyl-3,5-dioxabicyclo-octane [28] but is inferior to the cinnamaldehyde derivative 2-(2,2-dichloro-3-phenylcyclopropyl)-1,3-dioxolane. No pronounced selectivity in the cytotoxic effects of compound **12** was observed for a particular tumor cell line (the maximum SI value was 1.18 for A549 cells).

Considering the structure of the synthesized substances and their cytotoxicity we assumed that the toxicity of compound **12** was due to an increase in the amount of gem-dichlorocyclopropane fragments compared with compound **8**. This is confirmed by

Influence of compounds on cell viability (48 h, $M \pm m$)

Formula and compound number	IC_{50}, μM			
	Hek293	SH-SY5Y	MCF-7	A549
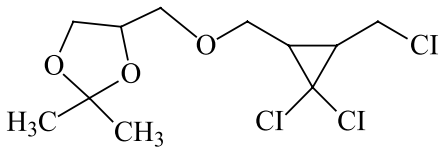 **8**	>100	>100	>100	>100
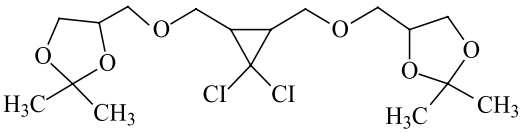 **9**	>100	>100	>100	>100
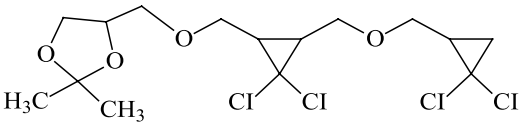 **12**	57.4 ± 4.3	86.2 ± 2.1 SI = 0.67**	72.7 ± 1.7 SI = 0.79**	48.8 ± 2.3 SI = 1.18**
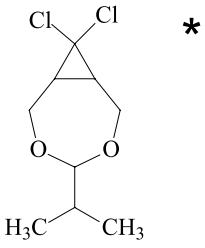 *	73.0 ± 5.7	93.2 ± 9.6 SI = 0.78**	21.0 ± 1.8 SI = 3.45**	56.0 ± 4.2 SI = 1.30**
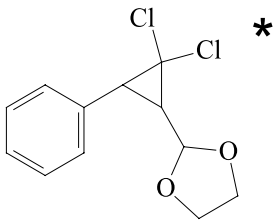 *	48.0 ± 3.1	58.67 ± 3.6 SI = 0.82**	27.6 ± 0.7 SI = 1.74**	33.7 ± 2.8 SI = 1.42**

Note: The results are presented as the arithmetic mean of three independent experiments (M), indicating the standard error of the mean ($\pm m$).

* Results from work [10].

** Selectivity Index (SI) is the ratio of the IC_{50} of the test compound for control HEK293 cells to IC_{50} for tumor cells.

comparing **12** with substances reported in [28]; the presence of the *gem*-dichlorocyclopropane group with the 1,3-dioxalane radical through oxygen in **12** reduces its negative impact on cell viability.

Thus, the analysis of compound **12** showed that an increase in the amount of *gem*-dichlorocyclopropane fragments caused cytotoxicity resulting from a change in the metabolic activity of the studied cells. The exact mechanism causing this effect is currently unknown and is the subject of our current research. Our results elaborate our understanding of the relationship of the structure of heterocyclic compounds containing *gem*-dichlorocyclopropane groups and/or 1,3-dioxalane radicals and their subsequent cytotoxic activity. Compounds **8**, **9**, and **12** may be promising candidates for the study of other types of biological activity.

CONCLUSIONS

Ethers containing *gem*-dichlorocyclopropane and 1,3-dioxolane fragments were synthesized in the presence of a catamine AB catalyst. The structures of the obtained substances were confirmed using mass spectrometry and NMR spectroscopy. Only one of several obtained compounds, 4-{[(2,2-dichloro-3-{[(2,2-dichlorocyclopropyl)methoxy]methyl} cyclopropyl)-methoxy]methyl}-2,2-dimethyl-1,3-dioxolane, had a negative impact on the metabolic activity of cells, regardless of their normal or tumor origin. Our analysis of the obtained data allowed us to establish that the toxic properties manifest due to an increase in the amount of *gem*-dichlorocyclopropane fragments in the candidate molecule and, subsequently, the cell.

Acknowledgments

The study was supported by the Ministry of Science and Higher Education of the Russian Federation, the agreement No. 075-15-2020-900 within the framework of the WCRC development program.

Authors' contribution

Sh.Sh. Dzhumaev – conducting research, reviewing publications on the topic of articles;

Y.G. Borisova – collecting and processing the material, writing the text of the article;

G.Z. Raskil'dina – collecting and processing the material, statistical processing;

U.Sh. Kuzmina – conducting biological research;

R.R. Daminev – consultation on planning, methodology and research implementation;

S.S. Zlotskii – development of the concept of the study, critical revision with the introduction of valuable intellectual content.

The authors declare no conflicts of interest.

REFERENCES

1. Yakovenko E.A., Raskil'dina G.Z., Mryasova L.M., Zlotsky S.S. Synthesis and herbicidal activity of some esters and amides that include saturated oxygen-containing heterocycles. *Khimiya i Tekhnologiya Organicheskikh Veshchestv = Chemistry and Technology of Organic Substances.* 2019;3(11):4–13 (in Russ.).

2. Stanislawski P.C., Willis A.C., Banwell M.G. *gem*-Dihalocyclopropanes as building blocks in natural-product synthesis: enantioselective total syntheses of *ent*-erythramine and 3-*epi*-erythramine. *Chem. Asian J.* 2007;2(9):1127–1136. https://doi.org/10.1002/asia.200700155

3. Sakhabutdinova G.N., Raskil'dina G.Z., Meshcheryakova S.A., Shumadalova A.V., Bortsova Yu.L., Kuzmina U.Sh., Zlotsky S.S., Sultanova R.M. Antioxidant and cytotoxic activity of a series of *O*- and *S*-containing macrocycles. *Izv. Vyssh. Uchebn. Zaved. Khim. Khim. Tekhnol. = Russ. J. Chem. & Chem. Tech.* 2020;63(3):82–88 (in Russ.). https://doi.org/10.6060/ivkkt.20206303.6118

4. Varfolomeev S.D., Nikiforov G.A., Vol'eva V.B., *et al.* Octane-increasing additive to petrol: RF Pat. 2365617. Publ. 27.08.2009. (in Russ.).

5. Küçük H.B., Yusufoğlu A.S., Mataracı E., Döşler S. Synthesis and biological activity of new 1,3-dioxolanes as potential antibacterial and antifungal compounds. *Molecules.* 2011;16(8):6806–6815. https://doi.org/10.3390/molecules16086806

СПИСОК ЛИТЕРАТУРЫ

1. Яковенко Е.А., Раскильдина Г.З., Мрясова Л.М., Злотский С.С. Получение и гербицидная активность некоторых сложных эфиров и амидов, включающих насыщенные кислородсодержащие гетероциклы. *Химия и технология органических веществ.* 2019;3(11):4–13.

2. Stanislawski P.C., Willis A.C., Banwell M.G. *gem*-Dihalocyclopropanes as building blocks in natural-product synthesis: enantioselective total syntheses of *ent*-erythramine and 3-*epi*-erythramine. *Chem. Asian J.* 2007;2(9):1127–1136. https://doi.org/10.1002/asia.200700155

3. Сахабутдинова Г.Н., Раскильдина Г.З., Мещерякова С.А., Шумадалова А.В., Борцова Ю.Л., Кузьмина У.Ш., Злотский С.С., Султанова Р.М. Антиоксидантная и цитотоксическая активность ряда *O*- и *S*-содержащих макроциклов. *Изв. вузов. Химия и хим. технология.* 2020;63(3):82–88. https://doi.org/10.6060/ivkkt.20206303.6118

4. Варфоломеев С.Д., Никифоров Г.А., Вольева В.Б. и др. Октаноповышающая добавка к бензину: пат. 2365617 РФ. Заявка 2008121078/04; заявл. 28.05.2008; опубл. 27.08.2009. Бюл. № 24.

5. Küçük H.B., Yusufoğlu A.S., Mataracı E., Döşler S. Synthesis and biological activity of new 1,3-dioxolanes as potential antibacterial and antifungal compounds. *Molecules.* 2011;16(8):6806–6815. https://doi.org/10.3390/molecules16086806

6. Genta M.T., Villa C., Mariani E., Loupy A., Petit A., Rizzetto R., Mascarotti A., Morini, F., Ferro M. Microwave-assisted preparation of cyclic ketals from a cineole ketone as potential cosmetic ingredients: solvent-free synthesis, odour evaluation, *in vitro* cytotoxicity and antimicrobial assays. *Int. J. Pharm.* 2002;231(1):11–20. https://doi.org/10.1016/S0378-5173(01)00821-3

7. Raskil'dina G.Z., Sakhabutdinova G.N., Purygin P.P., Bondareva N.A., Borisova Yu.G., Zlotsky S.S. Anticoagulant and antiaggregatory activities of a series of substituted 1,3-dioxacycloalkanes and *O*-, *S*-containing macrocycles. *Butlerovskie Soobshcheniya.* 2021;65(1):53–58 (in Russ.). Available from URL: https://butlerov.com/files/reports/2021/vol65/1/53/21-65-1-53-.pdf

8. Ovsyannikova M.N., Vol'eva V.B., Belostotskaya I.S., *et al.* Antibacterial activity of substituted 1,3-dioxolanes. *Pharm. Chem. J.* 2013;47(3):142–145. https://doi.org/10.1007/s11094-013-0913-6

9. Kailania M.H., Al-Bakrib A.G., Saadeha H., Al-Hiari Y.M. Preparation and Antimicrobial Screening of Novel 2,2-dichloro-cyclopropane–*cis*-dicarbamates and Comparison to their Alkane and *cis*-Alkene Analogs. *Jordan J. Chem.* 2012;7(3):239–252.

10. Soldatenkov A.T., Anh L.T., Hieu T.H., Nikitina E.V., Alarcon H.R. *Prirodnye biologicheski aktivnye veshchestva* (*Natural biologically active substances*). Hanoi: Znaniya; 2016. 376 p. (in Russ.).

11. Ozkanli F, Güney A, Caliş U, Uzbay T. Synthesis and anticonvulsant activity of some new dioxolane derivatives. *Arzneimittel-Forschung.* 2003;53(11):758–762. https://doi.org/10.1002/chin.200409098

12. Schmidt M., Ungvári J., Glöde J., Dobner B., Langner A. New 1,3-dioxolane and 1,3-dioxane derivatives as effective modulators to overcome multidrug resistance. *Bioorg. Med. Chem.* 2007;15(6):2283–2297. https://doi.org/10.1016/j.bmc.2007.01.024

13. Nguyen-Ba N., Lee N., Chan L., Zacharie B. Synthesis and antiviral activities of *N*-9-oxypurine 1,3-Dioxolane and 1,3-oxathiolane nucleosides. *Bioorg. Med. Chem. Lett.* 2000;10(19):2223–2226. https://doi.org/10.1016/S0960-894X(00)00452-2

14. Bera S., Malik L., Bhat B., Carrol S.S., MacCoss M., Olsen D.B., Tomassini J.E., Eldrup A.B. Synthesis and evaluation of optically pure dioxolanes as inhibitors of hepatitis C virus RNA replication. *Bioorg. Med. Chem. Lett.* 2003;13(24):4455–4458. https://doi.org/10.1016/j.bmcl.2003.09.008

15. Zapata-Sudo G., Pontes L.B., Gabriel D., Mendes T.C.F., Ribeiro N.M., Pinto A.C., Trachez M.M., Sudo R.T. Sedative–hypnotic profile of novel isatin ketals. *Pharmacol. Biochem. Behav.* 2007;86(4):678–685. https://doi.org/10.1016/j.pbb.2007.02.013

16. Ramazanov D.N., Dzhumbe A., Nekhaev A.I., Samoilov V.O., Maximov A.L., Egorova E.V. Reaction between glycerol and acetone in the presence of ethylene glycol. *Pet. Chem.* 2015;55(2):140–145. https://doi.org/10.1134/S0965544115020152

17. Barbosa S.L., Lima P.C. Oxygenated biofuels: Synthesis of fatty acid solketal esters with a mixture of sulfonated silica and $(Bu_4N)(BF_4)$ catalyst. *Catal. Commun.* 2019;120:76–79. https://doi.org/10.1016/j.catcom.2018.12.005

18. Sulistyo H., Huda E.N., Utami T.S., *et al*. Solketal Production by Glycerol Acetalization Using Amberlyst-15 Catalyst. *ASEAN J. Chem. Eng.* 2020;20(1):67–76. https://doi.org/10.22146/ajche.52455

6. Genta M.T., Villa C., Mariani E., Loupy A., Petit A., Rizzetto R., Mascarotti A., Morini, F., Ferro M. Microwave-assisted preparation of cyclic ketals from a cineole ketone as potential cosmetic ingredients: solvent-free synthesis, odour evaluation, *in vitro* cytotoxicity and antimicrobial assays. *Int. J. Pharm.* 2002;231(1):11–20. https://doi.org/10.1016/S0378-5173(01)00821-3

7. Раскильдина Г.З., Сахабутдинова Г.Н., Пурыгин П.П., Бондарева Н.А., Борисова Ю.Г., Злотский С.С. Антикоагуляционная и антиагрегационная активности ряда замещенных 1,3-диоксациклоалканов и *O*-, *S*-содержащих макроциклов. *Бутлеровские сообщения.* 2021;65(1):53–58. URL: https://butlerov.com/files/reports/2021/vol65/1/53/21-65-1-53-.pdf

8. Ovsyannikova M.N., Vol'eva V.B., Belostotskaya I.S., *et al.* Antibacterial activity of substituted 1,3-dioxolanes. *Pharm. Chem. J.* 2013;47(3):142–145. https://doi.org/10.1007/s11094-013-0913-6

9. Kailania M.H., Al-Bakrib A.G., Saadeha H., Al-Hiari Y.M. Preparation and Antimicrobial Screening of Novel 2,2-dichloro-cyclopropane–*cis*-dicarbamates and Comparison to their Alkane and *cis*-Alkene Analogs. *Jordan J. Chem.* 2012;7(3):239–252

10. Солдатенков А.Т., Ань Л.Т., Хиеу Ч.Х., Никитина Е.В., Аларкон Х.Р. *Природные биологически активные вещества*. Ханой: Знания; 2016. 376 с.

11. Ozkanli F, Güney A, Caliş U, Uzbay T. Synthesis and anticonvulsant activity of some new dioxolane derivatives. *Arzneimittel-Forschung.* 2003;53(11):758–762. https://doi.org/10.1002/chin.200409098

12. Schmidt M., Ungvári J., Glöde J., Dobner B., Langner A. New 1,3-dioxolane and 1,3-dioxane derivatives as effective modulators to overcome multidrug resistance. *Bioorg. Med. Chem.* 2007;15(6):2283–2297. https://doi.org/10.1016/j.bmc.2007.01.024

13. Nguyen-Ba N., Lee N., Chan L., Zacharie B. Synthesis and antiviral activities of *N*-9-oxypurine 1,3-Dioxolane and 1,3-oxathiolane nucleosides. *Bioorg. Med. Chem. Lett.* 2000;10(19):2223–2226. https://doi.org/10.1016/S0960-894X(00)00452-2

14. Bera S., Malik L., Bhat B., Carrol S.S., MacCoss M., Olsen D.B., Tomassini J.E., Eldrup A.B. Synthesis and evaluation of optically pure dioxolanes as inhibitors of hepatitis C virus RNA replication. *Bioorg. Med. Chem. Lett.* 2003;13(24):4455–4458. https://doi.org/10.1016/j.bmcl.2003.09.008

15. Zapata-Sudo G., Pontes L.B., Gabriel D., Mendes T.C.F., Ribeiro N.M., Pinto A.C., Trachez M.M., Sudo R.T. Sedative–hypnotic profile of novel isatin ketals. *Pharmacol. Biochem. Behav.* 2007;86(4):678–685. https://doi.org/10.1016/j.pbb.2007.02.013

16. Ramazanov D.N., Dzhumbe A., Nekhaev A.I., Samoilov V.O., Maximov A.L., Egorova E.V. Reaction between glycerol and acetone in the presence of ethylene glycol. *Pet. Chem.* 2015;55(2):140–145. https://doi.org/10.1134/S0965544115020152

17. Barbosa S.L., Lima P.C. Oxygenated biofuels: Synthesis of fatty acid solketal esters with a mixture of sulfonated silica and $(Bu_4N)(BF_4)$ catalyst. *Catal. Commun.* 2019;120:76–79. https://doi.org/10.1016/j.catcom.2018.12.005

18. Sulistyo H., Huda E.N., Utami T.S., *et al*. Solketal Production by Glycerol Acetalization Using Amberlyst-15 Catalyst. *ASEAN J. Chem. Eng.* 2020;20(1):67–76. https://doi.org/10.22146/ajche.52455

19. Fatimah I., Sahroni I., Fadillah G., *et al*. Glycerol to Solketal for Fuel Additive: Recent Progress in Heterogeneous Catalysts. *Energies.* 2019;12(15):2872. https://doi.org/10.3390/en12152872

20. Ilgen O., Yerlikaya S., Akyurek F.O. Synthesis of Solketal from Glycerol and Acetone over Amberlyst-46 to Produce an Oxygenated Fuel Additive. *Period. Polytech. Chem. Eng.* 2017;61(2):144–148. https://doi.org/10.3311/PPch.8895

21. Dmitriev G.S., Zanaveskin L.N., Terekhov A.V., *et al*. Technologies for processing of crude glycerol from biodiesel production: synthesis of solketal and its hydrolysis to obtain pure glycerol. *Russ. J. Appl. Chem.* 2018;91:1478–1485. https://doi.org/10.1134/S1070427218090100

22. Behr A., Eilting J., Irawadi K., Leschinski J., Lindner F., *et al.* Improved utilisation of renewable resources: New important derivatives of glycerol. *Green Chem.* 2008;10(1):13–30. https://doi.org/10.1039/B710561D

23. Raskil'dina G.Z., Valiev V.F., Sultanova R.M., Zlotsky S.S. Selective functionalization of the primary hydroxy group in triols. *Russ. J. Appl. Chem.* 2015;88(10):1599–1604. https://doi.org/10.1134/S1070427215100079

[Original Russian Text: Raskil'dina G.Z., Valiev V.F., Sultanova R.M., Zlotskii S.S. Selective functionalization of the primary hydroxy group in triols. *Zhurnal Prikladnoi Khimii.* 2015;88(10):1414–1419 (in Russ.).]

24. Valiev V.F., Raskildina G.Z., Mudrik T.P., Bogomazova A.A., Zlotsky S.S. Synthesis of polyfunctional vicinal glycoles. *Bashkir. khim. zh. = Bashkir Chem. J.* 2014:21(3):25–27 (in Russ.). Available from URL: http://bcj.rusoil.net/files/slider/BCJ_3_2014.pdf

25. Thankachan A.P., Sindhu K.S., Krishnan K.K., Anilkumar G. Recent advances in the syntheses, transformations and applications of 1,1-dihalocyclopropanes. *Org. Biom. Chem.* 2015;13(33):8780–8802. https://doi.org/10.1039/C5OB01088H

26. Fedoryński M. Syntheses of *gem*-Dihalocyclopropanes and Their Use in Organic Synthesis. *Chem. Rev.* 2003;103(4):1099–1132. https://doi.org/10.1021/cr0100087

27. Østby R.B., Didriksen T., Antonsen S.G., Nicolaisen S.S., Stenstrøm Y. Two-phase dibromocyclopropanation of unsaturated alcohols using flow chemistry. *Molecules.* 2020;25(10):2364–2376. https://doi.org/10.3390/molecules25102364

28. Raskil'dina G.Z., Kuzmina U.S., Dzhumaev S.S., *et al.* Synthesis and cytotoxic properties of some cyclic acetals of diols and their dichlorocyclopropyl derivatives. *Russ. Chem. Bull.* 2021;70:475–478. https://doi.org/10.1007/s11172-021-3111-9

[Original Russian Text: Raskil'dina G.Z., Kuzmina U.Sh., Dzhumaev Sh.Sh., Borisova Yu.G., Ishmetova D.V., Vakhitova Yu.V., Zlotskii S.S. Synthesis and cytotoxic properties of some cyclic acetals of diols and their dichlorocyclopropyl derivatives. *Izv. Akad. Nauk. Ser. Khim.* 2021;70(3):475–478 (in Russ.).]

19. Fatimah I., Sahroni I., Fadillah G., *et al*. Glycerol to Solketal for Fuel Additive: Recent Progress in Heterogeneous Catalysts. *Energies.* 2019;12(15):2872. https://doi.org/10.3390/en12152872

20. Ilgen O., Yerlikaya S., Akyurek F.O. Synthesis of Solketal from Glycerol and Acetone over Amberlyst-46 to Produce an Oxygenated Fuel Additive. *Period. Polytech. Chem. Eng.* 2017;61(2):144–148. https://doi.org/10.3311/PPch.8895

21. Dmitriev G.S., Zanaveskin L.N., Terekhov A.V., *et al.* Technologies for processing of crude glycerol from biodiesel production: synthesis of solketal and its hydrolysis to obtain pure glycerol. *Russ. J. Appl. Chem.* 2018;91:1478–1485. https://doi.org/10.1134/S1070427218090100

22. Behr A., Eilting J., Irawadi K., Leschinski J., Lindner F., *et al.* Improved utilisation of renewable resources: New important derivatives of glycerol. *Green Chem.* 2008;10(1):13–30. https://doi.org/10.1039/B710561D

23. Raskil'dina G.Z., Valiev V.F., Sultanova R.M., Zlotskii S.S. Selective functionalization of the primary hydroxy group in triols. *Russ. J. Appl. Chem.* 2015;88(10):1599–1604. https://doi.org/10.1134/S1070427215100079

24. Валиев В.Ф., Раскильдина Г.З., Мудрик Т.П., Богомазова А.А., Злотский С.С. Синтез полифункциональных вицинальных гликолей. *Баш. хим. журн.* 2014;21(3):25–27. http://bcj.rusoil.net/files/slider/BCJ_3_2014.pdf

25. Thankachan A.P., Sindhu K.S., Krishnan K.K., Anilkumar G. Recent advances in the syntheses, transformations and applications of 1,1-dihalocyclopropanes. *Org. Biom. Chem.* 2015;13(33):8780–8802. https://doi.org/10.1039/C5OB01088H

26. Fedoryński M. Syntheses of *gem*-Dihalocyclopropanes and Their Use in Organic Synthesis. *Chem. Rev.* 2003;103(4):1099–1132. https://doi.org/10.1021/cr0100087

27. Østby R.B., Didriksen T., Antonsen S.G., Nicolaisen S.S., Stenstrøm Y. Two-phase dibromocyclopropanation of unsaturated alcohols using flow chemistry. *Molecules.* 2020;25(10):2364–2376. https://doi.org/10.3390/molecules25102364

28. Раскильдина Г.З., Кузьмина У.Ш., Джумаев Ш.Ш., Борисова Ю.Г., Вахитова Ю.В., Злотский С.С. Синтез и цитотоксические свойства некоторых циклических ацеталей диолов и их дихлорциклопропановых производных. *Изв. АН. Сер. хим.* 2021;70(3):475–478.

About the authors:

Shahobiddin Sh. Dzhumaev, Postgraduate Student, Department of General, Analytical and Applied Chemistry, Ufa State Petroleum Technological University (1, Kosmonavtov ul., Ufa, 450064, Russia). E-mail: shakhob2993@mail.ru. https://orcid.org/0000-0002-1938-1478

Yulianna G. Borisova, Cand. Sci. (Chem.), Teacher, Department of General, Analytical and Applied Chemistry, Ufa State Petroleum Technological University University (1, Kosmonavtov ul., Ufa, 450064, Russia). E-mail: yulianna_borisova@mail.ru. Scopus Author ID 56526865000, ResearcherID P-9744-2017, https://orcid.org/0000-0001-6452-9454

Gul'nara Z. Raskil'dina, Cand. Sci. (Chem.), Associate Professor, Department of General, Analytical and Applied Chemistry, Ufa State Petroleum Technological University (1, Kosmonavtov ul., Ufa, 450064, Russia). E-mail: graskildina444@mail.ru. Scopus Author ID 56069888400, ResearcherID F-1619-2017, https://orcid.org/0000-0001-9770-5434

Ulyana Sh. Kuzmina, Cand. Sci. (Biol.), Researcher, Institute of Biochemistry and Genetics, Ufa Federal Research Center, Russian Academy of Sciences (71, Oktyabrya pr., Ufa, 450054, Russia). E-mail: ulia-bio@yandex.ru. ResearcherID I-9754-2018, https://orcid.org/0000-0001-7056-7895

Rustem R. Daminev, Dr. Sci. (Eng.), Professor, Director of Branch in Sterlitamak, Ufa State Petroleum Technological University, Branch in Sterlitamak (2, Oktyabrya pr., Sterlitamak, 453118, Russia). E-mail: daminew@mail.ru. Scopus Author ID 15026168000, https://orcid.org/0000-0001-8673-5240

Simon S. Zlotskii, Dr. Sci. (Chem.), Professor, Head of the Department of General, Analytical and Applied Chemistry, Ufa State Petroleum Technological University (1, Kosmonavtov ul., Ufa, 450064, Russia). E-mail: nocturne@mail.ru. Scopus Author ID 6701508202, ResearcherID W-6564-2018, https://orcid.org/0000-0001-6365-5010

Об авторах:

Джумаев Шахобиддин Шамсидинович, аспирант кафедры общей, аналитической и прикладной химии, ФГБОУ ВО «Уфимский государственный нефтяной технический университет» (450064, Россия, г. Уфа, ул. Космонавтов, д. 1). E-mail: shakhob2993@mail.ru. https://orcid.org/0000-0002-1938-1478

Борисова Юлианна Геннадьевна, к.х.н. преподаватель кафедры общей, аналитической и прикладной химии, филиал ФГБОУ ВО «Уфимский государственный нефтяной технический университет» (450064, Россия, г. Уфа, ул. Космонавтов, д. 1). E-mail: yulianna_borisova@mail.ru. Scopus Author ID 56526865000, ResearcherID P-9744-2017, https://orcid.org/0000-0001-6452-9454

Раскильдина Гульнара Зинуровна, к.х.н., доцент кафедры общей, аналитической и прикладной химии, ФГБОУ ВО «Уфимский государственный нефтяной технический университет» (450064, Россия, г. Уфа, ул. Космонавтов, д. 1). E-mail: graskildina444@mail.ru. Scopus Author ID 56069888400, ResearcherID F-1619-2017, https://orcid.org/0000-0001-9770-5434

Кузьмина Ульяна Шавкатовна, к.б.н., научный сотрудник, Институт биохимии и генетики УФИЦ РАН (450054, Россия, г. Уфа, пр. Октября, д. 71). E-mail: ulia-bio@yandex.ru. ResearcherID I-9754-2018, https://orcid.org/0000-0001-7056-7895

Даминев Рустем Рифович, д.т.н., профессор, директор филиала в г. Стерлитамак ФГБОУ ВО «Уфимский государственный нефтяной технический университет», филиал в г. Стерлитамак (453118, Россия, г. Стерлитамак, Октября пр-т, д. 2). E-mail: daminew@mail.ru. Scopus Author ID 15026168000. https://orcid.org/0000-0001-8673-5240

Злотский Семен Соломонович, д.х.н., заведующий кафедрой общей, аналитической и прикладной химии, ФГБОУ ВО «Уфимский государственный нефтяной технический университет» (450064, Россия, г. Уфа, ул. Космонавтов, д. 1). E-mail: nocturne@mail.ru. Scopus Author ID 6701508202, ResearcherID W-6564-2018, https://orcid.org/0000-0001-6365-5010

The article was submitted: February 16, 2021; approved after reviewing: March 10, 2021; accepted for publication: April 05, 2021.

Translated from Russian into English by H. Moshkov
Edited for English language and spelling by Enago, an editing brand of Crimson Interactive Inc.

SYNTHESIS AND PROCESSING OF POLYMERS AND POLYMERIC COMPOSITES

СИНТЕЗ И ПЕРЕРАБОТКА ПОЛИМЕРОВ И КОМПОЗИТОВ НА ИХ ОСНОВЕ

ISSN 2686-7575 (Online)
https://doi.org/10.32362/2410-6593-2021-16-2-167-175
UDC 541.64+543.51

RESEARCH ARTICLE

Synthesis of thermosensitive copolymers of *N*-isopropylacrylamide with 2-aminoethylmethacrylate hydrochloride

Vladimir R. Duflot[1], Andrey V. Gaivoronsky[1,2,@], Ekaterina I. Lobanova[1]

[1]Karpov Institute of Physical Chemistry, Obninsk, 249033 Россия
[2]MIREA – Russian Technological University (M.V. Lomonosov Institute of Fine Chemical Technologies), Moscow, 119571 Russia
[@]Corresponding author, e-mail: andrei.gaivoronsky@yandex.ru

Abstract

Objectives. *Due to the increasing number of oncological diseases, active research into developing new radiopharmaceuticals is underway. Thermosensitive copolymers have valuable physicochemical properties that can be harnessed to develop therapeutic radiopharmaceuticals for treating solid tumors. The aim of this study was to develop a method for producing thermosensitive copolymers that can find use as radionuclide carriers to create therapeutic radiopharmaceuticals for treating solid tumors.*

Methods. *Using radical copolymerization in polar solvents, we synthesized water-soluble copolymers based on N-isopropyl acrylamide and 2-aminoethyl methacrylate hydrochloride. The resulting copolymers were characterized in terms of molecular composition and hydrodynamic properties using gel permeation chromatography, IR spectroscopy, potentiometry, and viscometry. Changes in optical density during temperature scanning helped determine the phase transition temperature (PTT) of aqueous copolymer solutions.*

Results. *We developed a method for preparing copolymers of N-isopropylacrylamide with 2-aminoethyl methacrylate using radical copolymerization in water and isopropanol with a content of 2-aminoethyl methacrylate hydrochloride in a copolymer up to 23 mol %. We studied how the second comonomer affected the PTT of the aqueous copolymer solutions. An increase in the content of 2-aminoethyl methacrylate in the copolymer caused the PTT to increase. We found that the change in the PTT depending on the content of 2-aminoethyl methacrylate units in the copolymer had a straightforward relationship with its content up to 17 mol %. The use of physiological saline as a solvent led to a temperature decrease of the phase transition by two degrees.*

Conclusions. *The method of producing thermosensitive copolymers by radical copolymerization in isopropanol does not allow creating a radionuclide carrier. Solutions of the obtained low-molecular weight oligomers form coacervate solutions, which will inevitably cause the radionuclide to spread throughout the body. The copolymers obtained by radical copolymerization in water with the content of the second comonomer 2-aminoethyl methacrylate from 10–17 mol % can be used as a radionuclides carrier provided that a physiological solution of sodium chloride is used as a solvent.*

Keywords: *N-isopropylacrylamide, 2-aminoethyl methacrylate, thermosensitive copolymers, radical polymerization, phase transition temperature*

For citation: Duflot V.R., Gaivoronsky A.V., Lobanova E.I. Synthesis of thermosensitive copolymers of *N*-isopropylacrylamide with 2-aminoethylmethacrylate hydrochloride. *Tonk. Khim. Tekhnol. = Fine Chem. Technol.* 2021;16(2):167–175 (Russ., Eng.). https://doi.org/10.32362/2410-6593-2021-16-2-167-175

НАУЧНАЯ СТАТЬЯ

Синтез термочувствительных сополимеров *N*-изопропилакриламида с гидрохлоридом 2-аминоэтилметакрилата

В.Р. Дуфлот[1], А.В. Гайворонский[1,2,@], Е.И. Лобанова[1]

[1]Научно-исследовательский физико-химический институт им. Л.Я. Карпова, Обнинск, 249033 Россия
[2]МИРЭА – Российский технологический университет (Институт тонких химических технологий им. М.В. Ломоносова), Москва, 119571 Россия
[@]Автор для переписки, e-mail: andrei.gaivoronsky@yandex.ru

Аннотация

Цели. *В связи с увеличением числа онкологических заболеваний ведутся активные поиски в разработке новых радиофармацевтических препаратов. В этом аспекте значительный интерес представляют термочувствительные сополимеры, обладающие комплексом ценных физико-химических свойств. Данная работа посвящена разработке метода получения термочувствительных сополимеров, которые могут быть использованы в качестве носителя радионуклидов для создания терапевтического радиофармпрепарата для лечения солидных опухолей.*
Методы. *Методом радикальной сополимеризации в полярных растворителях синтезированы водорастворимые сополимеры на основе N-изопропилакриламида и гидрохлорида 2-аминоэтилметакрилата. Полученные сополимеры были охарактеризованы по составу молекулярным и гидродинамическим характеристикам с использованием гель-проникающей хроматографии, ИК-спектроскопии, потенциометрии и вискозиметрии. Температуру фазового перехода водных растворов сополимеров определяли по изменению оптической плотности от температуры.*
Результаты. *Был разработан метод получения сополимеров N-изопропилакриламида с 2-аминоэтилметакрилатом радикальной сополимеризацией в воде и 2-пропаноле с содержанием гидрохлорида 2-аминоэтилметакрилата в сополимере до 23 моль-звено %. Изучено влияние второго сомономера на температуру фазового перехода водных растворов сополимеров. Увеличение содержания 2-аминоэтилметакрилата в сополимере приводит к смещению температуры фазового перехода, повышая ее. Установлено, что изменение температуры фазового перехода в зависимости от содержания звеньев 2-аминоэтилметакрилата*

в сополимере имеет прямолинейную з ависимость при его содержании до 17 моль-звено %. Использование в качестве растворителя физиологического раствора хлорида натрия приводит к снижению температуры фазового перехода на два градуса.

Выводы. *Метод получения термочувствительных сополимеров радикальной сополимеризацией при использовании в качестве растворителя 2-пропанола не позволяет создать носитель радионуклида. Растворы полученных низкомолекулярных олигомеров образуют коацерватные растворы, что неизбежно приведет к распространению радионуклида по организму. Сополимеры, полученные методом радикальной сополимеризацией в воде с содержанием второго сомономера 2-аминоэтилметакрилат от 10 до 17 моль-звено %, могут быть использованы в качестве носителя радионуклидов только при условии, что в качестве растворителя используются физиологический раствор хлорида натрия.*

Ключевые слова: *N-изопропилакриламид, 2-аминоэтилметакрилат, термочувствительные сополимеры, радикальная полимеризация, температура фазового перехода*

Для цитирования: Дуфлот В.Р., Гайворонский А.В., Лобанова Е.И. Синтез термочувствительных сополимеров *N*-изопропилакриламида с гидрохлоридом 2-аминоэтилметакрилата. *Тонкие химические технологии.* 2021;16(2):167–175. https://doi.org/10.32362/2410-6593-2021-16-2-167-175

INTRODUCTION

A modern and effective method of treating cancer is brachytherapy. Microsource introduction inside tumor or near-tumor tissues enables to localize ionizing radiation in the immediate vicinity of cancer cells. The related disadvantages of this method are the complexity and high costs of producing microsources. Around 40 to 80 microsources are needed to treat a disease such as prostate cancer. Their number strongly depends on the severity of the disease [1].

An analog of expensive microsources is the use of polymeric carriers of radionuclides, namely thermosensitive (co)polymers, the aqueous solutions of which have a lower critical dissolution temperature in the temperature range below the physiological temperature of the human body [2]. The aqueous solution of a thermosensitive copolymer, with which the radionuclide is chelated, is introduced into a tumor, undergoes a phase transition and forms a dense gel. The latter acts as a local radiation source. For these purposes, thermosensitive copolymers based on *N*-isopropylacrylamide (NIPA) can be used [3, 4]. The phase transition temperature (PTT) of an aqueous solution of poly-*N*-isopropylacrylamide (PNIPA) homopolymer lies in the range of 32°C, and does not depend on the chain length of the polymer molecule.

The work [5] describes methods of synthesizing polymer-protein thermosensitive conjugates based on PNIPA. The use of these thermosensitive polymer-protein conjugates as radionuclide carriers presents difficulties due to phase transition peculiarities that occur in the pH range between 3.5 and 5.5. In physiological conditions (pH 7.35–7.45), the polymer-protein conjugate cannot form a dense gel and will inevitably spread throughout the body. The authors of [6] developed and patented [7] a method for producing a thermosensitive polymer-protein iodine-containing radiopharmaceutical (RP) with radiochemical purity (RCP) of 95–98%. In this work, we used a polymer-protein conjugate of PNIPA and a globular protein (bovine serum albumin) as a matrix, to the tyrosine groups of which the ^{131}I radionuclide is covalently attached. Related disadvantages include the RP complexity and multistep manufacturing. Purifying RPs from ternary poly-*N*-isopropylacryamide-^{131}I hydrate complexes using the column method increases the RCP, but decreases drug concentration [8].

Study [9] describes an RP based on a thermosensitive carrier, a NIPA-allylamine copolymer with a chelator, and a diethylenetriaminepentaacetic acid (DTPA) added to the amino groups by esterification. A potential disadvantage of this carrier is the low content of DTPA groups, which is due to the lack of a sufficient number of allylamine units in the copolymer, to which DTPA units are attached. In addition, when synthesizing this copolymer, the authors failed to obtain samples of the carrier copolymer with a viscosity average molecular weight M_η > 40 kDa. The reason for this is the chain transfer to the monomer, the so-called “allyl degradation transfer of the chain.” Low-molecular PNIPA

compounds form a colloidal system similar to that of milk dispersion. Therefore, in the drag, the authors had to use a PNIPA polymer thickener that had an average molecular weight $M_\eta \leq 100$ kDa to create a polymeric spatial network [10].

A small number of chelating groups for binding a radionuclide can limit the radiopharmaceutical's maximum efficacy of treating tumors. Increasing the number of functional amino groups in the thermosensitive copolymer should help solve this problem. Replacing the allyl monomer with a methacrylic monomer containing amino groups should increase the molecular weight of the thermosensitive copolymer and eliminate the need for a polymer thickener. 2-Aminoethyl methacrylate hydrochloride (AEM HC) can be used as a comonomer.

The aim of this work is to develop a method of producing thermosensitive copolymers based on NIPA–AEM, with AEM content of up to 23 mol %, study their molecular and hydrodynamic properties, and determine how the number of AEM units in the copolymer affect the phase transition temperature of aqueous solutions of NIPA–AEM copolymers.

EXPERIMENTAL

We used the following reagents in our work: *N*-isopropylacrylamide 97% (*Sigma-Aldrich*, Missouri, USA); *tert*-butyl hydroperoxide 70% aqueous solution (*Sigma-Aldrich*); 2,2-azobisisobutyronitrile (*Vekton*, St. Petersburg, Russia); diethyl ether, chemically pure (*MEDKHIMPROM*, Balashikha, Moscow oblast, Russia); 1,2-dichloroethane, chemically pure (*Ekos-1*, Staraya Kupavna, Moscow oblast, Russia); 2-propanol, chemically pure (*Khimkomplekt*, country of origin: Netherlands); monoethanolamine, chemically pure (*Ekos-1*); methacryloyl chloride, pure (*Ekos-1*). The bidistillate was obtained in a laboratory bidistiller BE-4 (*Livam*, Belgorod, Russia). Methacryloyl chloride was distilled twice before use. Diethyl ether was purified from peroxides [11] and distilled before use. The AEM HC monomer was derived by acylation according to the method proposed in [12] and the yield was 89%. The reaction product was purified twice by recrystallization from dichloroethane. IR spectroscopy helped determine the monomer structure. IR spectra were recorded by an FSM1202 IR Fourier spectrometer (*Infraspek*, St. Petersburg, Russia) in KBr pellets.

Copolymers **1**–**4** (Table 1) were obtained by homogeneous radical copolymerization in 2-propanol. The polymerization was initiated by 2,2-azobisisobutyronitrile. Its concentration in all reactions was the same: 0.024 mol/L. Oxygen was removed by a triple freeze-thaw cycle followed by evacuation after which the ampoules were sealed and thermostated. After a certain time, the ampoules opened, and the contents were precipitated in diethyl ether under vigorous stirring. The formed precipitate was filtered off on a Buchner funnel and dried in vacuum.

Copolymers **5**–**12** (Table 2) were obtained by radical precipitation copolymerization in water. The initial copolymer concentration in all reactions was 0.01 mol/L. Oxygen was removed by blowing argon for 10 min. Then the ampoules were sealed and thermostated. After a certain time, the ampoules opened and lyophilized in a Christ alpha 2-4 LSC plus lyophilizer (*Martin Christ Gefriertrocknungsanlagen*, Germany). Then the samples were dissolved in 10 mL 2-propanol and precipitated into diethyl ether under vigorous stirring. The formed precipitate was filtered off on a Buchner funnel and dried in vacuum.

The quantitative content of AEM HC units was monitored by NH_2 groups using direct and reverse potentiometric titration in ethanol that was previously purified from aldehydes [13]. IR spectrometry helped determine the qualitative structure in KBr pellets in the following absorption bands: 3500–3300 cm^{-1} (ν NH_2), 2974–2887 cm^{-1} (ν CH_3), 1734 cm^{-1} (ν C=O), 1653 cm^{-1} (ν C=O), 1541 cm^{-1} (δ NH_2), 1460 cm^{-1} (δ CH_3), and 1074 cm^{-1} (ν C–O–C).

The copolymer IR band at 1653 cm^{-1} is attributed to the stretching vibrations of the absorption bands (C=O) of the amide group in the associated state. The 1734 cm^{-1} band corresponds to the stretching vibrations of the carbonyl group (C=O) absorption bands of the 2-aminoethyl methacrylate hydrochloride copolymer unit. Furthermore, there is a spectral band at 2380–2840 cm^{-1}, which is characteristic of amino group salt [14].

The intrinsic viscosity of copolymer solutions was determined in a 0.5 M aqueous solution of $LiNO_3$ at 20°C in an Ubbelohde viscometer (*Labtech*, Moscow, Russia). The value of the viscosity average molecular weight M_η of the copolymers was determined using the Mark-Kuhn-Houwink equation [15]. The coefficient values of the PNIPA homopolymer were defined as $K = 4.7 \times 10^{-4}$, $\alpha = 0.61$.

Gel permeation chromatography in dimethylformamide was employed to determine the weight-average (M_w) and number-average (M_n) molecular weights of the copolymers (*Labtech*, Moscow, Russia), which contained 0.1 wt % LiBr. The experiments were carried out at 50°C with the use of a GPC-120 chromatograph (*Polymer Laboratories*, United Kingdom). A differential refractometer was used as a detector. For separation, two PLgel 5 μm MIXED B columns ($M = (5 \times 10^2)$–(1×10^7)) (*Agilent Technologies*, California, USA) were used. The copolymer molecular weight (MW) was calculated

according to calibration measurements conducted against narrow-dispersed polymethyl methacrylate standards.

The PTT values of the copolymer aqueous solutions were determined from the temperature dependence of optical density, obtained by an Agilent 8453 UV-vision spectrophotometer (*Agilent Technologies*). Copolymers were preliminarily purified from HCl with an equimolar amount of 0.1 N KOH solution in water at T = 50°C for 2 h.

Low-molecular compounds were removed by dialysis in water for 2 days in dialysis bags (*Orange Scientific OrDial*, Belgium) with a pore size of 12–14 kDa. The copolymer concentration in the test solutions in all samples was c_{pol} = 1 wt %. The solvents used were double-distilled water and a 0.9% NaCl solution.

RESULTS AND DISCUSSION

Table 1 presents the synthesis conditions and copolymer properties obtained by radical copolymerization in 2-propanol. Statistical copolymers containing AEM HC units from 18.2 to 27.3 mol % were obtained. The low MW values and copolymer conversions stem from the chain transfer to the solvent. Such a low copolymer MW prevents them from being used as radionuclide carriers without using a thickener. Study [16] demonstrated that thermosensitive copolymers based on *N*-isopropylacrylamide with MW $\leq 40 \times 10^3$ are excreted mostly by the kidneys within 48 h. Therefore, the use of copolymers with MW $\leq 40 \times 10^3$ as radionuclide carriers is not appropriate.

Copolymers obtained by radical precipitation copolymerization in water demonstrated higher conversion efficiencies and MW values compared to those of copolymers prepared in 2-propanol. Table 2 presents the copolymerization conditions and MW characteristics. An aqueous solution of copolymer **5** synthesized at a high temperature demonstrated pronounced opalescence compared to that of sample **6** synthesized at 50°C. The opalescence in the copolymer solution most likely indicates macromolecule crosslinking during their synthesis. To this end, all subsequent copolymers were synthesized at 50°C.

An increase in the molar fraction of AEM HC in the monomer mixture results in higher copolymer yield, but decreases its MW. The molecular mass decrease observed with the increased starting monomer concentration is most likely due to the AEM HC ionic effects: that affect the capture of the radical of the growing chain (i.e., prevent chain growth). Study [17] reported similar results. The authors explain this effect by a possible chain transfer to the monomer and the polymer. The study showed that the amino group content in the obtained copolymers is higher than the initial concentrations and does not depend on the conversion rate.

The narrow molecular weight distribution (MWD) that certain samples demonstrate is probably due to fractionation at the isolation and purification stages. The typical MWD curves for some samples are shown in Fig. 1. The M_w values of copolymers **10**–**12** obtained at an initial AEM HC concentration below 0.1 mol/L exceed 10^5. Comparison of copolymers **6**–**9** derived under the same conditions indicates that polydispersity naturally increases as conversion increases. Considering a number of parameters, we conclude that the most optimal samples, which can be recommended for use as RP precursors, are samples **6** and **7**.

The phase transition temperature (PTT) value is a crucial factor in the copolymer use as thermosensitive radionuclide carriers. The human body temperature ranges between 34.4 and 37.8°C [18] and strongly depends on the circadian rhythms of the human body. Proceeding from this condition, the PTT of copolymer aqueous solutions for designing RP should not exceed 34°C. The PTT measurements of aqueous

Table 1. Synthesis conditions and properties of copolymers synthesized in 2-propanol

No.	$[M_1]$, mol/L	$[M_2]$, mol/L	Temperature, °C	Time, h	Conversion, %	$[m_2]$, mol %	$M_\eta \times 10^{-5}$
1	0.72	0.04	50	72	16.3	27.3	0.08
2				96	23.9	18.2	0.15
3			60	72	20.9	20.7	0.12
4			70	72	20.0	21.1	0.11

Note: $[M_1]$ – *N*-isopropylacrylamide, $[M_2]$ – 2-aminoethyl methacrylate hydrochloride, $[m_2]$ – 2-aminoethyl methacrylate hydrochloride units.

Table 2. Synthesis conditions and properties of copolymers synthesized in water

No.	$[M_1]$, mol/L	$[M_2]$, mol/L	Time, min	Temperature, °C	Conversion, %	$[m_2]$, mol %	PTT, °C	PTT 0.9% NaCl, °C	$M_\eta \times 10^{-5}$	$M_n \times 10^{-5}$	$M_w \times 10^{-5}$	M_w/M_n
5	0.9	0.1	15	70	87.1	13.3	33.2	31.0	–	–	–	–
6			15	50	36.5	23.5	–	39.8	11.6	2.6	5.5	2.1
7			37	50	68.5	17.7	33.8	32.8	13.0	1.5	4.3	2.9
8			60	50	92.8	10.9	33.0	31.1	7.7	0.9	3.0	3.5
9			120	50	96.6	10.2	32.9	31.0	7.8	0.8	5.3	6.7
10	0.925	0.075	60	50	60.6	17.7	–	–	–	5.9	12.2	2.1
11	0.95	0.05		50	57.9	9.6	–	–	–	7.4	17.4	2.4
12	0.97	0.03		50	45.9	6.6	–	–	–	6.8	17.1	2.5

Note: $[M_1]$ – *N*-isopropylacrylamide, $[M_2]$ – 2-aminoethyl methacrylate hydrochloride, $[m_2]$ – 2-aminoethyl methacrylate hydrochloride units.

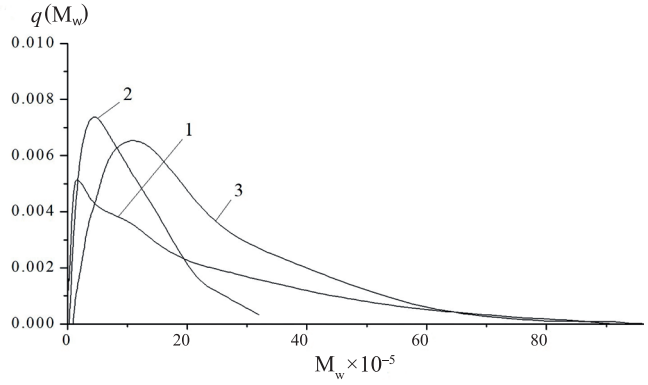

Fig. 1. Molecular weight distribution curves of copolymers: (1) No. **12** ($M_w = 17.1 \times 10^5$); (2) No. **6** ($M_w = 5.5 \times 10^5$); (3) No. **10** ($M_w = 12.2 \times 10^5$); $q(M_w)$ – weight fraction of macromolecules.

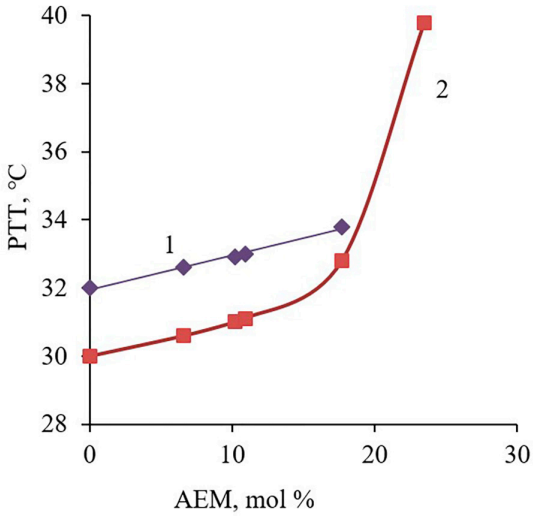

Fig. 2. The dependence of phase transition temperature (PTT) on the content of 2-aminoethyl methacrylate (AEM) in the copolymer: water (1) and 0.9% NaCl (2).

solutions of the obtained copolymers showed that an increase in the AEM fraction follows a linear growth (Fig. 2). When the AEM content in the copolymer exceeded 17.7 mol %, no phase transitions were observed in aqueous solutions. This is probably due to the increased hydrophilic interactions between the increased number of AEM units and water molecules.

Figure 3 shows the turbidity curves of 1% aqueous solutions of a number of copolymers. Organoleptically, copolymer **9** had a dense elastic gel-like structure, while copolymers **7** and **8** formed a coacervate solution in the form of a milk

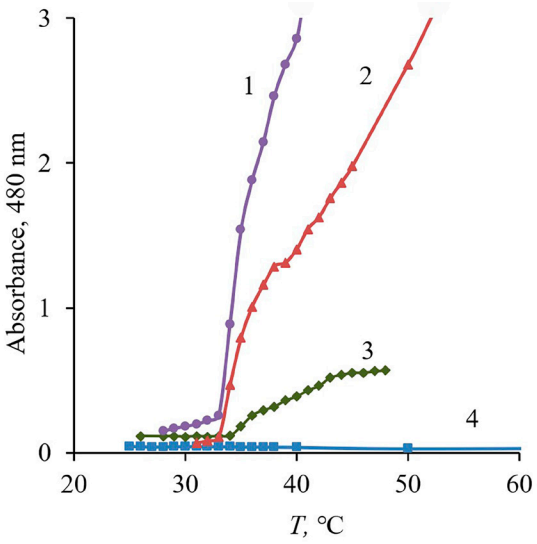

Fig. 3. Turbidity curves of 1% copolymer aqueous solutions: (1) No. **9**, (2) No. **8**, (3) No. **7**, (4) No. **6**.

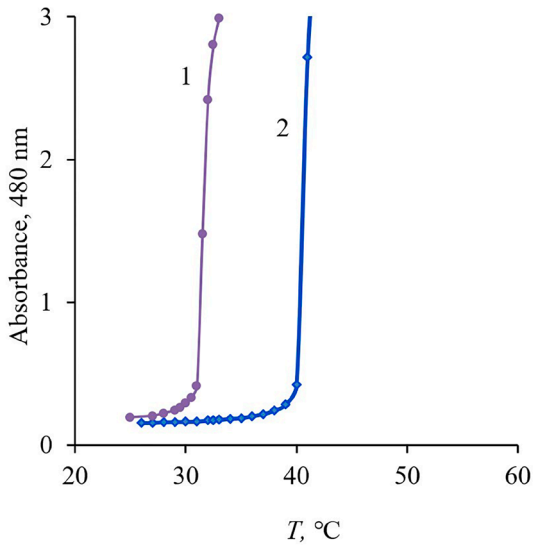

Fig. 4. Turbidity curves of solutions of copolymers prepared in saline: (1) No. **10**, (2) No. **6**.

dispersion. The disperse state of the copolymer after the phase transition does not ensure radionuclide retention in a specific place. The use of saline (a 0.9% NaCl solution) as a solvent causes a decrease in PTT by about two degrees (curve 2 in Fig. 4). Salt molecules are known to be actively participate in the destruction of hydrogen bonds formed between water molecules and macromolecules of both PNIPA homopolymers and copolymers, causing the coil-globule transition. Thus, at a NaCl concentration of 1 mol/L, salt molecules the PNIPA homopolymer to collapse even at room temperature [2]. A characteristic feature of the phase transition in a saline solution is a sharp change in optical density in a very narrow temperature range, indicating the formation of a dense structure of the AEM gel.

CONCLUSIONS

Water-soluble copolymers based on *N*-isopropylacrylamide and 2-aminoethyl methacrylate hydrochloride with different content of amino groups were synthesized by radical copolymerization in water. The resulting copolymers were characterized in terms of molecular composition and hydrodynamic properties using gel permeation chromatography, IR spectroscopy, and viscometry. The study investigated how 2-aminoethyl methacrylate affected the PTT of aqueous copolymer solutions. Increase of the content of 2-aminoethyl methacrylate in the copolymer increases the PTT. The change in the PTT depending on the content of 2-aminoethyl methacrylate units in the copolymer was found to demonstrate a linear relationship up to 17 mol %.

Acknowledgments

The authors are especially grateful to E.V. Chernikova for participating and assisting in the work.

Authors' contributions

V.R. Duflot – management and scientific consulting;

A.V. Gaivoronsky – planning and conducting research, collecting and analyzing experimental materials, writing the manuscript;

E.I. Lobanova – collection of materials of the experiments.

The authors declare no conflicts of interest.

REFERENCES

1. Kaprin A.D., Biryukov V.A., Chernichenko A.V., Koryakin A.V., Polyakov V.A., Karyakin O.B., Galkin V.N., Apolikhin O.I., Ivanov S.A., Sivkov A.V., Oschepkov V.N., Alekseev B.Ya., Obukhov A.A., Lepilina O.G. Interstitial radiotherapy therapy (brachytherapy) of prostate cancer. Own experience of the National Medical Research Radiological Center of the Ministry of Health of Russia. *Russ. Med. Zh. = RMJ.* 2017;25(27):2011–2014 (in Russ.).

СПИСОК ЛИТЕРАТУРЫ

1. Каприн А.Д., Бирюков В.А., Черниченко А.В., Корякин А.В., Поляков В.А., Карякин О.Б., Галкин В.Н., Аполихин О.И., Иванов С.А., Сивков А.В., Ощепков В.Н., Алексеев Б.Я., Обухов А.А., Лепилина О.Г. Внутритканевая лучевая терапия (брахитерапия) рака предстательной железы. Собственный опыт работы национального медицинского исследовательского радиологического центра Минздрава России. *Рус. мед. журн.* 2017;25(27):2011–2014.

2. Galaev I.Y. “Smart” polymers in biotechnology and medicine. *Russ. Chem. Rev.* 1995;64(5):471–489. https://doi.org/10.1070/RC1995v064n05ABEH000161

[Galaev I.Yu. “Smart” polymers in biotechnology and medicine. *Usp. Khim.* 1995;64(5):505–524 (in Russ.).]

3. Weller R.E., Lind M.E., Fisher D.R., *et al*. Stimulus sensitive gel with radioisotope and methods of making. US Patent US6296831B1, 2001. Oct. 2.

4. Weller R.E., Lind M.E., Fisher D.R., Gutovska A., Campbell A.A. Stimulus Sensitive Gel with Radioisotope and Methods of Making. US Patent US6869588B2, 2005. Mar. 22.

5. Cao Z., Jin Y., Zhang B., Miao Q., Ma C. A novel temperature- and pH-responsive polymer-biomolecule conjugate composed of casein and poly(*N*-isopropylacrylamide). *Iran. Polym. J.* 2010;19(9):689–698.

6. Bolbet N.M., Duflot R.V., Dubova E.A., Gaivoronsky A.V., Lobanova E.I. Altynnikova T.V. Synthesis and properties of thermosensitive polymer protein conjugates labeled with radioactive isotopes of iodine. *Aktual. Prob. Gum. i Estestv. Nauk = Actual Prob. Human. and Nat. Sciences.* 2013;6(53):30–39 (in Russ.).

7. Bolbit N.M., Dubova E.A., Duflot V.R., Gaivoronsky A.V. Thermosensitive polymer-protein iodine-containing radiopharmaceutical: RF Pat. 255447. Publ. 10.01.2015 (in Russ.).

8. Bolbit N.M., Duflot V.R., Dubova E.A., Altynnikova T.V. Heat-sensitive radiopharmaceutical for local radiotherapy on the basis of the ^{131}I-radiolabeled polymer-protein conjugate. *V mire nauchnykh otkrytii.* 2013;7–3(43):30–48 (in Russ.).

9. Petriev V.M., Tishchenko V.K., Smorizanova O.A., *et al*. Novel radiopharmaceutical, Sm-153-labelled thermoresponsive polymer, for local radiotherapy of solid tumors. *Radiatsiya i risk = Radiation and Risk.* 2018;27(1):66–76 (in Russ.). https://doi.org/10.21870/0131-3878-2018-27-1-66-76

10. Bolbit N.M., Dubova E.A., Duflot V.R., Zamaraeva T.V., Lobanova E.I., Rybkin N.I. Method for producing a thermosensitive radiopharmaceutical agent: RF Pat. 2665140. Publ. 28.08.2018 (in Russ.).

11. Gitis S.S., Glaz A.I., Ivanov A.V. *Praktikum po organicheskoi khimii: Organicheskii sintez* (*Workshop on organic chemistry: Organic synthesis*). Moscow: Vysshaya shkola; 1991. 303 p. (in Russ.).

12. Korshunov M.A, Mikhlin V.S., Bondarenko F.N. Interaction of amine-alkylaminoalkanols with esters and acid chlorides of acrylic and methacrylic acids. *Zh. Org. khim.* 1969;5(2):254–263 (in Russ.).

13. *Gosudarstvennaya Farmakopeya Rossiiskoi Federatsii XIV* (*State Pharmacopoeia of the Russian Federation XIV*). Moscow: Gos. Med. Izd. 2018. V. 1. 1470 p. (in Russ.).

14. Pavia D.L., Lampman G.M., Kriz G.S., Vyvyan J.A. *Introduction to Spectroscopy*: 5th ed. Cengage Learning; 2009. 752 p. ISBN 978-1-285-46012-3

15. Bocias G., Houdret D., Hiopolos J. Positively charged amphiphilic polymers based on poly(*N*-isopropylacrylamide): phase behavior and shear-induced thickening in aqueous solutions. *Macromolecules.* 2000;33(8):2929–2935. https://doi.org/10.1021/ma991409f

16. Bertrand N., Fleischer J.G., Wasan K.M., Leroux J.-C. Pharmacokinetics and biodistribution of *N*-isopropylacrylamide copolymers for the design of pH-sensitive liposomes. *Biomaterials.* 2009;30(13):2598–2605. http://doi.org/10.1016/j.biomaterials.2008.12.082

17. Loginova N.N., Gavurina R.K., Alexandrova M.L. Polymerization of *N*,*N*-diethylaminoethylmethacrylate hydrochloride in aqueous solutions. *Vysokomolek. soed. = Polym. Sci.* 1969;11(9):643–645 (in Russ.).

2. Галаев И.Ю. Умные полимеры в биотехнологии и медицине. *Успехи химии.* 1995;64(5):505–524. https://doi.org/10.1070/RC1995v064n05ABEH000161

3. Weller R.E., Lind M.E., Fisher D.R., *et al.* Stimulus sensitive gel with radioisotope and methods of making: US Patent US6296831B1, 2001. Oct. 2.

4. Weller R.E., Lind M.E., Fisher D.R., Gutovska A., Campbell A.A. Stimulus Sensitive Gel with Radioisotope and Methods of Making. US Patent US6869588B2, 2005. Mar. 22.

5. Cao Z., Jin Y., Zhang B., Miao Q., Ma C. A novel temperature- and pH-responsive polymer-biomolecule conjugate composed of casein and poly(*N*-isopropylacrylamide). *Iran. Polym. J.* 2010;19(9):689–698.

6. Больбит Н.М., Дуфлот В.Р., Дубова Е.А., Гайворонский А.В., Лобанова Е.И., Алтынникова Т.В. Синтез и свойства термочувствительных полимер белковых коньюгатов, меченых изотопами радиоактивного йода. *Актуал. Пробл. Гуманит. и Естеств. Наук.* 2013;6(53):30–39.

7. Больбит Н.М., Дубова Е.А., Дуфлот В.Р., Гайворонский А.В. Термочувствительный полимер-протеиновый йодсодержащий радиофармпрепарат: Пат. 2554472 РФ. Заявка № 2013127985/15; заявл. 20.06.2013; опубл. 10.01.2015. Бюл. № 1.

8. Больбит Н.М., Дуфлот В.Р., Дубова Е.А., Алтынникова Т.В. Термочувствительный радиофармпрепарат для локальной радиотерапии на основе меченого изотопом ^{131}I полимер-белкового коньюгата. *В мире научных открытий.* 2013;7–3(43):30–48.

9. Петриев В.М., Тищенко В.К., Сморызанова О.А., Михайловская А.А., Больбит Н.М., Дуфлот В.Р., Гайворонский А.В., Морозова Н.Б., Якубовская Р.И. Новый радиофармпрепарат на основе термочувствительного полимера и ^{153}Sm для локальной радионуклидной терапии солидных опухолей. *Радиация и риск.* 2018;27(1):66–76. https://doi.org/10.21870/0131-3878-2018-27-1-66-76

10. Больбит Н.М., Дубова Е.А., Дуфлот В.Р., Замарева Т.В., Лобанова Е.И., Рыбкин Н.И. Способ получения термочувствительного радиофармпрепарата: Пат. 2665140 РФ. Заявл. 31.05.2016; опубл. 28.08.2018. Бюл. № 20.

11. Гитис С.С., Глаз А.И., Иванов А.В. *Практикум по органической химии: Органический синтез.* М.: Высшая школа; 1991. 303 с.

12. Коршунов М.А., Михлин В.С., Бондаренко Ф.Н. Взаимодействие амин-алкиламиноалканолов с эфирами и хлорангидридами акриловой и метакриловой кислот. *Журн. орган. химии.* 1969;5(2):254–263.

13. *Государственная Фармакопея Российской Федерации XIV.* М.: Гос. мед. изд-во; 2018. Т. 1. 1470 с.

14. Pavia D.L., Lampman G.M., Kriz G.S., Vyvyan J.A. *Introduction to Spectroscopy*: 5th ed. Cengage Learning; 2009. 752 p. ISBN 978-1-285-46012-3

15. Bocias G., Houdret D., Hiopolos J. Positively charged amphiphilic polymers based on poly(*N*-isopropylacrylamide): phase behavior and shear-induced thickening in aqueous solutions. *Macromolecules.* 2000;33(8):2929–2935. https://doi.org/10.1021/ma991409f

16. Bertrand N., Fleischer J.G., Wasan K.M., Leroux J.-C. Pharmacokinetics and biodistribution of *N*-isopropylacrylamide copolymers for the design of pH-sensitive liposomes. *Biomaterials.* 2009;30(13):2598–2605. http://doi.org/10.1016/j.biomaterials.2008.12.082

17. Логинова Н.Н., Гавурина Р.К., Александрова М.Л. Полимеризация гидрохлорида *N*,*N*-диэтиламиноэтилметакрилата в водных растворах. *Высокомолекул. соед.* 1969;11(9):643–645.

18. Sund-Levander M., Forsberg C., Wahren L.K. Normal oral, rectal, tympanic and axillary body temperature in adult men and women: a systematic literature review. *Scand. J. Caring. Sci.* 2002;16(2):122–128. http://doi.org/10.1046/j.1471-6712.2002.00069.x

18. Sund-Levander M., Forsberg C., Wahren L.K. Normal oral, rectal, tympanic and axillary body temperature in adult men and women: a systematic literature review. *Scand. J. Caring. Sci.* 2002;16(2):122–128. http://doi.org/10.1046/j.1471-6712.2002.00069.x

About the authors:

Vladimir R. Duflot, Dr. Sci. (Chem.), Director for Innovation, Obninsk Branch, Karpov Institute of Physical Chemistry (6, Kievskoe sh., Obninsk, Kaluga oblast, 249033, Russia). E-mail: duflot@karpovipc.ru. Scopus Author ID 6701534854, ResearcherID A-7104-2014, https://orcid.org/0000-0002-1546-3572

Andrey V. Gaivoronsky, Engineer, Obninsk Branch, Karpov Institute of Physical Chemistry (6, Kievskoe sh., Obninsk, Kaluga oblast, 249033, Russia); Postgraduate Student, S.S. Medvedev Department of Chemistry and Technology of Macromolecular Compounds, M.V. Lomonosov Institute of Fine Chemical Technologies, MIREA – Russian Technological University (86, Vernadskogo pr., Moscow, 119571, Russia). E-mail: andrei.gaivoronsky@yandex.ru. https://orcid.org/0000-0003-4131-7365

Ekaterina I. Lobanova, Lead Engineer, Obninsk Branch, Karpov Institute of Physical Chemistry (6, Kievskoe sh., Obninsk, Kaluga oblast, 249033, Russia). E-mail: lobanova@karpovipc.ru. https://orcid.org/0000-0002-8328-2132

Об авторах:

Дуфлот Владимир Робертович, д.х.н., директор по инновационной деятельности акционерного общества «Ордена Трудового Красного Знамени научно-исследовательский физико-химический институт им. Л.Я. Карпова» (249033, Россия, Калужская обл., г. Обнинск, Киевское шоссе, д. 6). E-mail: duflot@karpovipc.ru. Scopus Author ID 6701534854, ResearcherID A-7104-2014, https://orcid.org/0000-0002-1546-3572

Гайворонский Андрей Владимирович, инженер акционерного общества «Ордена Трудового Красного Знамени научно-исследовательский физико-химический институт им. Л.Я. Карпова» (249033, Россия, Обнинск, Киевское шоссе, д.6); аспирант кафедры химии и технологии высокомолекулярных соединений им. С.С. Медведева Института тонких химических технологий им. М.В. Ломоносова ФГБОУ ВО «МИРЭА – Российский технологический университет» (119571, Россия, Москва, пр-т Вернадского, д. 86). E-mail: andrei.gaivoronsky@yandex.ru. https://orcid.org/0000-0003-4131-7365

Лобанова Екатерина Игоревна, ведущий инженер акционерного общества «Ордена Трудового Красного Знамени научно-исследовательский физико-химический институт им. Л.Я. Карпова» (249033, Россия, Обнинск, Киевское шоссе, д. 6) E-mail: lobanova@karpovipc.ru. https://orcid.org/0000-0002-8328-2132

The article was submitted: May 05, 2020; approved after reviewed: September 23, 2020; accepted for publication: April 02, 2021.

Translated from Russian into English by M. Povorin
Edited for English language and spelling by Enago, an editing brand of Crimson Interactive Inc.

SYNTHESIS AND PROCESSING OF POLYMERS AND POLYMERIC COMPOSITES

СИНТЕЗ И ПЕРЕРАБОТКА ПОЛИМЕРОВ И КОМПОЗИТОВ НА ИХ ОСНОВЕ

ISSN 2686-7575 (Online)
https://doi.org/10.32362/2410-6593-2021-16-2-176-183
UDC 661.717.5

RESEARCH ARTICLE

Development of a polyurea-based composition with an extended life span

Sergei V. Romanov[1], Olga A. Botvinova[1], Evgenii A. Timakov[2], Larisa A. Chizhova[2], Yuri T. Panov[2,@]

[1]Production Company Elast PU, Vladimir, 600026 Russia
[2]Alexander and Nikolay Stoletovs Vladimir State University, Vladimir, 600014 Russia
[@]Corresponding author, e-mail: tpp_vlgu@mail.ru

Abstract

Objectives. *Improvement of the technology for obtaining polymer-sprayed coatings based on polycarbodiimides (polyureas) with high chemical, hydrolytic, and abrasive resistance and improved physical and mechanical properties, as well as obtainment of polyurea compositions with a lifetime of at least 5 min without loss performance characteristics (i.e., "hand-applied" polyureas) suitable for repair of coatings already in use.*

Methods. *The reaction rate between isocyanate and amino groups is almost a hundred times higher than that between isocyanate and hydroxyl groups, necessitating the use of special high-performance and high-pressure installations equipped with self-cleaning mixing chambers and heating of components. The following are determined from the obtained materials: strength, elongation at break according to the standard method, Taber abrasion, and Shore hardness.*

Results. *Three methods of slowing down the reaction are investigated: 1) the synthesis of prepolymers with the content of NCO groups from 10.5% to 18%; 2) the addition of a plasticizer into the prepolymer in the amount of 1–10 mass parts; and 3) the introduction of polyesters into the composition and radiation of the so-called "hybrid" systems. When using 14% polyesters with a molecular weight of 2000 Da, only "hybrid" systems make it possible to obtain compositions with a lifetime of more than 5 min. At the same time, the tensile strength decreases by 20%, and the abrasion increases by 40%; however, such "hybrid" systems have a higher adhesion force and are cheaper than pure polyureas, allowing them to be used as "repair" systems.*

Conclusions. *The developed composition and technology of applying "hybrid" systems allow for the repair of existing coatings without using specialized devices. "Manual" polyurea is easy to use and does not require special training.*

Keywords: *polyurea, lifetime, polymer coatings, physical and mechanical properties*

For citation: Romanov S.V., Botvinova O.A., Timakov E.A., Chizhova L.A., Panov Yu.T. Development of a polyurea-based composition with an extended life span. *Tonk. Khim. Tekhnol. = Fine Chem. Technol.* 2021;16(2):176–183 (Russ., Eng.). https://doi.org/10.32362/2410-6593-2021-16-2-176-183

НАУЧНАЯ СТАТЬЯ

Разработка композиции на основе полимочевины с увеличенным сроком жизни

С.В. Романов[1], О.А. Ботвинова[1], Е.А. Тимаков[2], Л.А. Чижова[2], Ю.Т. Панов[2,@]

[1]Производственная компания «Эласт ПУ», Владимир, 600026 Россия
[2]Владимирский государственный университет им. Александра Григорьевича и Николая Григорьевича Столетовых, Владимир, 600014 Россия
[@]Автор для переписки, e-mail: tpp_vlgu@mail.ru

Аннотация

Цели. *Совершенствование технологии получения полимерных напыляемых покрытий на основе поликарбодиимидов (полимочевин), с высокой химической, гидролитической и абразивной стойкостью и улучшенными физико-механическими показателями, а также, получение полимочевинных композиций с временем жизни не менее 5 мин без потери эксплуатационных характеристик (полимочевин «ручного» нанесения), пригодных для ремонта уже эксплуатирующихся покрытий.*
Методы. *Скорость реакции между изоцианатными и аминогруппами практически в сто раз превышает скорость реакции между изоцианатными и гидроксильными группами, что вызывает необходимость использовать специальные высокопроизводительные установки высокого давления, оснащенные самоочищающимися смесительными камерами и обогревом компонентов. У полученных материалов определяли прочность, удлинение на разрыв по стандартной методике, истираемость по Таберу и твердость по Шору.*
Результаты. *Исследованы три способа замедления реакции: во-первых, синтез предполимеров с содержанием NCO-групп от 10.5% до 18%; во-вторых, введение в предполимер пластификатора в количестве 1–10 масс.ч.; в-третьих, введение в композицию полиэфиров и получения «гибридных» систем. Показано, что только «гибридные» системы при использовании полиэфиров с молекулярной массой 2000 Да, в количестве 14% позволяют получить композиции с временем жизни более 5 мин. При этом прочность на разрыв снижается на 20%, истираемость увеличивается на 40%, но такие «гибридные» системы имеют более высокую силу адгезии и дешевле по сравнению с чистыми полимочевинами, что позволяет использовать их в качестве «ремонтных» систем.*
Выводы. *Разработанный состав и технология нанесения «гибридных» систем позволяют производить ремонтные работы существующих покрытий без применения специализированных устройств. Полимочевина «ручного» нанесения удобна в эксплуатации и не требует специальной подготовки.*

Ключевые слова: *полимочевина, время жизни, полимерные покрытия, физико-механические свойства*

Для цитирования: Романов С.В., Ботвинова О.А., Тимаков Е.А., Чижова Л.А., Панов Ю.Т. Разработка композиции на основе полимочевины с увеличенным сроком жизни. *Тонкие химические технологии.* 2021;16(2):176–183. https://doi.org/10.32362/2410-6593-2021-16-2-176-183

INTRODUCTION

The technology of obtaining polymer-sprayed coatings based on polycarbodiimides (polyureas) has been developing at an outstripping pace in the recent years. This is associated with the high chemical, hydrolytic, and abrasive resistance of these coatings and their excellent physical and mechanical properties[1,2].

A wide range of properties, which can be obtained due to a change in the structure of the polyurea composition, makes it suitable for use in many areas: in construction [1, 2], in the field of protection of mining and processing equipment [3, 4]. Unlike polyurethane and rubber, which are also actively used in the mining and processing, polyurea can be applied as a lining composition not only in the factory; there are no restrictions on the geometry of the protected surface.

This study aimed to develop repair compounds that can be manually applied to any of the most difficult surfaces. Moreover, the properties of such compositions should be comparable to those of the original polyurea coating. This goal was achieved by using hybrid polyurethane–polyurea coatings. When developing this system, the authors proceeded from the theoretical premises described in the study of S.V. Romanov (see Footnote 1).

Polyureas are an ideal material for covering large surfaces with high strength and low abrasion, which can only be applied to the surface using high-pressure (more than 100 atm) installations. After the warranty period, cracks and chips appear on the coating, which must be eliminated. For such cases, a hand-applied composition is used, which is mainly in contact with the original polyurea. The adhesion to which is a priori very high.

To obtain polyurea in the coating technology, only high-pressure installations equipped with a self-cleaning mixing chamber and heating of components are used because of the very short lifetime of the composition [5, 6]. This factor determines another indisputable advantage of polyureas, which consists in their almost complete insensitivity to the surrounding moisture.

Figure 1 schematically shows the reaction of the polyurea formation.

The disubstituted urea reacts with the isocyanate group to form biuret (Fig. 2).

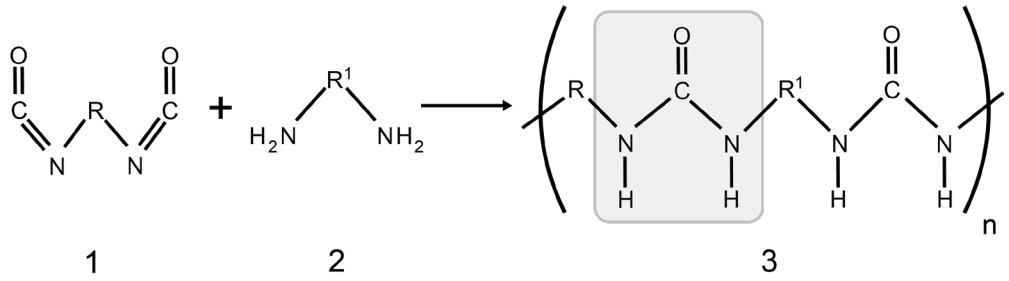

Fig. 1. Process of the polyurea formation: (1) diisocyanate, (2) polyester amine, and (3) polyurea.

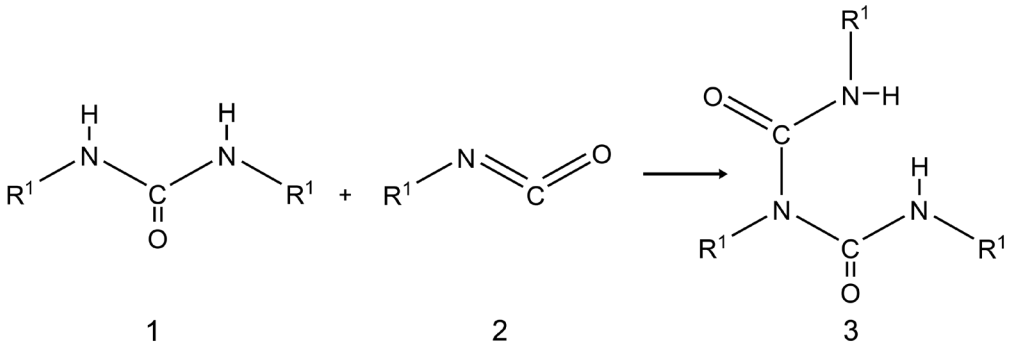

Fig. 2. Biuret production process: (1) disubstituted urea, (2) isocyanate, and (3) biuret.

[1] Romanov S.V. Sprayablepolyureas with extended service life in extreme conditions: Cand. Sci. Thesis. Kazan: KNR TU; 2019. 127 p. (in Russ.).
[2] Timakova K.A. Development of the composition and production technology of one-pack non-foaming polyurethane sealant based on domestic polyesters: Cand. Sci. Thesis. Vladimir: VGU; 2018. 136 p. (in Russ.).

The isocyanate component is called component B. It is a prepolymer containing isocyanate groups at the ends of the macromolecule, allowing the classification of polyurea as a class of polyurethane coatings [5, 6].

The market share of polyurea products is growing annually. Along with this, the number of problems associated with this product is also increasing. One of the urgent tasks is to solve the need for the local repair of polyurea coatings. It is not economically feasible to use polyurea with a short lifetime for every repair because it is a substance that cannot be applied without the help of special equipment. Therefore, studies are underway to slow down the reaction of obtaining polyurea [7].

MATERIALS AND METHODS

The following materials were used to obtain a polyurea coating: mixture used as the amine component (component A) was Jeffamine D-2000 (a mixture of polyoxypropylene amines with ~2000 Da molecular weight); Jeffamine T-5000 (a mixture of polyoxypropylene amines with ~5000 Da molecular weight) (*Houfa*, China), Deadta 80 (*Dow Chemical Company*, Midland, Michigan, USA), and Polilink 4200 (*ACETO GmbH*, Germany) were used as crosslinking agents, as well as the adhesion promoter was Silquest A187 (*Momentive*, Russia).

Isocyanate component (component B): a prepolymer synthesized from propylene glycol and polyisocyanate was used (Millionate MR200 (*Khimtrast*, Russia)) with a mass fraction of NCO groups of 10.5–18% [7–10]. We also used a plasticizer (i.e., dioctyl phthalate) from *Vitakhim* (Russia) and a modifier (i.e., polyester) Coradol 56-200 with 2000 Da molecular weight from *Himseil* (Russia).

The prepolymer preparation technique was similar to that described in the above study of Romanov.

The sample's tensile strength and elongation were determined using standard methods on a GP2DLC-0.5 universal tensile testing machine (*Tochpribor*, Russia). The tensile strength and the elongation at break were determined according to GOST 21751-76[3] on blades of Type 1 with a 3.0 ± 0.2 mm thickness at 100 mm/min clamping speed of the tensile testing machine.

Taber abrasion was determined on a Taber rotary platform abrasion tester model 5135/5155 (*TABER® Industries*, USA), disk H18, 1000 cycles. Meanwhile, hardness was determined according to GOST 263-75[4] on a device for measuring the material hardness according to Shore A on 6 mm-thick samples on a TVR-D installation (*Metrotest*, Russia).

RESULTS AND DISCUSSION

Polyurea has become an excellent solution for waterproofing large areas. The lifetime of this two-component system in its classical design does not exceed 10–15 s [11–13].

Several advantages and disadvantages are associated with such a short lifetime. First is the need for expensive and difficult-to-maintain equipment, which largely hinders the use of polyurea systems.

Polyurea systems are currently classified as follows according to their lifetime:

– "classic" polyurea: lifetime of up to 20 s;

– "slow" polyurea: lifetime from 3 to 4 min; and

– "manual" polyurea: lifetime of more than 5 min.

The lifetime is taken to be the gelation time, that is, the time after which the composition stops flowing from the glass rod.

The application of the "classic" and "slow" polyureas is impossible without pressure washers; hence, they cannot be used for most local repairs. "Manual" polyureas do not require special equipment. The composition lifetime allows them to be applied through manual stirring.

Unlike "classical" polyureas, "manual" systems have not been sufficiently studied.

In studies on the retardation of polyurea compositions, prepolymers have been synthesized with the content of NCO groups from 10.5% to 18%.

The reaction rate decreases with the decrease in the content of the NCO groups in the system, albeit this decrease being very small, as shown by the table below.

A decrease in the content of the NCO groups in component B leads to a decrease in the coating hardness, which is unacceptable. To avoid this, further studies are advised to rely on a formulation with an NCO-group content of at least 12.5%.

The first step in solving this problem is to use the strategy of introducing a small amount of plasticizer into component A of the system.

Figures 3 and 4 illustrate graphs of the lifetime dependence and performance characteristics of polyureas on the plasticizer percentage in the system.

[3] GOST 21751-76 Sealants. Determination method of tensile strength, ultimate elongation at break and deformation set after break. Moscow: Izd. Standartov; 1983.

[4] GOST 263-75. Rubber. Method for determination of Shore A hardness. Moscow: Izd. Standartov; 1983.

Performance characteristics of coatings with different contents of the NCO-groups in component B

Content of NCO groups in component B, %	System lifetime, s	Shore hardness, units
10.5	14	60A
12.5	11	75A
14.0	9	80A
15.5	7	92A
18.0	5	70D

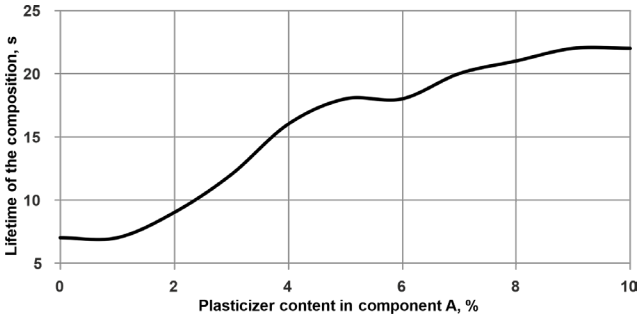

Fig. 3. Dependence of the composition lifetime on the plasticizer percentage in component A of the system.

The graphs show that the maximum possible amount of plasticizer that can be introduced into component A of the system does not exceed 5%. With the addition of a larger amount of plasticizer, the system lifetime significantly increases, but the physicomechanical parameters dramatically decrease. When 5% is added, these indicators practically do not deteriorate. Such indicators as abrasion and elongation at break even slightly increase.

However, the system lifetime can be increased only slightly. This indicator has a positive effect on the spreading of the polyurea system and, consequently, on the adhesion of the composition

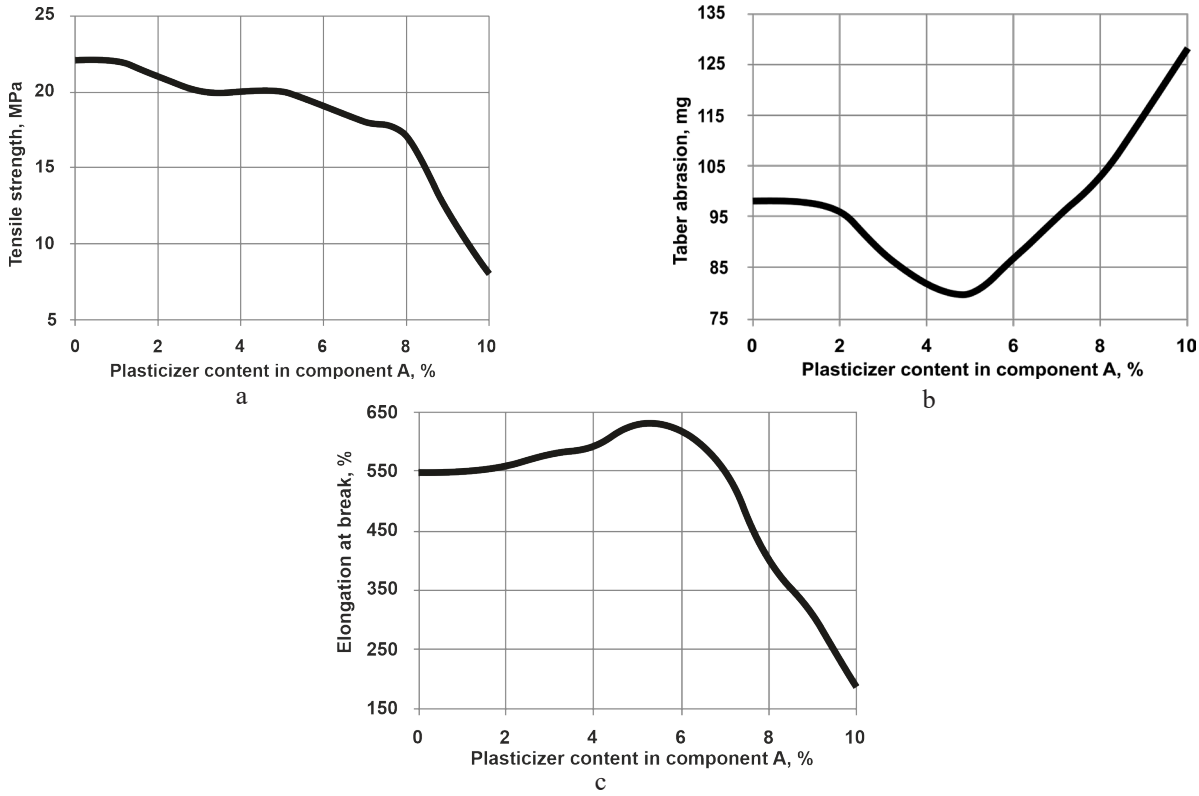

Fig. 4. Dependence of the tensile strength of the composition (a), abrasion (b), and elongation at break (c) on the plasticizer percentage in component A of the system.

to the substrate. The resulting time is not allow working with this system without the help of additional equipment.

In our opinion, the main solution for slowing down the polyurea formation is to transfer the system to the "hybrid" system category, in which, along with polyester amines, polyesters (i.e., Coradol 56-200) are introduced into component A. As a consequence, both polyurea and polyurethane groups are formed during the reaction.

Hybrid systems have a number of advantages. The lifetime of such systems is somewhat longer; thus, they spread better, have high adhesion, and take the complex geometry of the protected surface well. They are somewhat cheaper compared to pure polyureas and are not inferior in terms of performance characteristics. However, due to their chemical composition, their sensitivity to moisture significantly increases, making it impossible to work with them in humid climates or bad weather conditions.

Polyesters with high-molecular weights were selected for this research, and we expected that additional spatial hindrances would give an additional increase in the system lifetime.

Figures 5 and 6 present graphs of the system lifetime and the main physical and mechanical parameters depending on the polyester percentage (molecular weight: 2000 Da) in component A of the system.

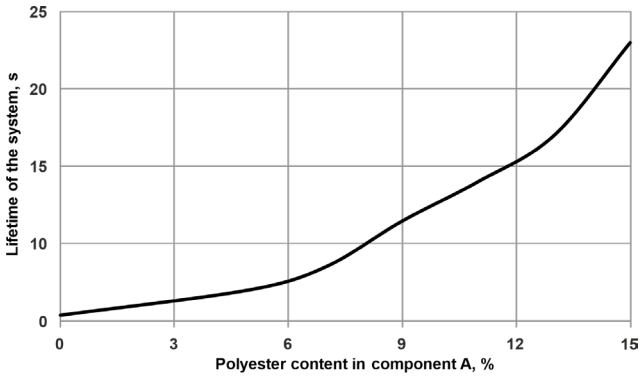

Fig. 5. Dependence of the composition lifetime on the polyester content in component A of the system.

Introducing high-molecular weight polyester increases the lifetime of the polyurea composition to the required values (5 min) and increases its abrasion while the tensile strength and elongation are reduced to an acceptable level. This allows this system to be used as a "manual" one.

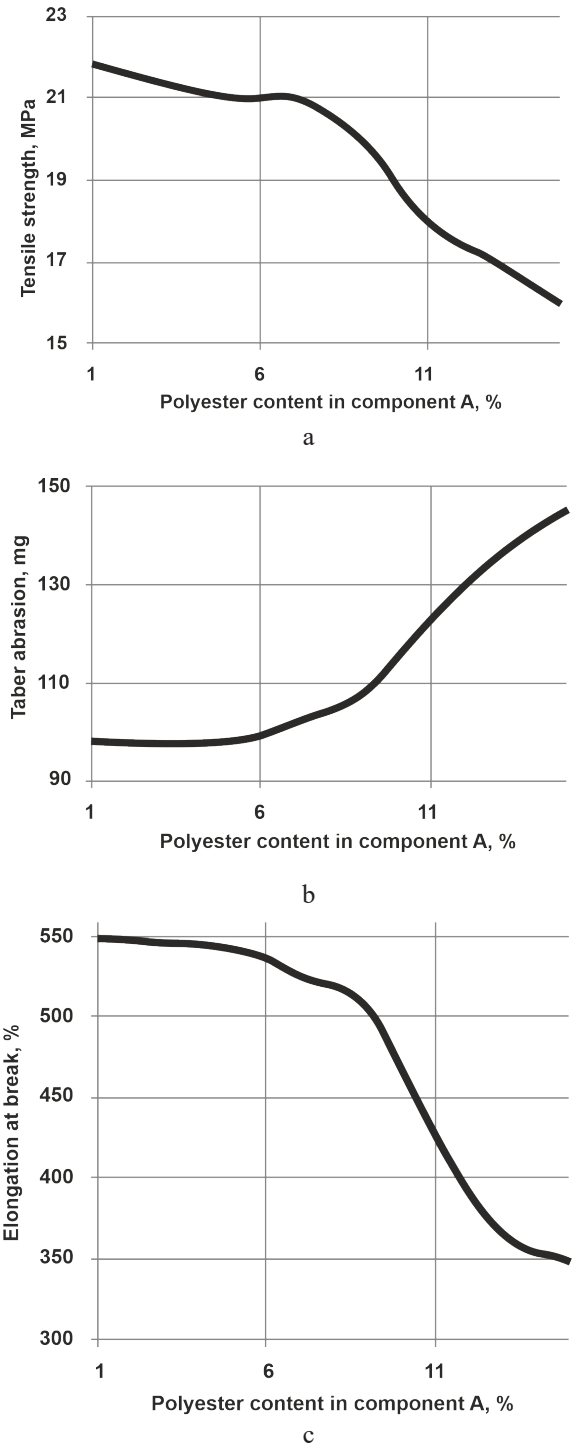

Fig. 6. Dependence of the tensile strength (a), composition abrasion (b), and elongation at break (c) on the polyester content in component A of the system.

CONCLUSIONS

In this study, a polyurea composition with a lifetime of more than 5 min can be obtained with a curing rate of approximately 30 times slower than the original composition because of the partial replacement of amine groups with less active hydroxyl groups and because of the introduction of 10–15%

polyester with ~2000 Da molecular weight into the system. The resulting systems have the required strength characteristics and higher adhesive properties. This composition of "manual" application can be used for the repair of polyurea coatings without needing high-pressure installations.

Authors' contribution

All authors equally contributed to the study.

The authors declare no conflicts of interest.

REFERENCES

1. Szycher M. S*zycher's handbook of polyurethanes*. Boca Raton: Taylor & Francis Group CRC Press; 2013. 1092 p.

2. Ryszkowska J. Supermolecular structure, morphology and physical properties of urea-urethane elastomers. *Polimery.* 2012;57(11–12):775–902. Available from URL: https://studylib.net/doc/18145915/supermolecular-structure--morphology-and-physical-propert

3. Wolf A.T. (Ed.). Durability of Building and Construction Sealants and Adhesives. V. 3. *Journal of ASTM International Selected Technical Papers STP1545*. 2010. XVII. 417 p. ISBN 978-0-8031-3426-3.

4. Stengard R.A. High-pressure impingement mixing-route to faster, better PU parts. *Plast. Tech.* 1974;41–44.

5. Zafar F., Sharmin E. *Polyurethane.* Rijeka, Croatia: InTech; 2012. 480 p. ISBN 978-953-51-0726-2

6. Saunders J.H., Hansen R.H. The mechanism of foam formation. In: *Plastic foams.* Part 1. Frisch K.C., Saunders J.H. (Eds.). New York: Marcel Dekker; 1972. P. 3–108.

7. Botvinova O.A., Panov Y.T., Romanov S.V. Producing Bicomponent Sealants Based on Polyaspartate Urea Resins. *Polym. Sci. Ser. D.* 2020;13(4):407–413. https://doi.org/10.1134/S1995421220040048

8. Steiner E.C., Pelletier R.R., Trucks R.O. A study of the polymerization of propylene oxide catalyzed by anhydrous potassium hydroxide. *J. Amer. Chem. Soc.* 1964;86(21):4678–4686. https://doi.org/10.1021/ja01075a031

9. Van Maris R., Tamano Y., Yoshimura H., Gay K.M. Polyurethane Catalysis by Tertiary Amines. *J. Cell. Plast.* 2005;41(4):305–322. https://doi.org/10.1177%2F0021955X05055113

10. Ward R.S., Jones R.L. Polyurethanes and Silicone Polyurethane Copolymers. In book: *Comprehensive Biomaterials* II. V. 1. 2017. P. 570-619. https://doi.org/10.1016/B978-0-08-100691-7.00179-8

11. Vahabi H., Rastin H., Movahedifar E., Antoun K., Brosse N., *et al*. Flame Retardancy of Bio-Based Polyurethanes: Opportunities and Challenges. *Polymers.* 2020;12(6):1234. https://doi.org/10.3390/polym12061234

12. Sándor N., Gelade E., van Maris R., Rácz G. Effect of melamine on the foam kinetics of polyurethane model system. *Models Chem.* 1997;134(2):253–263. https://doi.org/10.1002/(SICI)1097-4628(19980307)67:10<1739::AID-APP7>3.0.CO;2-K

13. Vreenegoor N.C. The Foamax process for making flat-top flexible polyurethane slabstock foams. *Plast. Rub. Proc.* 1977;2(1):30–32.

About the authors:

Sergei V. Romanov, Cand. Sci. (Eng.), Director of the Production Company Elast-PU (21a, Gastello ul., Vladimir, 600026, Russia). E-mail: Romanov-elastpu@mail.ru. https://orcid.org/0000-0002-5152-4678

Olga A. Botvinova, Researcher, Production Company Elast-PU (21a, Gastello ul., Vladimir, 600026, Russia). E-mail: ermolaeva_olya@inbox.ru. https://orcid.org/0000-0003-0217-8446

Evgenii A. Timakov, Assistant, Chemical Technologies Department, Institute of Architecture, Construction, and Energy, Alexander and Nikolay Stoletovs Vladimir State University (87, Gor'kogo ul., Vladimir, 600026, Russia). E-mail: okakie@yandex.ru. Scopus Author ID 57219018403, https://orcid.org/0000-0003-3312-0810

Larisa A. Chizhova, Associate Professor, Chemical Technologies Department, Institute of Architecture, Construction, and Energy, Alexander and Nikolay Stoletovs Vladimir State University (87, Gor'kogo ul., Vladimir, 600026, Russia). E-mail: lar-chizhova@mail.ru. https://orcid.org/0000-0003-2838-2349

Yuri T. Panov, Dr. Sci. (Eng.), Professor, Head of the Chemical Technologies Department, Institute of Architecture, Construction, and Energy, Alexander and Nikolay Stoletovs Vladimir State University (87, Gor'kogo ul., Vladimir, 600026, Russia). E-mail: tpp_vlgu@mail.ru. https://orcid.org/0000-0001-8528-1195

Об авторах:

Романов Сергей Викторович, к.т.н., директор ООО «Эласт-ПУ» (Россия, 600026, Владимир, ул. Гастелло, д. 21а). E-mail: Romanov-elastpu@mail.ru. https://orcid.org/0000-0002-5152-4678

Ботвинова Ольга Андреевна, научный сотрудник лаборатории ООО «Эласт-ПУ» (Россия, 600026, Владимир, ул. Гастелло, д. 21а). E-mail: ermolaeva_olya@inbox.ru. https://orcid.org/0000-0003-0217-8446

Тимаков Евгений Александрович, ассистент кафедры химических технологий Института архитектуры, строительства и энергетики ФГБОУ ВО «Владимирский государственный университет им. Александра Григорьевича и Николая Григорьевича Столетовых» (Россия, 600000, Владимир, ул. Горького, д. 87). E-mail: okakie@yandex.ru. Scopus Author ID 57219018403, https://orcid.org/0000-0003-3312-0810

Чижова Лариса Анатольевна, доцент кафедры химических технологий Института архитектуры, строительства и энергетики ФГБОУ ВО «Владимирский государственный университет им. Александра Григорьевича и Николая Григорьевича Столетовых» (Россия, 600000, Владимир, ул. Горького, д. 87). E-mail: lar-chizhova@mail.ru. https://orcid.org/0000-0003-2838-2349

Панов Юрий Терентьевич, д.т.н., профессор, заведующий кафедрой химических технологий Института архитектуры, строительства и энергетики ФГБОУ ВО «Владимирский государственный университет им. Александра Григорьевича и Николая Григорьевича Столетовых» (Россия, 600000, Владимир, ул. Горького, д. 87). E-mail: tpp_vlgu@mail.ru. https://orcid.org/0000-0001-8528-1195

The article was submitted: December 11, 2020; approved after reviewed: March 05, 2021; accepted for publication: April 12, 2021.

Translated from Russian into English by H. Moshkov
Edited for English language and spelling by Enago, an editing brand of Crimson Interactive Inc.

CHEMISTRY AND TECHNOLOGY OF INORGANIC MATERIALS
ХИМИЯ И ТЕХНОЛОГИЯ НЕОРГАНИЧЕСКИХ МАТЕРИАЛОВ

ISSN 2686-7575 (Online)

https://doi.org/10.32362/2410-6593-2021-16-2-184-191

UDC 538.945

RESEARCH ARTICLE

Transmission coefficients of superconducting particles

Anton V. Matasov[@], Armen A. Dovmalov, Daria M. Babyshkina

National Research University MPEI, Moscow, 111250 Russia
[@]Corresponding author, e-mail: matasov_av93@mail.ru

Abstract

Objectives. *There is no general theory of superconductivity capable of fully describing this phenomenon, which imposes its own difficulties in the search for new superconducting materials, as well as in the study of their properties. In particular, the electrodynamics of a superconducting system is unexplored. With the aim of a possible further description of the electrodynamics of superconductors, the temperature dependences of the energy parameters of a Cooper pair in the potential field of Abrikosov vortex were analyzed.*

Methods. *The basis for the obtained results of the work was the consideration of the transmission coefficient for a superconducting particle in the approximation of the Wentzel–Kramers–Brillouin method, as well as the relationship between the critical temperature and the London penetration depth and the coherence length based on the model of plasmon destruction of the superconducting state.*

Results. *The dependences of the lifetime of a particle in a potential well, penetration depth, frequency of impacts of a particle against a potential barrier, blurring of the energy level, transmission coefficient, and potential and kinetic energy of a particle on temperature were obtained. The characteristic values of these parameters were obtained at absolute zero for various cuprate, organic, and other superconducting materials. The dependences of the critical electric potential on temperature, as well as the London penetration depth, coherence length, and electric potential on the transmission coefficient at different temperatures were obtained. The form of the dependences qualitatively corresponds to the experimental data.*

Conclusions. *The results obtained can be used to construct a general theory of superconductivity, describe the electrodynamics of a superconducting state, and develop new superconductors with higher critical currents.*

Keywords: *theory of superconductivity, Cooper pair, Abrikosov vortex, electrodynamics of superconductors*

For citation: Matasov A.V., Dovmalov A.A., Babyshkina D.M. Transmission coefficients of superconducting particles. *Tonk. Khim. Tekhnol. = Fine Chem. Technol.* 2021;16(2):184–191 (Russ., Eng.). https://doi.org/10.32362/2410-6593-2021-16-2-184-191

НАУЧНАЯ СТАТЬЯ

О коэффициенте прохождения сверхпроводящей частицы

А.В. Матасов[@], А.А. Довмалов, Д.М. Бабышкина

Национальный исследовательский университет «МЭИ», Москва, 111250 Россия
[@]Автор для переписки, e-mail: matasov_av93@mail.ru

Аннотация

Цели. *Общая теория сверхпроводимости, способная полностью описать данное явление, отсутствует, что накладывает свои трудности в поиске новых сверхпроводящих материалов и исследовании их свойств. В частности, неисследованной является электродинамика сверхпроводящей системы. С целью возможного дальнейшего описания электродинамики сверхпроводников в работе рассматриваются температурные зависимости энергетических параметров куперовской пары в потенциальном поле вихря Абрикосова.*

Методы. *Основой для полученных результатов работы являлось рассмотрение коэффициента прохождения сверхпроводящей частицы в приближении метода Вентцеля–Крамерса–Бриллюэна, а также связь критической температуры с лондоновской глубиной проникновения и длиной когерентности на основе модели плазмонного разрушения сверхпроводящего состояния.*

Результаты. *Получены зависимости времени жизни частицы в потенциальной яме, глубины проникновения, частоты ударов частицы о потенциальный барьер, размытости энергетического уровня, коэффициента прохождения, потенциальной, кинетической энергии частицы от температуры. Получены характерные значения данных параметров при абсолютном нуле для различных купратных, органических и других сверхпроводящих материалов. Получены зависимости критического электрического потенциала от температуры, лондоновской глубины проникновения, длины когерентности; электрического потенциала от коэффициента прохождения при разных значениях температуры. Вид зависимостей качественно соответствует экспериментальным данным.*

Выводы. *Полученные результаты могут быть использованы для построения общей теории сверхпроводимости, описании электродинамики сверхпроводящего состояния, разработки новых сверхпроводников, обладающих более высокими значениями критических токов.*

Ключевые слова: *теория сверхпроводимости, куперовская пара, вихрь Абрикосова, электродинамика сверхпроводников*

Для цитирования: Матасов А.В., Довмалов А.А., Бабышкина Д.М. О коэффициенте прохождения сверхпроводящей частицы. *Тонкие химические технологии.* 2021;16(2):184–191. https://doi.org/10.32362/2410-6593-2021-16-2-184-191

INTRODUCTION

Based on the works of Abrikosov [1] and the discovery of Abrikosov vortices, the electrodynamics of the superconducting state is mainly described through the motion of the vortex lattice [2]. Mechanical models of motion consider the forces of viscous friction, pinning of vortices, and forces that deform the lattice. However, this approach does not consider the quantum nature of the Abrikosov vortex and the phenomenon of superconductivity. Another common approach to describing the dynamics of the superconducting state is the solitonic theory of superconductivity [3]. This approach considers nonlinear excitations, which often leads to difficulties in obtaining an accurate solution, and although the solitonic theory accounts for some differential characteristics of cuprate superconductors it does not apply to all superconducting materials.

The absence of a general theory describing the electrodynamics of the superconducting state means that to give a generalized theoretical description of the current–voltage characteristics of most superconducting compounds, which is extremely important for their wider application, is difficult.

In this study, we analyze a model of the motion of a Cooper pair in an Abrikosov vortex. This problem has been considered [4] using a framework that estimated the relationship between the coherence length and London penetration depth, as well as solving the one-dimensional Schrodinger equation, which is important for constructing a general theory of superconductivity and the electrodynamics of the superconducting state. We investigated the dependences of various energy parameters of a superconducting particle on temperature, including its transmission coefficient, which formed the basis of a qualitative model describing the current-voltage characteristics of superconductors.

TEMPERATURE DEPENDENCES OF THE ENERGY PARAMETERS OF THE COOPER PAIR IN THE POTENTIAL FIELD OF THE ABRIKOSOV VORTEX

We estimated the dependence of the transmission coefficient of a superconducting particle D through the potential barrier of the Abrikosov vortex U. The region of the Abrikosov vortex where the energy of a superconducting particle can be efficiently dissipated is the non-superconducting inner cylindrical region. In this region, one can assume that the energy of the Abrikosov vortex is constant in the limit $\xi << \lambda$, where ξ is the coherence length, which is the characteristic size of the Cooper pair, and λ is the London penetration depth, which is the characteristic depth of penetration of the external magnetic field into the superconductor. [5] Then, using the quasi-classical Wentzel–Kramers–Brillouin approximation [6], we obtained the following expression for the transmission coefficient:

$$D(T) = \frac{e^{-4\xi(T)\sqrt{\frac{2m}{\hbar^2}(U(T)-E(T))}}}{(1+0.25e^{-4\xi(T)\sqrt{\frac{2m}{\hbar^2}(U(T)-E(T))}})^2}, \quad (1)$$

where m is the mass of the Cooper pair (in this paper it is twice the mass of the electron), $\hbar$ is the Dirac constant, and E is the energy of the Cooper pair.

The potential energy is the energy of the Abrikosov vortex, which is generally expressed in terms of the Bessel function K_0 [5] and is often normalized to a certain unit of length. In this paper, the coherence length was used as the unit of length:

$$U(T) = \frac{\Phi_0^2 \xi(E)}{4\pi\mu_0\lambda(T)^2} K_0\left(\frac{\xi(T)}{\lambda(T)}\right), \quad (2)$$

where Φ_0 is the magnetic flux quantum, μ_0 is the magnetic constant, and λ is the London penetration depth.

Using the analogy of an energy gap, the energy of a superconducting particle can be expressed as $E = 2kT_c$, where T_c is the critical temperature, i.e., the temperature at which a material transitions to the superconducting state. Building on the relationship between the critical temperature, London penetration depth, and coherence length obtained in [7], we expressed the particle energy in terms of these characteristic lengths:

$$E(T) = \hbar c / \lambda(T) \sqrt{\frac{4\pi\alpha\xi(T)}{\lambda(T)}}, \quad (3)$$

where c is the speed of light and α is the fine structure constant.

The dependences of the measured ξ and λ on temperature were determined using standard expressions:

$$\xi(T) = \frac{\xi(0)}{\sqrt{1-\left(\frac{T}{T_c}\right)^4}}, \quad (4)$$

$$\lambda(T) = \frac{\lambda(0)}{\sqrt{1-\left(\frac{T}{T_c}\right)^4}}, \quad (5)$$

We plotted the dependences of the energies and the transmission coefficient on the temperature for the $YBa_2Cu_3O_7$ superconductor at $\lambda(0) = 180$ nm, $\xi(0) = 0.4$ nm, and $T_c = 90.8$ K [8] (Figs. 1 and 2).

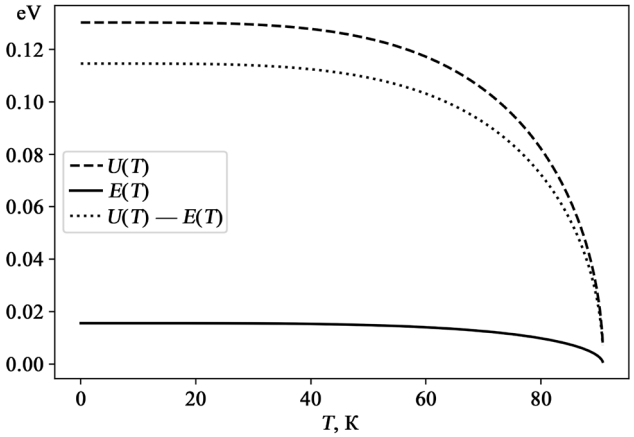

Fig. 1. Dependence of the potential, U, and kinetic, E, energies and the energy difference on temperature for $YBa_2Cu_3O_7$.

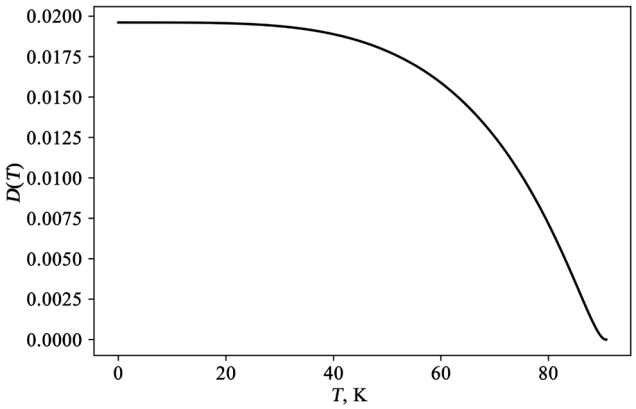

Fig. 2. Dependence of the transmission coefficient on temperature for $YBa_2Cu_3O_7$.

Based on the obtained transmission coefficient, we were able to obtain the dependence of the frequency of the particle impacting on the barrier n, the lifetime of the particle in the well t, the depth of penetration under the potential barrier L, and the blurring of the energy level on the temperature T [6]:

$$n(T) = \frac{1}{4\lambda(T)}\sqrt{\frac{2E(T)}{m}} \quad (6)$$

$$t(T) = \frac{1}{n(T)D(T)} \quad (7)$$

$$L(T) = \frac{\hbar}{2\sqrt{2m(U(T) - E(T))}} \quad (8)$$

$$\Delta E(T) = h / t(T) \quad (9)$$

From this we found that the potential and kinetic energies of the particle, the transmission coefficient, the number of collisions per unit time, and the blurring of the energy gap decreased with increasing temperature; however, the penetration depth and lifetime of the Cooper pair in the non-superconducting region of the vortex increased with increasing temperature.

We then calculated the characteristic values of (1)–(3), (6), (8), and (9) for cuprate, organic, and some other type-II superconductors at T = 0 K (Table 1). For this analysis, materials were selected which validated the expression (3) and corresponded with the calculated (T_c*) and experimental (T_c) critical temperatures (Table 2).

Based on the obtained dependence of the transmission coefficient of the Cooper pair on temperature, we constructed a qualitative model for describing the current-voltage characteristics of superconductors.

In the first approximation we assumed that the energy of the Abrikosov vortex does not depend on

Table 1. Typical values of the energy parameters of some superconductors at T = 0 K

Material	$D(0)$	$U(0)$, eV	$E(0)$, eV	$n(0)$, s^{-1}	$L(0)$, m	$\Delta E(0)$, eV
$La_{1.85}Sr_{0.15}CuO$	0.021	0.042	5.606×10^{-3}	1.827×10^{10}	3.623×10^{-10}	1.567×10^{-6}
$YBa_2Cu_3O_7$	0.02	0.13	0.016	7.29×10^{10}	2.04×10^{-10}	5.909×10^{-6}
$Bi_2Sr_2CuO_{6+x}$	1.55×10^{-3}	0.025	3.234×10^{-3}	7.457×10^{9}	4.638×10^{-10}	4.779×10^{-8}
$Bi_2Sr_2CaCu_2O_{8+x}$	2.636×10^{-11}	0.193	0.016	4.459×10^{10}	1.642×10^{-10}	4.86×10^{-15}
$HgBa_2CuO_{4+x}$	9.739×10^{-7}	0.175	0.016	5.325×10^{10}	1.734×10^{-10}	2.144×10^{-10}
$HgBa_2CaCu_2O_{6+x}$	1.242×10^{-12}	0.336	0.027	8.337×10^{10}	1.24×10^{-10}	4.281×10^{-16}
$HgBa_2Ca_2Cu_3O_{8+x}$	6.248×10^{-11}	0.318	0.026	8.437×10^{10}	1.277×10^{-10}	2.18×10^{-14}
κ-$(BEDT\text{-}TTF)_2Cu(NCS)_2$	0.108	0.011	1.794×10^{-3}	4.623×10^{9}	7.366×10^{-10}	2.059×10^{-6}
$(BEDT\text{-}TTF)_2Cu[N(CN)_2]Br$	0.233	0.01	1.928×10^{-3}	5.883×10^{9}	7.534×10^{-10}	5.674×10^{-6}
β_L-$(BEDT\text{-}TTF)_2\vert_3$	0.088	2.098×10^{-3}	4.08×10^{-4}	6.055×10^{8}	1.68×10^{-9}	2.21×10^{-7}
β-$(BEDT\text{-}TTF)_2\vert Br_2$	1.164×10^{-64}	0.014	1.121×10^{-3}	7.025×10^{8}	5.978×10^{-10}	3.382×10^{-70}
β-$(BEDT\text{-}TTF)_2\vert Au_2$	8.041×10^{-23}	0.011	1.002×10^{-3}	8.302×10^{8}	7.076×10^{-10}	2.760×10^{-28}
CNT(5,0)	1.139×10^{-13}	0.027	2.59×10^{-3}	3.513×10^{9}	4.429×10^{-10}	1.654×10^{-18}
$NbSe_2$	5.705×10^{-4}	0.012	1.626×10^{-3}	2.82×10^{9}	6.695×10^{-10}	6.653×10^{-9}
H_2S(155 HPa)	1.471×10^{-18}	0.468	0.034	1.019×10^{11}	1.047×10^{-10}	6.200×10^{-22}

Note: BEDT-TTF is bis(ethylendithio)tetratiafulvalen and CNT(5,0) is a carbon nanotube with a chirality of (5,0).

Table 2. Comparison of the calculated (T_c*) and experimental (T_c) critical temperatures of various superconductors

Material	ξ, nm	λ, nm	T_c^*, K	T_c, K	Reference
$La_{1.85}Sr_{0.15}CuO$	0.7	430	32.5	34	[8]
$YBa_2Cu_3O_7$	0.4	180	90.8	92.4	[8]
$Bi_2Sr_2CuO_{6+x}$	1.5	800	18.8	13	[9]
$Bi_2Sr_2CaCu_2O_{8+x}$	2	200–300 at 300	94.3	94	[9]
$HgBa_2CuO_{4+x}$	1.2	200–450 at 252	94.9	95	[9]
$HgBa_2CaCu_2O_{6+x}$	1.7	205	154	127	[9]
$HgBa_2Ca_2Cu_3O_{8+x}$	1.5	130–200 at 200	150	135	[9]
κ-$(BEDT\text{-}TTF)_2Cu(NCS)_2$	0.8	500–2000 at 961	10.41	10.4	[9]
$(BEDT\text{-}TTF)_2Cu[N(CN)_2]Br$	0.5–1.2 at 0.5	550–1500 at 783	11.19	11.2	[9]
β_L-$(BEDT\text{-}TTF)_2\|_3$	2	3500	2.37	1.5	[9]
β-$(BEDT\text{-}TTF)_2\|Br_2$	44–46 at 44	4000–5000 at 5000	6.5	2.2	[9]
β-$(BEDT\text{-}TTF)_2\|Au_2$	18–25 at 18	4000	5.81	4.2	[9]
CNT(5,0)	6.6–12 at 6.6	1430–1570 at 1520	15.03	15	[10]
$NbSe_2$	2.5	1500	9.44	7	[9]
H_2S(155 HPa)	2.15	189	195.56	190–203	[11]

the external applied electric field, allowing us to add to the energy of the particle E the dependence on the applied potential φ as follows: $E(T, \varphi) = E(T) + 2q\varphi$, where q is the charge of the electron.

Then the critical electric potential was defined as $\varphi_c = (U - E)/2q$ (Fig. 3). We also determined the dependence of the critical potential on the characteristic lengths that determine the superconducting state (Fig. 4).

The dependence of the electric potential on the transmission coefficient at different temperatures is shown in Fig. 5, which physically represents a qualitative description of the current-voltage characteristic of superconductors.

RESULTS AND DISCUSSION

The obtained dependences of various energy parameters of superconducting materials were mainly expressed in terms of the characteristic lengths that determine the superconducting state, the London penetration depth, and the coherence length. The determination of the transmission coefficient was obtained based on the dependence of the characteristic lengths on temperature, which is not generally described by equations in the form of (4) and (5) [12] but instead requires specific consideration for a particular superconducting material.

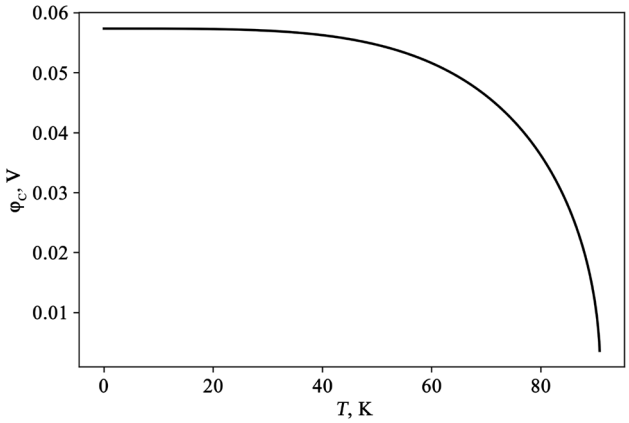

Fig. 3. Dependence of the critical electric potential (φ_c) value on temperature for $YBa_2Cu_3O_7$.

We found that the considered dependence of the particle energy on temperature has a similar form to the dependence of the energy gap on temperature.

According to our obtained characteristic values of the energy parameters shown in Table 2, we concluded that some organic materials with large London penetration depths, as well as H_2S, are significantly knocked out of the materials. These organic materials are less accurately described by the expression for the critical temperature given in [7], which may indicate

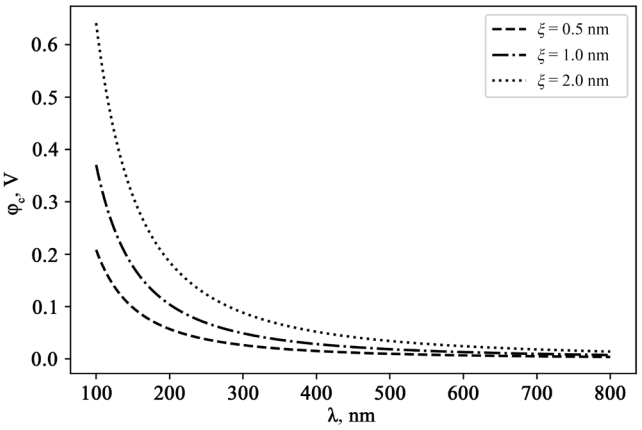

Fig. 4. Dependence of the value of the critical electric potential (φ_c) on the London depth of penetration for various fixed coherence lengths.

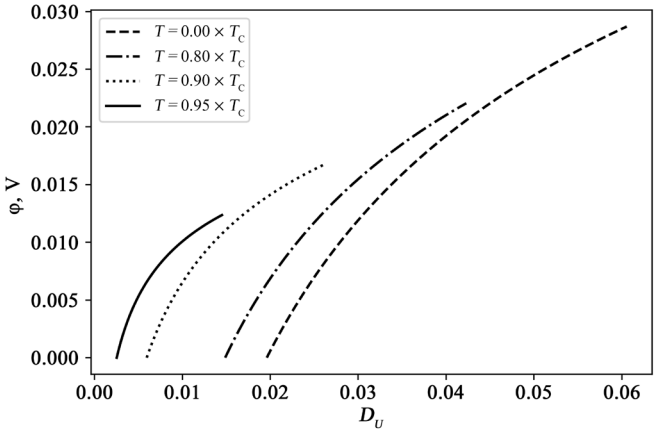

Fig. 5. Dependence of the electric potential on the transmission coefficient at different temperatures for $YBa_2Cu_3O_7$.

that their effective characteristic lengths match the experimental critical temperatures more closely. The obtained values for H_2S indicate that superconducting properties around room temperature require an increase in the energy of the Abrikosov vortex.

The direct proportionality of the transmission coefficient to the tunnel current means that the obtained dependence $\varphi(D)$ (Fig. 5) has a direct relationship with the current-voltage characteristics of superconducting materials and, as we have demonstrated, has a similar form to experimental measurements in this area [13, 14].

In this study, the dependence on the electric potential φ was given by adding the kinetic energy required to accelerate the particles; however, to improve the accuracy of the model, we found that it was necessary to determine all the dependences on external factors for the parameters of a superconducting material through the dependences on the London penetration depth and coherence length. Despite this, the obtained dependence of the critical potential on the temperature has a form that can describe the experimental data but can also easily be reduced to the traditional linear dependence of the critical current on the temperature in the region of the phase transition of the Bardeen-Cooper-Schrieffer theory [15] and experimental power approximations. The critical electric potential, as well as the kinetic energy of the superconducting particle and its critical temperature, increased with increasing coherence length and decreased with increasing London penetration depth.

CONCLUSIONS

In this study, the dependences of various energy parameters on temperature were obtained with the dependence of the transmission coefficient being especially relevant to the future construction of a general theory of the electrodynamics of superconductors.

The characteristic values of these energy parameters can be used to evaluate the fundamental and applied properties associated with the mechanisms of superconductivity.

The obtained dependences of the critical electric potential on temperature and the transmission coefficient qualitatively matched the corresponding experimental measurements and can be used to construct a theory of superconductivity, which itself can be used to develop new superconductor based current-conducting devices. In the future, we regard the dependence of the characteristic lengths on the electric potential to be of interest in the building of a more accurate model of the current-voltage characteristics of superconductors.

Authors' contribution

The contribution of each of the authors was to jointly set tasks, solve them, and discuss the results. The authors made an equal contribution to the calculation part of the work, the preparation of the article for publication, and the use of software to create a visualization of the obtained dependencies.

The authors declare no conflicts of interest.

REFERENCES

1. Abrikosov A.A. The magnetic properties of superconducting alloys. *J. Phys. Chem. Solids.* 1957;2(3):199–208. https://doi.org/10.1016/0022-3697(57)90083-5

2. Matsushita T. *Flux Pinning in Superconductors*. Part of the Springer Series in Solid-State Sciences book series. V. 178. Springer-Verlag Berlin Heidelberg; 2014. 475 p. https://doi.org/10.1007/978-3-642-45312-0

3. Mourachkine A. *High-Temperature Superconductivity in Cuprates. The Nonlinear Mechanism and Tunneling Measurements.* Part of the Fundamental Theories of Physics book series. V. 125. Kluwer Academic Publishers; 2002. 317 p. https://doi.org/10.1007/0-306-48063-8

4. Matasov A.V., Cherkasov A.P., Kholodny D.S. and Mikhaylov I.A. Cooper Pair in the Potential Field of Abrikosov Vortex. In: *2020 International Youth Conference on Radio Electronics, Electrical and Power Engineering (REEPE)*. Moscow, Russia; 2020. 4 p. https://doi.org/10.1109/REEPE49198.2020.9059113

5. Schmidt V.V., Müller P., Ustinov A.V. The *Physics of Superconductors: Introduction to Fundamentals and Applications*. Springer-Verlag Berlin Heidelberg; 1997. 207 p. https://doi.org/10.1007/978-3-662-03501-6

6. Davydov A.S. *Quantum Mechanics*. 2nd ed. Oxford, New York: Pergamon Press; 1976. 637 p.

7. Matasov A.V. Prediction of the critical temperature of unconventional superconductors based on the plasmon mechanism. In: *AIP Conference Proceedings.* 2019;2163(1):020005. https://doi.org/10.1063/1.5130084

8. Tsipenyuk Yu.M. *Fizicheskie osnovy sverkhprovodimosti* (*Physical foundations of superconductivity*). Moscow: MIPT Publishing House: Fizmatkniga; 2003; 158 p. ISBN 5-89155-099-7

9. Kleiner R., Buckel W. *Superconductivity: An Introduction*. Germany: Wiley-VCH Verlag GmbH and Co; 2016. 496 p.

10. Wang Z., Shi W., Lortz R., Sheng P. Superconductivity in 4-Angstrom carbon nanotubes – a short review. *Nanoscale.* 2012;4(1):21–41. https://doi.org/10.1039/C1NR10817D

11. Talantsev E.F., Crump W.P., Tallon J.L. Universal scaling of the self-field critical current in superconductors: from sub-nanometre to millimetre size. Sci. Rep. 2017;7(1):10010. https://doi.org/10.1038/s41598-017-10226-z

12. Prozorov R., Giannetta R.W. TOPICAL REVIEW: Magnetic penetration depth in unconventional superconductors. *Supercond. Sci. Technol.* 2006;19(8):R41–R67. https://doi.org/10.1088/0953-2048/19/8/R01

13. Ozkan H., Topal U., Gasanly N.M., Albiss B., Kayed T. Voltage-current characteristics of the thallium-based ceramic superconductors. *Supercond. Sci. Technol.* 1999;12(9):592. https://doi.org/10.1088/0953-2048/12/9/303

14. Sun Y., Zhao W., Wang J. *et al*. Voltage-current properties of superconducting amorphous tungsten nanostrips. *Sci. Rep.* 2013;3:2307. https://doi.org/10.1038/srep02307

15. Original Article. Ambegaokar V., Baratoff A. Tunneling Between Superconductors. *Phys. Rev. Lett.* 1963;10(11):486. https://doi.org/10.1103/PhysRevLett.10.486

Erratum. Ambegaokar V., Baratoff A. Tunneling Between Superconductors. *Phys. Rev. Lett.* 1963;11(2):104. https://doi.org/10.1103/PhysRevLett.11.104

About the authors:

Anton V. Matasov, Postgraduate Student, Department of Physics and Technology of Electrotechnical Materials and Components, Institute of Electrical Engineering and Electrification, National Research University MPEI (14, Krasnokazarmennaya ul, Moscow, 111250, Russia). E-mail: matasov_av93@mail.ru. Scopus Author ID 57208886094, ResearcherID Q-9794-2017, https://orcid.org/0000-0001-6092-5089

Armen A. Dovmalov, Student, Department of Physics and Technology of Electrotechnical Materials and Components, Institute of Electrical Engineering and Electrification, National Research University MPEI (14, Krasnokazarmennaya ul., Moscow, 111250, Russia). E-mail: armenbbb80821@gmail.com. https://orcid.org/0000-0002-4285-7876

Daria M. Babyshkina, Student, Department of Physics and Technology of Electrotechnical Materials and Components, Institute of Electrical Engineering and Electrification, National Research University MPEI (14, Krasnokazarmennaya ul., Moscow, 111250, Russia). E-mail: dashababyshkina@gmail.com. https://orcid.org/0000-0001-7893-5525

Об авторах:

Матасов Антон Владимирович, аспирант кафедры физики и технологии электротехнических материалов и компонентов Института электротехники и электрификации ФГБОУ ВО «Национальный исследовательский университет «МЭИ» (111250, Россия, Москва, ул. Красноказарменная, д. 14). E-mail: matasov_av93@mail.ru. Scopus Author ID 57208886094, ResearcherID Q-9794-2017, https://orcid.org/0000-0001-6092-5089

Довмалов Армен Арменович, студент кафедры физики и технологии электротехнических материалов и компонентов Института электротехники и электрификации ФГБОУ ВО «Национальный исследовательский университет «МЭИ» (111250, Россия, Москва, ул. Красноказарменная, д. 14). E-mail: armenbbb80821@gmail.com. https://orcid.org/0000-0002-4285-7876

Бабышкина Дарья Максимовна, студент кафедры физики и технологии электротехнических материалов и компонентов Института электротехники и электрификации ФГБОУ ВО «Национальный исследовательский университет «МЭИ» (111250, Россия, Москва, ул. Красноказарменная, д. 14). E-mail: dashababyshkina@gmail.com. https://orcid.org/0000-0001-7893-5525

The article was submitted: Novemder 25, 2020; approved after reviewing: February 02, 2021; accepted for publication: March 31, 2021.

Translated from Russian into English by N. Isaeva
Edited for English language and spelling by Enago, an editing brand of Crimson Interactive Inc.

MIREA – Russian Technological University
78, Vernadskogo pr., Moscow, 119454, Russian Federation.
Publication date *April 30, 2021.*
Not for sale

МИРЭА – Российский технологический университет
119454, РФ, Москва, пр-кт Вернадского, д. 78.
Дата опубликования *30.04.2021.*
Не для продажи

www.finechem-mirea.ru